Bericht des Instituts für Aerodynamik und Strömungstechnik

Report of the Institute of Aerodynamics and Flow Technology

IB 124-2010/2

Implementation, verification and validation of empirical transition criteria for airfoil and rotary wing applications using the DLR FLOWer code

Christoph Heister

Herausgeber:
Deutsches Zentrum für Luft- und Raumfahrt e.V.
Institut für Aerodynamik und Strömungstechnik
Lilienthalplatz 7, Germany, 38108 Braunschweig

ISSN 1614-7790

Stufe der Zugänglichkeit: 1
Braunschweig, im Februar 2010

Institutsdirektor:
Prof. Dr.-Ing. habil. C.-C. Rossow

Verfasser:
Dipl.-Ing. Christoph Heister

Abteilung: $C^2A^2S^2E$
Abteilungsleiter:
Prof. Dr.-Ing. N. Kroll

Der Bericht enthält:
95 Seiten
67 Bilder
19 Tabellen
24 Literaturstellen

Abstract

This report covers the implementation, verification and validation of a transition prediction method for airfoil and rotary wing applications based on the DLR-FLOWer code. The prediction method features five empirical criteria according to minimum pressure, laminar separation, Michel, van Driest & Blumer and Arnal, Habiballah & Delcourt (AHD). The criteria's equations will be briefly summarized. The prediction method's algorithm and it's implementation into the DLR's structured flow solver FLOWer will be described. Validation has been carried out for the Somer's airfoil ($M_\infty = 0.3$, $\alpha = [-5°, 15°]$) as well as the CAST10 airfoil ($M_\infty = 0.73$, $\alpha = -0.25°$). A verification of the implemented method has been done using the ONERA 7A rotor hover test case. Finally, the method is applied to a recent rotor geometry in hover, representing an industrial application case.

Zusammenfassung

Der vorliegende Bericht behandelt die Implementierung, Verifizierung und Validierung einer Methodik zur Transitionsvorhersage für den strukturierten Strömungslöser FLOWer. Die Implementierung wurde im Hinblick auf Anwendungen für Profil- und Rotorrechnungen vorgenommen. Zu den verwendeten empirischen Vorhersagekriterien zählen Kriterien nach minimalem Druck, laminarer Ablösung, Michel, van Driest & Blumer und Arnal, Habiballah & Delcourt (AHD). Es wird eine analytische Darstellung der Kriterien sowie des implementierten Vorhersagealgorithmus gegeben. Eine Validierung erfolgt für das Somers Profil ($M_\infty = 0.3$, $\alpha = [-5°, 15°]$) und das CAST10 Profil ($M_\infty = 0.73$, $\alpha = -0.25°$). Die Anwendbarkeit empirischer Transitionskriterien für einen Rotor im Schwebeflug wird durch Rechnungen für den ONERA 7A Rotor aufgezeigt und die Ergebnisse mit Resultaten der ONERA verifiziert. Abschliessend wird die Vorhersagemethodik an einem industriellen Schwebeflugfall getestet.

Contents

Symbols

Latin Symbols

Symbol	Units	Explanation
c	m	chord length
c_p	$-$	pressure coefficient
c_P	$-$	power coefficient
c_T	$-$	thrust coefficient
FM	$-$	figure of merit
H	$-$	form factor
k	m^2/s^2	specific kinetic turbulence energy
M	$-$	mach number
p	N/m^2	local pressure
r	$-$	relaxation factor
R	m	rotor radius
Re	$-$	Reynolds number
Re_{δ_1}	$-$	Reynolds number based on displacement thickness
Re_{δ_2}	$-$	Reynolds number based on momentum thickness
s	m	arc length
Tu	$-$	turbulence level
u	m/s	wall tangential velocity
U_e	m/s	velocity at boundary layer edge
U_∞	m/s	free stream velocity
y	m	wall normal coordinate

Greek Symbols

Symbol	Units	Explanation
α	$^\circ$	angle of attack
δ	m	boundary layer thickness
δ_1	m	displacement thickness
δ_2	m	momentum thickness
Θ_c	$^\circ$	geometric angle of attack
Λ	$-$	Pohlhausen factor
$\overline{\Lambda}_2$	$-$	averaged Pohlhausen factor
μ	$Pa \cdot s$	dynamic viscosity
μ_{Tu}	$Pa \cdot s$	eddy viscosity
ν	m^2/s	kinematic viscosity
ρ	kg/m^3	density

Subscripts

Subscript	Explanation
cr	critical location
e	boundary layer edge
i	wall tangential index
j	wall normal index
n	prediction step
th	Thwaites approximation
tr	transition location
∞	far field value

1 Introduction

The behaviour of the boundary layer in the context of rotary wing aerodynamics has been an area of great interest throughout the years. This is due to the fact, that the state of the boundary layer significantly effects the generated drag and maximum attainable lift of airfoils and rotary wings. With respect to a helicopter rotor, boundary layer transition is of particular importance since accurate prediction of torque and hence power is essential in emerging designs. It has been shown for generic rotor geometries, that accounting for a laminar-turbulent boundary layer in the Navier-Stokes computations has a positive influence on the rotor's efficiency by 3 to 4.5 counts [5], compared to assuming the flow as fully turbulent. The comparison presented in [5] has been done by *prescribing* areas of laminar and turbulent flow within the computational domain.
This report focuses on a method to *predict* the development of the boundary layer state with respect to rotary wing applications, using the DLR's block structured flow solver FLOWer in combination with empirical transition criteria.
Chapter 2 of this report gives an overview of the FLOWer code and how it handles regions of laminar or turbulent flow in general. Chapter 3 summarizes the empirical criteria implemented into the code. The evaluation of the required boundary layer parameters is described in chapter 4. An explanation of the prediction algorithm is given in chapter 5. Chapter 6 and 7 present the results of the validation and verification test cases. A first application to a rotor in hover, representing a recent industrial rotor geometry, is described in chapter 8. A conclusion of the obtained results will be given in chapter 9. An outlook to possible future improvements and developments is included in chapter 10.

The research activities of this report are based on a cooperation with EUROCOPTER Deutschland company.

2 DLR FLOWer code

A brief summary of the DLR flow solver FLOWer is given, which has been used for the research activites described in this report. Additionally, a short overview of modeling laminar and turbulent flow regions in FLOWer is included because of the importance to the presented transition prediction method.

2.1 General features

The block-structured flow solver FLOWer solves the compressible three-dimensional Reynolds averaged Navier-Stokes equations for rigid bodies in arbitrary motion. A finite-volume method with second order upwind or central space discretization including scalar or matrix artifical dissipation is used to solve the equations. Cell centered and cell vertex formulations are provided for space discretization. The discrete equations are integrated explicitly using a multistage Runge-Kutta scheme. To accelerate convergence for steady computations, the FLOWer code features several techniques, including local time stepping, implicit residual smoothing and multigrid acceleration. For time accurate computations the implicit dual time stepping method is employed. The code has been parallelized according to the MPI library specification. Additionally the Chimera technique enhances the flexibility of handling complex geometries and independently moving bodies. Preconditioning is used for low speed flow simulation. Various turbulence models are available, ranging from eddy viscosity to full differential Reynolds stress models. For additional information concerning the FLOWer code see for example [10], [11], and [12].

2.2 Laminar and turbulent flow regions

The aim of the transition prediction method it to generate physically feasible regions of laminar, turbulent and transitional flow within the computational grid. The generation of flow regions in FLOWer is controlled by a real value called LTFLAG. Each cell vertex or cell center holds a LTFLAG value, labeling it's flow state to be treated as:

- LTFLAG = 0 - laminar,
- LTFLAG = 1 - turbulent or
- LTFLAG =]0,...,1[- transitional.

Turbulence model	LTFLAG influence
Algebraic	$\mu_{tu} = (1 - LTFLAG)\,\mu_{lam} + LTFLAG \cdot \mu_{tu}$
One equation	$S_{tu} = min(S_{full}, S_{lim})$ with: $S_{lim} = LTFLAG \cdot S_{full}$ and: $S_{full} = P + Diff - D$
Two equation	$\vec{S}_{tu} = \begin{bmatrix} P_k - D_k \\ P_\omega - D_\omega \end{bmatrix}$ with: $P_{k/\omega} = min(P_{k/\omega},\, C^{LTFLAG} \cdot D_{k/\omega})$

Table 2.1: Influence of LTFLAG value on turbulence model transport equations used for modeling regions of laminar, transitional and turbulent flow.

Within *laminar* and *transitional* flow regions LTFLAG influences the source term S_{tu} of the turbulence model transport equation in such a way that its value is lower or equal to zero [13]. Consequently suppression of turbulence production P is enforced, allowing for turbulence destruction D only.

Within *turbulent* flow regions LTFLAG allows the source term S_{tu} to be evaluated normally according to the activated turbulence model.

The transition prediction method presented in this report will use the LTFLAG value in order to generate flow regions according to the evaluation of the empirical criteria (see chapter 3).

Table 2.1 schematically summarizes the influence of the LTFLAG value with respect to different turbulence models implemented in FLOWer.

3 Empirical transition criteria

Empirical transition criteria are often used for practical applications because of their uncomplicated introduction in engineering prediction methods. Generally they are established by using experimental data obtained in low turbulence wind tunnels or flight tests and account for streamwise instabilities of 2D flows [2].

Rotor airfoils typically exhibit a steep adverse pressure gradient in chordwise direction [14]. The chordwise pressure distribution has been found to have a strong influence on the behaviour of transition onset on rotating blades [17], when neglecting unsteady effects. Within the presented approach for transition prediction, the empircal criteria will be evaluated along the grid lines in chordwise direction. Possible influences of cross flow instabilities or rotational forces on the boundary layer development will not be captured.

Depending on the criterion, various influences on the boundary layer flow can be accounted for, like:

- pressure gradients,
- flow reversal,
- free stream turbulence or
- amplification of Tollmien-Schlichting instabilities.

In the following, five empirical criteria will be presented, which were used during the research activities - minimum pressure, laminar separation, Michel, van Driest & Blumer and Arnal, Habiballah & Delcourt.

3.1 Minimum pressure

This pragmatic criterion is suited for a flow driven by a pressure gradient. Laminar flow is assumed to persist, as long as the flow is accelerated by a negative pressure gradient. Transition to turbulence will occur with the encounter of a positive (adverse) pressure gradient.
The pressure distribution will be evaluated along a grid line starting from the stagnation point to the trailing edge, for the suction and pressure side respectively. A pressure minimum at point i will be detected, if the following conditions are satisfied:

$$p_{i-1} \geq p_i < p_{i+1} \qquad \text{or} \qquad p_{i-1} > p_i \leq p_{i+1} \tag{3.1}$$

and

$$\left.\frac{dp}{ds}\right|_{i-1} \leq 0 < \left.\frac{dp}{ds}\right|_{i+1} \qquad \text{or} \qquad \left.\frac{dp}{ds}\right|_{i-1} < 0 \leq \left.\frac{dp}{ds}\right|_{i+1} \tag{3.2}$$

Onset of transition will be set to the location of the *first* detected pressure minimum.

3.2 Laminar separation

This criterion detects flow reversal within laminar separation bubbles forming due to an adverse pressure gradient. Transition onset will be set to the first node location *i* with reversal of the wall tangential velocity *u*:

$$u_{i-1,j+1} \cdot u_{i+1,j+1} \leq 0 \tag{3.3}$$

$$\left.\frac{\partial p}{\partial s}\right|_{i-1,j+1} > 0 \qquad \text{and} \qquad \left.\frac{\partial p}{\partial s}\right|_{i+1,j+1} > 0 \tag{3.4}$$

The wall tangential velocity *u* is taken at the first inner grid point above the wall. Additionally, the presence of a positive pressure gradient has to be fulfilled, in order to prevent a stagnation point detection by mistake.

3.3 Michel

The Michel criterion has been developed to predict transition with respect to pressure gradient effects [2]. Transition will be set depending on a correlation of two Reynold numbers: Re_s based on the arc length in streamwise (here: chordwise) direction and Re_{δ_2} based on momentum thickness of the boundary layer.

A version of the Michel criterion, as published in the year 1951 [18], was used by Hill, Shaw and Qin for transition prediction on a rotary wing [9]. This version of the Michel criterion is implemented in the ROT version of the FLOWer code:

$$Re_{\delta_2} = 2,94 \cdot Re_{s,tr}^{0,4} \qquad \text{(FLOWer ROT version)} \tag{3.5}$$

A later version of the Michel criterion, published 1952 [19], is available as default in the MAIN version of the FLOWer code:

$$Re_{\delta_2} = 1,174 \cdot Re_{s,tr}^{0,46} \qquad \text{(FLOWer MAIN version)} \tag{3.6}$$

with

$$Re_{\delta_2} = \frac{U_e \cdot \delta_2}{\nu_e} \tag{3.7}$$

$$Re_s = \frac{U_e \cdot s}{\nu_e} \tag{3.8}$$

$$\nu_e = \frac{\mu_e}{\rho_e} \tag{3.9}$$

If not stated otherwise, the version of 1951 will be used for the computations, because a succesfull application to airfoils and an isolated rotor in hover has been demonstrated in [9].

The momentum thickness δ_2 can be evaluated by the Thwaites approximation [22] or by direct integration of the boundary layer values (see chapter 4).

3.4 van Driest and Blumer

The criterion proposed by van Driest & Blumer [23] combines the consideration of pressure gradient and free stream turbulence. Transition onset will be predicted, depending on the boundary layer thickness Reynolds number Re_δ, the Pohlhausen parameter Λ and the free stream turbulence level Tu. The formulation of the criterion is given as:

$$9860 = Re_{\delta,tr}(1 - 0,0485\Lambda_{tr} + 3,36\, Re_{\delta,tr}\, Tu^2) \tag{3.10}$$

with

$$Re_\delta = \frac{U_e \cdot \delta}{\nu_e} \tag{3.11}$$

$$\Lambda = \frac{dU_e}{ds}\delta^2 \frac{1}{\nu_e} \tag{3.12}$$

$$Tu = \frac{1}{U_e}\sqrt{\frac{2}{3}\, k_e} \tag{3.13}$$

and

$$\nu_e = \frac{\mu_e}{\rho_e} \tag{3.14}$$

The boundary layer thickness δ will be detected according to Stock & Haase [21] (see chapter 5.3).

3.5 Arnal, Habiballah and Delcourt

The AHD criterion has been developed for transition prediction, accouting for pressure gradient and free stream turbulence effects [2]. The incompressible version has been implemented during this work. This version sees frequent use by the ONERA, for fixed [6] as well as rotary wing applications [4].

The criterion evaluates transition onset based on the Reynolds number of the boundary layer momentum thickness Re_{δ_2}, the averaged Pohlhausen factor $\bar{\Lambda}_2$ and the free stream

turbulence level Tu. The critical Reynolds number $Re_{\delta_2,cr}$ characterizes the stability of the flow. The following relation has to be fulfilled at the location of transition onset:

$$Re_{\delta_2,tr} - Re_{\delta_2,cr} = -206 \cdot exp\,(25,7\overline{\Lambda}_{2,tr})\,(ln(16,8\,Tu) - 2,77\,\overline{\Lambda}_{2,tr}) \tag{3.15}$$

with

$$Re_{\delta_2} = \frac{U_e \cdot \delta_2}{\nu_e} \tag{3.16}$$

$$Re_{\delta_2,cr} = exp(\frac{52}{H} - 14,8) \tag{3.17}$$

$$\overline{\Lambda}_2 = \frac{1}{s - s_{cr}} \int_{s_{cr}}^{s} \left(\frac{\delta_2^2}{\nu_e} \frac{U_e}{ds} \right) ds \tag{3.18}$$

$$Tu = \frac{1}{U_e} \sqrt{\frac{2}{3}\,k_e} \tag{3.19}$$

and

$$H = \frac{\delta_1}{\delta_2} \tag{3.20}$$

$$s_{cr} = \frac{Re_{\delta_2,cr} \cdot \nu_e}{U_e} \tag{3.21}$$

$$\nu_e = \frac{\mu_e}{\rho_e} \tag{3.22}$$

The momentum thickness δ_2 can be evaluated by the Thwaites approximation [22] or direct integration of the boundary layer values.

The displacement thickness δ_1 necessary for the form factor H will be directly integrated based on the boundary layer values (see chapter 4).

To assure a valid evaluation of $Re_{\delta_2,cr}$, the shape factor is assumed to be in the range of $2.0 < H < 3.1$.
The turbulence level's default is assumed to be $Tu = 1 \cdot 10^{-3}$ [2], representing a physically feasible lower bound, if not otherwise a greater value exists from the flow solution.

4 Two dimensional boundary layer parameters

The empirical criteria presented in chapter 3 rely on the evaluation of the laminar boundary layer parameters in order to predict transition onset. A summary of the employed parameter definitions for the two dimensional case is given, since the criteria do not account for three dimensional effects.

The evaluation of the integral boundary layer parameters strongly depends on the correct detection of the boundary layer edge (see chapter 5.3) as well as the grid resolution of the viscous layer (see chapter F).

4.1 Displacement thickness

The displacement thickness can be interpreted as the amount streamlines around a body are deflected due to the thickening of the boundary layer. The compressible, integral definition reads as [24]:

$$\delta_1 = \int_0^{\delta} \left(1 - \frac{\rho}{\rho_e}\frac{u}{U_e}\right) dy \tag{4.1}$$

The thickness of the viscous layer δ is assumed to be known.

4.2 Momentum thickness

The momentum thickness represents an equivalent boundary layer thickness due to skin friction induced momentum loss. Two different approaches are implemented into the flow solver - an incompressible approximation and the integral formulation respecting compressibility.

4.2.1 Thwaites approximation

The momentum thickness can be approximated for incompressible laminar flow regions according to Thwaites [22]. The approximation takes into account the wall pressure and

the running length s. This allows a formulation independend of further boundary layer parameters.

$$\delta_{2,th}^2 = \frac{0,45\,\nu_e}{U_e^6} \int_0^s U_e^5\, ds \tag{4.2}$$

with

$$U_e = U_\infty \sqrt{1 - c_{p,\,wall}} \tag{4.3}$$

$$\nu_e = \frac{\mu_e}{\rho_e} \tag{4.4}$$

The pressure gradient normal to the wall in the viscous layer is assumed to be zero.

4.2.2 Integral, compressible formulation

The compressible, integral thickness is defined as [24]:

$$\delta_2 = \int_0^\delta \frac{\rho}{\rho_e} \frac{u}{U_e} \left(1 - \frac{u}{U_e}\right) dy \tag{4.5}$$

The boundary layer thickness δ is assumed to be known.

5 Implementation

The transition prediction method is directly implemented in the FLOWer code. It is hereby part of the iterative solution procedure. The method uses the internally computed flow solution of the code to evaluate the boundary layer parameters as presented in chapter 4. The evaluation is done along grid lines, assuming global alignment to the dominant flow direction. Please refer to [7] or appendix F summarizing further requirements for the grids to be used in order to work properly with the prediction algorithm.

5.1 Algorithm

According to [13], the flow field will be initalized to fully laminar before execution of the first transition prediction step. This is found to support the early detection of laminar separation points, serving as an approximation of transition onset and thereby stabilizing the RANS computation.

It may be mentioned that fully turbulent initialization is also possible but not used during the presented computations.

The prediction is triggered at user defined intervals, this means iteration steps. Consequently for each airfoil section, an algorithm will be run through, which is basically organized as follows:

1. Detection of stagnation point;
2. Application of laminar separation criterion (see chapter 3.2);
3. Detection of boundary layer edge;
4. Calculation of the boundary layer parameters (see chapter 4);
5. Evaluation of the minimum pressure, Michel, van Driest & Blumer or AHD criterion - relaxation of transition onset;
6. Prescription of transitional region's extent;
7. Initialization of laminar/turbulent flow regions via LTFLAG;

Steps two to seven will be done for each airfoil section side, resulting from a partitioning by the stagnation and trailing edge point.

Step two will be skipped if the minimum pressure criterion has been selected. This allows for a robust prediction capability, independend of boundary layer parameters.

5.2 Detection of stagnation point

Two different approaches are available for stagnation point detection - based solely on maximum pressure or on a combination of flow reversal and maximum pressure.

5.2.1 Maximum pressure

This procedure evaluates a known pressure distribution in order to find the stagnation point. The evalulation starts from the middle node on one section side, proceeds over the leading edge and ends at the middle node on the other section side. A pressure maximum at point i will be detected, if the following conditions are satisfied:

$$p_{i-1} \leq p_i > p_{i+1} \qquad \text{or} \qquad p_{i-1} < p_i \geq p_{i+1} \tag{5.1}$$

and

$$\left.\frac{dp}{ds}\right|_{i-1} \geq 0 > \left.\frac{dp}{ds}\right|_{i+1} \qquad \text{or} \qquad \left.\frac{dp}{ds}\right|_{i-1} > 0 \geq \left.\frac{dp}{ds}\right|_{i+1} \tag{5.2}$$

Of all detected points, the one representing the absolute maximum pressure is assumed as stagnation point.

5.2.2 Flow reversal with maximum pressure

This algorithm looks for a zero wall tangential velocity u by comparing its absolute value to a tolerance level ϵ_{tol}. Additionally, a velocity reversal will be detected, if there exists a sign changeover of detected zero point clusters.

$$|u_i| < \epsilon_{tol} \qquad \text{and} \qquad sgn(u_{c-1}) \neq sgn(u_{c+1}) \tag{5.3}$$

Of all detected zero velocity points with flow reversal, the one with the absolute maximum pressure is assumed the stagnation point.

5.3 Detection of boundary layer edge

In order to derive the state of flow parameters or integrate the thickness of the boundary layer edge, the viscous layer thickness δ has to be known (see chapter 4). A method after Stock & Haase [21] is employed to detect the viscous layer thickness, using wall normal profiles of the wall tangential velocity from the flow solution. A diagnostic function F is formulated as follows:

$$F(y) = y^a \left(\frac{du}{dy}\right) \tag{5.4}$$

resulting in

$$\delta = \epsilon \cdot y_{max} \tag{5.5}$$

Constant	laminar	turbulent	transitional
a	$3,9$	$1,0$	$(1 - LTFLAG) \cdot 3,9 + LTFLAG \cdot 1,0$
ϵ	$1,294$	$1,936$	$(1 - LTFLAG) \cdot 1,294 + LTFLAG \cdot 1,936$

Table 5.1: Constants of the diagnostic function acoording to Stock & Haase [21] with respect to boundary layer flow state.

y_{max} is the wall normal distance, for which $F = F_{max}$. The constants a and ϵ of the diagnostic function are summarized in Table 5.1 for the laminar, turbulent and, in interpolated form, for the transitional region.

The method of Stock & Haase gives feasible results in the laminar flow regime. This is a fundamental requirement for calculating the integral laminar boundary layer parameters δ_1 and δ_2 introduced.
In the turbulent flow regime though, problems were observed when trying to detect the boundary layer edge. This is due to a peak of the diagnostic function $F(y)$ occuring very close to the wall. Consequently, this peak will be detected as a maximum, resulting in a very small boundary layer thickness. To improve the detection in the *turbulent* regime, the maximum search of the diagnostic function $F(y)$ has been adapted to look for the second maximum, skipping the first one representing the peak of the diagnostic function. Investigations are undertaken by the Institut für Aerodynamik und Gasdynamik (IAG) of the Universität Stuttgart as part of a diploma thesis to improve the boundary layer detection method [16]. The improved detection method will be selectable in the central version of the FLOWer code. It is not used within the presented activities.

5.4 Evaluation of transition onset

The empirical criteria according to Michel, van Driest & Blumer and AHD are defined for laminar, attached flows. To assure a valid evaluation of the criteria, the extent of attached flows is determined by the laminar separation criterion. Thus, the laminar separation criterion has precedence over the above mentioned criteria. This is assured by the following procedure:

1. Evaluation of empirical criterion;
2. If laminar separation has been detected, assume as onset point;
3. If laminar separation has not been detected, relax onset of empirical criterion;
4. Set onset point;

Transition onset movement $\Delta = \left(x_{cr}^T - x_{n-1}^T\right)$	Relaxation technique
downstream $(\Delta > 0)$	$x_n^T = x_{n-1}^T + \lvert r \rvert \cdot r \cdot \Delta$
upstream $(\Delta < 0)$	$x_n^T = x_{n-1}^T + r \cdot \Delta$
upstream 'shift' $(\lvert\Delta\rvert > r \cdot c)$	$x_n^T = x_{n-1}^T$

Table 5.2: Relaxation techniques of transition onset depending on difference to previous detected position.

If laminar separation is detected during a transition prediction step, an area of attached laminar flow will be initialized. The empirical criterion will evaluate the boundary layer of this area in the next prediction step.

The procedure explained above assumes, that the employed empirical criterion does not account for laminar separation bubbles, in order to avoid interference with the laminar separation criterion.

5.5 Relaxation of transition onset

During early computations for the Somers and CAST10 airfoils, oscillations in the convergence history of the transion onset position could be observed, especially for moderate and high angles of attack. The periodic shift of transition onset negatively influenced the convergence behaviour which in consequence also showed periodic oscillations.

In order to damp the oscillations, an existing relaxation procedure was modified. The goal of the modification is to assure a continuous evolution of the onset point from the trailing edge in upstream direction [13]. Additionally, unphysical large shifts of the onset position in upstream direction due to an unconverged flow state will be avoided. Table 5.2 summarizes the employed relaxation technique.

As illustration, a relaxation factor of $r = 0.5$ is assumed. This allows an onset shift of 25% chord in downstream direction and 50% onset shift in upstream direction. If the movements exceeds 50% of the chord length, the new onset position will be ignored and replaced by the one of the previous prediction step.
For $r = 1$ an unrestricted movement of the new transition location is possible, suitable to capture instationary flow phenomena.
A value of $r = 0$ denies any movement of transition location, preserving the location of the first prediction step or a laminar separation point.

5.6 Determination of transitional region's extent

The extent of a transitional region behind the onset point is defined as an amount of preset grid points in the form of user input. A default of five grid points was used throughout the present work.

6 Validation test cases

For a first validation, the transition prediction method is applied to two different airfoil testcases: a low Mach number flow over the Somers airfoil [20] at various angles of attack and a transsonic flow over the CAST10 airfoil [8] at a fixed angle of attack.

For transition prediction, empirical criteria according to minimum pressure, Michel, van Driest & Blumer and AHD will be used.

The computational procedure for transition prediction is divided into two steps:

1. a fully turbulent computation (full multigrid) to converge the lift and drag coefficients;
2. a restart (simple multigrid) with activated transition prediction and laminar initialization;

The procedure above is based on best practice experience gained during transition prediction with the FLOWer code in combination with e^N - database methods [13]. It favours the early detection of laminar separation points as first approximation of transition onset, which enhances the stability of the RANS computation (see also chapter 5).

The above procedure will be used for all computations for the sake of consistency and comparability of the results among each other. For the Somers testcase 1100 / 1000 cycles will be run, the CAST10 testcase is computed with 2700 / 7500 cycles respectively.

For the Somers testcase, the influence of selected turbulence models on the computed transition location will be investigated in chapter 6.1.5.

6.1 Somers airfoil

The computations for the Somers airfoil are performed on a single block mesh (see figure A.1) with about 24.600 grid points, 73 in wall normal direction and 337 in tangential direction. The boundary layer is resolved with approximately 40 grid points. Mach number is $M = 0.3$ for a Reynolds number of $Re = 4.0 \cdot 10^6$. Angles of attack vary in steps of two degrees from -4° to $+14^\circ$, covering the range of the experimental data.

Transition prediction will be called at intervalls of 50 cycles.

The Baldwin-Lomax turbulence model is used at first for it's robustness. Computations with further turbulence models will be presented in chapter 6.1.5.

Option	Setting	FLOWer parameter	Value
Stagnation point detection	flow reversal + c_p-max	TRACSTAGMETH	2
Relaxation	none	TRACRELAX	1.0
Prediction frequency	user specified	TRACFREQ	50
Laminar zone thickness	user specified	TRACTHICKN	41

Table 6.1: FLOWer parameter for transition prediction on Somers airfoil using the minimum pressure criterion.

6.1.1 Minimum pressure

Transition onset is evaluted with respect to the minimum pressure location. The settings used for the calculation are summarized in table 6.1.

Figure A.2 shows the convergence history of the density residual, lift coefficient and drag coefficient for an angle of attack of $\alpha = 0°$. The introduction of laminar flow regions initially causes small disturbances with respect to the coefficients but comes to a level state after the second prediction step (100 iterations). A decrease of the drag coefficient by 21% can be observed due to the reduced skin friction coefficent of the present laminar flow regions. The lift coefficient experiences a minor increase by 4%. The density residual converges progressively after the restart.

Figure A.3 shows the convergence of the transition locations for the upper and lower side of the airfoil as a function of the prediction steps. Throughout all prediction steps the transition onset remains at a fixed position indicating a stable location of the pressure minimum throughout the prediction procedure.

Figure A.4 compares experimental [20] and computed transition locations using the minimum pressure criterion, in the range from $-4°$ to $+14°$. Observing the development of transition onset for the airfoil's upper side, a gradual shift of transition onset towards the leading edge takes place with increasing angle of attack. Onset starts at 33% chord position for $\alpha = -4°$ and settles near the leading edge for $\alpha = [10°, 14°]$. This behaviour represents the shift of the pressure peak on the airfoil's upper side. For the airfoil's lower side, transition onset shows the opposite trend compared to the upper side. For $\alpha = -4°$ onset is located at the leading edge, gradually shifting in downstream direction for $\alpha = +4°$. Only minor downstream movements are observed until $\alpha = +14°$ is reached.

In summary, the trends of the experimental data are captured. The agreement between numerical and experimental determined transition onset is poor however. Transition onset for both upper and lower side is predicted at a more upstream position than the experiment with an average offset of 15% chord length. A maximum offset of 32% can be observed on the airfoil's lower side for $\alpha = 0°$.

6.1.2 Michel

Transition onset is evaluted with respect to the Michel criterion [18]. The Thwaites approximation is used for calculating the momentum thickness [22]. Table 6.2 summarizes the employed transition settings.

Option	Setting	FLOWer parameter	Value
Stagnation point detection	flow reversal + c_p-max	TRACSTAGMETH	2
Relaxation	moderate, $\alpha =]-4°, 6°[$	TRACRELAX	0.35
	enforcing, $\alpha =]8°, 14°[$	TRACRELAX	0.0
Prediction frequency	user specified	TRACFREQ	50
Laminar zone thickness	user specified	TRACTHICKN	41
Calculation of δ_2	Thwaites approximation	TRATHWAITES(1)	1.0

Table 6.2: FLOWer parameter for transition prediction on Somers airfoil using the Michel criterion.

Figure A.5 shows the convergence history of the density residual, lift coefficient and drag coefficient for an angle of attack of $\alpha = 0°$. Small excitements in the convergence of the coefficients and density residual can be seen during the first six prediction steps after the restart. With the seventh prediction step, the transition onset locations settle at positions of 38% and 39% chord respectively, as can be seen in Figure A.6. With the stabilization of the transition locations, the density residual decreases progressively , bringing the lift and drag coefficients to convergence. A decrease of the drag coefficient by 39% can be observed due to the reduced skin friction coefficent within the present laminar flow region. The lift coefficient experiences a minor increase by 9%.

A comparison of experimental [20] and computed transition onset data is given in figure A.7 for the range from $-4°$ to $+14°$. For the airfoil's upper side, a linear shift of transition onset in upstream direction can be observed with increasing angle of attack. Onset starts at 48% chord position for $\alpha = -4°$ and settles at the leading edge for $\alpha = +14°$. For the airfoil's lower side, transition onset shows the opposite trend compared to the upper side. For $\alpha = -4°$ onset is located at 11% chord, gradually travelling in downstream direction for $\alpha = +2°$ and changing into a flat curve with then only minor shifts until $\alpha = +14°$ is reached. From $\alpha = 8°$ onwards, the relaxation factor has to be changed from 0.35 to 0.0 due to transition onset oscillations. The oscillations result from an alternation of a laminar separation point and an onset point of the Michel criterion at further downstream position. These positions are in conflict with each other throughout the remaining prediction steps. To damp the oscillations, a relaxation factor of 0.0 is used, favouring the laminar separation point as transition onset point.

Overall, the trends of the experimental data are reproduced very closely. Transition onset for both upper and lower side is predicted at a slightly more upstream position than the experiment with an average offset of 3% chord length. A maximum offset of 14% can be observed for $\alpha = 0°$ on the lower side.

6.1.3 van Driest & Blumer

Transition onset is evaluted with respect to the van Driest & Blumer criterion. Boundary layer thickness is detected according to the method of Stock & Haase [21], using the settings presented in table 6.3.

Figure A.9 shows the convergence of the transition locations on the upper and lower side

Option	Setting	FLOWer parameter	Value
Stagnation point detection	flow reversal + c_p-max	TRACSTAGMETH	2
Relaxation	moderate	TRACRELAX	0.35
Prediction frequency	user specified	TRACFREQ	50
Laminar zone thickness	user specified	TRACTHICKN	41

Table 6.3: FLOWer parameter for transition prediction on Somers airfoil using the van Driest & Blumer criterion.

of the airfoil as a function of the prediction steps for $\alpha = 0°$. As a result from the laminar initalization (see chapter 5.1), laminar separation points on the upper and lower side of the airfoil are detected at 56% chord during the first prediction step. During the second prediction step, another laminar separation point, moving in upstream direction, is detected on the upper side. On the lower side, transition onset is detected by the van Driest & Blumer criterion. Onset positions on both sides smoothly converge in upstream direction and remain stable after the fifth prediction step throughout the remaining prediction cycles.

The convergence of the transition onset points is reflected in the convergence behaviour of the density residuum and the lift and drag coefficient shown in figure A.8. Peaks in the curve of the density residual at intervalls of 50 iterations mark the prediction steps. After 250 iterations the lift and drag coefficients become stable and the density residual is reduced progressivly due the stable onset position. A decrease of the drag coefficient by 34% can be observed due to the reduced skin friction coefficent of the present laminar flow regions. The lift coefficient experiences a minor increase by 8%.

Figure A.10 compares experimental [20] and computed transition locations in the range from $-4°$ to $+14°$. For the airfoil's upper side, a gradual shift of transition onset towards the leading edge takes place with increasing angle of attack. Onset starts at 37% chord length for $\alpha = -4°$ and settles at the leading edge for $\alpha = +14°$. For the airfoil's lower side, transition onset shows the opposite trend compared to the upper side. For $\alpha = -4°$ onset is located at 16% chord, gradually shifting in downstream direction for $\alpha = +2°$, with then only minor shifts until $\alpha = +14°$ is reached.

Generally speaking, the trends of the experimental data is well captured. Transition onset for all points on the airfoil's upper and lower side is predicted at a more upstream position than the experiment with an average of 8% offset in chord length. A maximum offset of 14% can be observed on the lower side for $\alpha = 0°$.

6.1.4 AHD

Transition onset is evaluated with respect to the AHD criterion. For calculation of the momentum thickness, the approximation according to Thwaites [22] is used. Displacement thickness is calculated based on the integral boundary layer parameter (see chapter 5). Table 6.4 summarizes the settings used for the prediction procedure.

The convergence history of the density residual, lift coefficient and drag coefficient is shown for an angle of attack of $\alpha = 0°$ in figure A.11. The transition prediction procedure

Option	Setting	FLOWer parameter	Value
Stagnation point detection	flow reversal + c_p-max	TRACSTAGMETH	2
Relaxation	moderate	TRACRELAX	0.35
Prediction frequency	user specified	TRACFREQ	50
Laminar zone thickness	user specified	TRACTHICKN	41
Calculation of δ_1	integral	-	-
Calculation of δ_2	Thwaites approximation	TRATHWAITES(1)	1.0

Table 6.4: FLOWer parameter for transition prediction on Somers airfoil using the AHD criterion.

causes small peaks in the curve of the density residual at intervalls of 50 iterations, marking the executed prediction steps. After 250 iterations, this equals five prediction steps, the lift and drag coefficients become stable and the density residual is reduced progressivly due to a stablilization of the transition onset position, as shown in A.12. Due to the reduced skin friction coefficent within the present laminar flow region, a decrease of the drag coefficient by 37% can be observed. The lift coefficient experiences a minor increase by 8%, as with results of the previous criteria.

Figure A.12 shows the convergence of the transition locations on the upper and lower side of the airfoil as a function of the prediction steps for $\alpha = 0°$. Laminar separation points on the upper and lower side of the airfoil are detected at 56% chord during the first prediction step, possible by laminar initalization (see chapter 5.1). During the second prediction step, another laminar separation point, moving in upstream direction, is detected on the upper side. On the lower side, transition onset is detected by the AHD criterion. Onset positions on both sides travel in upstream direction and converge after the 7th prediction step. The onsets remain stable throughout the remaining prediction cycles.

A comparison of experimental [20] and computed transition locations is given in figure A.13 in the range from $-4°$ to $+14°$. For the airfoil's upper side, with increasing angle of attack, a slightly S-shaped curve represents the shift of the onset locations in upstream direction. The onset starts at 42% chord position for $\alpha = -4°$ and ends at the leading edge for $\alpha = +14°$. On the airfoil's lower side, for $\alpha = -4°$, onset is located at 6% chord, linearily shifting downstream until $\alpha = +2°$. From $\alpha = +2°$ to $\alpha = 14°$ the curve of transition onset flatens, again in an S-shaped manner.

Overall, the trends of the experimental data are closely captured. Transition onset for both upper and lower side is predicted at a sligthly more upstream position than the experiment, showing in an average of 4% offset in chord length. Maximum offset of 17% can be observed on the aifoils lower side for $\alpha = 0°$.

6.1.5 Influence of selected turbulence models

In order to investigate a possible influence of turbulence models on the location of transition onset, a study is conducted for the Somers airfoil testcase. Within this study, the empirical transition criteria are employed in combination with four different turbulence

models, including the

- Baldwin-Lomax model,
- Spalart-Allmaras model,
- Wilcox k-ω model and
- SST k-ω model;

As with the validation cases, transition prediction will be done covering angles of attack in the range $[-4°; 14°]$, using the minimum pressure, Michel, van Driest & Blumer and AHD criterion. The corresponding parameter sets used for the calculations are identical to the ones given in tables 6.1, 6.2, 6.3 and 6.4. The CFL number is set to 7.5. For all calculations employing the SST k-ω turbulence model, the CFL number has to be reduced to 3.5 and 1.5 at $\alpha = 12°$ and $14°$ for numerical stability.

Minimum pressure criterion

Calculated transition onset positions using the minimum pressure criterion are shown in figure A.14, comparing the investigated turbulence models. As can be seen, the turbulence models' influence on the prediction quality of the minimum pressure criterion is very small. The location of onset varies by maximum 4% chord length. Convergence of the density residual and transition location is benign for all investigated turbulence models up to $\alpha = 10°$.

Minor oscillations occur at $\alpha > 12°$ using the Spalart-Allmaras and SST k-ω turbulence models.

In general, the most stable convergence behaviour was obtained using the Baldwin-Lomax or Wilcox k-ω turbulence model, even at high angles of attack.

Michel criterion

The transition onset locations for the Michel criterion [18] in combination with the investigated turbulence models are given in figure A.15. The criterion's prediction quality is almost unaffected by the investigated turbulence models up to $\alpha = 8°$. Within this range, onset differences among the computations are below 2% chord length. Convergence of the density residual and transition onset location is benign for all turbulence models up to $\alpha = 12°$.

Recalling the prediction strategy used for the validation computation of the Michel criterion (see chapter 6.1.2), the detection of laminar separation points is again favoured for $\alpha > 8°$. On the upper side, laminar separation points are detected 6-8% more downstream of chord using the Baldwin-Lomax and SST k-ω model, compared to the Spalart-Allmaras and Wilcox k-ω computations. On the lower side, laminar separation can not be detected at $\alpha = 14°$ using the Wilcox k-ω model. Oscillations of the onset locations occur for the SST k-ω turbulence model at $\alpha = 14°$.

For the Michel criterion the best prediction quality together with non oscillating convergence behaviour, especially at high angles of attack, is achieved with the Baldwin-Lomax turbulence model.

van Driest & Blumer criterion

Figure A.16 presents the transition locations for the investigated turbulence models using the van Driest & Blumer criterion. The criterion's prediction quality is almost unaffected by the turbulence models up to $\alpha = 12°$. Differences in onset locations vary by maximum 4% chord length among the calculated results. Convergence of the density residual and transition location is benign for all turbulence models up to $\alpha = 10°$.

Concerning the Spalart-Allmaras, Wilcox k-ω and SST k-ω model, the relaxation factor is adjusted to 1.0 for $\alpha > 10°$ in order to obtain convergence of the transition location. Strong oscillations without convergence are only encountered at $\alpha = 14°$ for the SST k-ω model.

Concluding, the best prediction quality for the van Driest & Blumer criterion combined with stable convergence behaviour is obtained with the Baldwin-Lomax or Wilcox k-ω turbulence model, especially for high angles of attack.

AHD criterion

Transition locations predicted with the AHD criterion are shown in figure A.17, comparing the investigated turbulence models. The AHD criterion's prediction results are nearly unaffected by the use of different turbulence models, with maximum differences of just 2% chord length up to $\alpha = 12°$. For all turbulence models, convergence of the density residual and transition location is benign up to $\alpha = 12°$.

For the Wilcox k-ω model, slight oscillations of the onset location occur on the lower side at $\alpha = 14°$. This is due to an alternation between the AHD and laminar separation criterion. For the SST k-ω model, strong oscillations set in for $\alpha = 14°$, preventing onset convergence on the lower side. The same holds true for the Spalart-Allmaras model.

In summary, the AHD criterion's prediction and convergence behaviour was very stable using the Baldwin-Lomax and Wilcox k-ω model, especially at high angles of attack.

6.1.6 Conclusion

Among the empirical criteria, the AHD criterion features the best applicability for the Somers testcase. With an average offset for the transition location of 4% chord length in upstream direction, it is in good agreement to the experimental data. Thus, it is more accurate than the minimum pressure (upstream by 15%) and van Driest & Blumer criterion (upstream by 8%), while comparable to the Michel criterion (upstream by 3%). The AHD criterion's convergence behaviour is good, with a more robust detection behaviour at high angles of attack compared to the Michel criterion.

The prediction accuracy of the individual empirical criteria shows no significant dependence on the investigated range of turbulence models for the Somers testcase. Con-

Option	Setting	FLOWer parameter	Value
Stagnation point detection	c_p-max	TRACSTAGMETH	1
Relaxation	none	TRACSTAGMETH	1.0
Prediction frequency	user specified	TRACFREQ	250
Laminar zone thickness	user specified	TRACTHICKN	30

Table 6.5: FLOWer parameter for transition prediction on CAST10 airfoil using the minimum pressure criterion.

vergence is stable for all investigated turbulence models up to $\alpha = 12°$. The choice of turbulence models mainly affects the convergence behaviour at angles of attack higher than $\alpha = 12°$. With respect to the AHD criterion, the Baldwin-Lomax and Wilcox k-ω turbulence models proof to give stable prediction and convergence behaviour over the whole range of angles of attack.

For completeness, it should be mentioned that the influence of the grid resolution on the criteria's prediction quality has been investigated in [16] for the Somers testcase ($\alpha = 0.01°$). Results for grids with 336x72, 448x128 and 896x256 points have been compared, with approximately 30, 40 and 70 points in the laminar boundary layer. For the AHD criterion in combination with the Thwaites approximation, the location of transition onset has been found to be almost independed of the grid resolution. The same holds true for the Michel and minimum pressure criterion. Strong influence was observed for the van Driest & Blumer criterion.

6.2 CAST 10 airfoil

For the CAST10 testcase computations, a two block (C-H) mesh with a total of approximately 41.400 grid points is used (see figure B.1). The first block represents the airfoil, using 107 points in wall normal direction and 357 points in tangential direction. The boundary layer is resolved with approximately 20 points. The second block models the blunt trailing edge with 61 points along the edge and 51 points in the wake.

Mach number is $M = 0.73$ for a Reynolds number of $Re = 3.9 \cdot 10^6$ with $T_i = 293K$ at an angle of attack of $\alpha = -0.25°$. The external turbulence level in the wind tunnel is equal to $Tu = 0.001$. This setup corresponds to the experimental conditions for natural transition conditions discribed in [8]. The Wilcox k-ω turbulence model is used for all computations.

Transition prediction will be called at intervalls of 250 cycles.

6.2.1 Minimum pressure

As first case, transition onset is evaluated with the minimum pressure criterion. Table 6.5 summarizes the transition prediction parameter used for the computation.

The convergence history of the density residual as well as lift and drag coefficient is shown in figure B.2. The density residual decreases progressively, bringing the coefficients to

a level state. The activation of the transition prediction introduces initial disturbances to the flow solution which diminish after five prediction steps (1300 iterations). Initial convergence rate of the densitiy residual equals the rate of the fully turbulent calculation. From iteration cycle 4500 on, residual convergence starts to osciallate in a periodic pattern, recurring every 1000 iterations. This periodic behaviour is reflected in the curves of the coefficients for lift and drag. The influence of the present laminar flow regions on the coefficients can still be seen. The drag coefficient decreases by approximately 6% while the lift coefficient increases by 7%.

Looking at figure B.3 the reason for the oscillation can be found in an oscillation of the transition onset itself on the airfoil's upper side. Transition onset is detected initially at 13% of chord, slowly shifting in downstream direction for the next five prediction steps to 20% chord length. Here, a sudden shift in upstream direction occurs, back to the initally detected position of 13% chord. During the remaining prediction steps this behaviour repeats at an intervall of four prediction steps. Onset on the airfoil's lower side remains constant, located near the leading edge. This is due to a suction peak near the leading edge, resulting from the negative angle of attack (see figure B.4). This peak is detected by the minimum pressure criterion as transition onset point through the prediction process.

The airfoil's computed pressure distribution and laminar / turbulent flag LTFLAG are shown in figure B.4. For comparison, the experimental pressure distribution and onset locations from [8] are included.
Looking at the airfoil's upper side, the transition onset is predicted at the shock position, upstream of the measured transition position by 28% chord length. For the lower side, the predicted transition onset is located at a suction peak, 60% chord upstream compared to the experimental position.
In summary, the minimum pressure criterion is not suited to model transtion onset for the CAST10 airfoil test case. On the airfoil's upper side, an oscillation of transition onset occures, possibly to an interaction of the minimum pressure criterion and the shock position. On the lower side, a suction peak at the leading edge prevents the minimum pressure criterion from finding a transition onset position located further downstream.

6.2.2 Michel

As second case, the Michel criterion [18] is used for transition prediction. Momentum thickness is approximated according to Thwaites [22]. Table 6.6 summarizes the transition parameter used for the computation with activated transition prediction.

Figure B.5 shows the convergence history for the density residual as well as for the lift and drag coefficients. Convergence behaviour of the coefficients is very good as the residual decreases steadily during the fully turbulent computation. With the coefficients converged, a restart with activated transition prediction is done. The activation initially results in a distubance of the coefficients before they converge again after 3000 iterations, which equals 12 prediction steps. The density residual decreases progressively. With the introduction of laminar flow regions, the drag coefficient decreases by 30%, the lift coefficient increases by 9%.

Figure B.6 shows the convergence of the predicted transition locations using the Michel criterion. For the aifoil's upper side, the onset position is initially located at the trailing

Option	Setting	FLOWer parameter	Value
Stagnation point detection	c_p-max	TRACSTAGMETH	1
Relaxation	moderate	TRACRELAX	0.5
Prediction frequency	user specified	TRACFREQ	250
Laminar zone thickness	user specified	TRACTHICKN	30
Calculation of δ_2	Thwaites approximation	TRATHWAITES(1)	1.0

Table 6.6: FLOWer parameter for transition prediction on CAST10 airfoil using the Michel criterion.

Option	Setting	FLOWer parameter	Value
Stagnation point detection	flow reversal + c_p-max	TRACSTAGMETH	2
Relaxation	moderate	TRACRELAX	0.5
Prediction frequency	user specified	TRACFREQ	250
Laminar zone thickness	user specified	TRACTHICKN	41

Table 6.7: FLOWer parameter for transition prediction on CAST10 airfoil using the van Driest & Blumer criterion.

edge. During the next two prediction steps, laminar separation points are detected at approximately 65% chord length. The onset position smoothly shifts in upstream direction, converging after ten prediction steps at 23% chord length.
On the airfoil's lower side, laminar separation is detected during the second prediction step at 56 % chord length. The position is held constant during the remaining prediction steps. This behaviour indicates the use of strong relaxation in upstream direction (as explaind in chapter 5.5). The Michel criterion is prevented from abruptly changing the transition location more than 30% chord length in upstream direction between predition steps, since in this case a relaxation factor of 0.3 is used.

A comparison between the experimental [8] and computed transition locations and pressure distributions is given in figure B.7. On the airfoil's upper side, the transition position detected by the Michel criterion is located at the position of the shock. This location is upstream of the experimental position by 24% chord length. On the lower side, transition onset is detected downstream of the global pressure minimum at 56% chord length, detected by the laminar separation criterion. The predicted onset is in close proximity to the experimentally determined position, differing by 6% in upstream direction. While the comparison with experiment for the airfoil's lower side is satisfying, the result on the upper side is in fair agreement with experiment.

6.2.3 van Driest & Blumer

During the third case, transition prediction is done with the help of the van Driest & Blumer criterion. Boundary layer thickness is determined according to Stock & Haase, as presented in chapter 5.3. Table 6.7 summarizes the settings used for the transition prediction process.

Option	Setting	FLOWer parameter	Value
Stagnation point detection	flow reversal + c_p-max	TRACSTAGMETH	2
Relaxation	moderate	TRACRELAX	0.3
Prediction frequency	user specified	TRACFREQ	250
Laminar zone thickness	user specified	TRACTHICKN	30
Calculation of δ_1	integral	-	-
Calculation of δ_2	Thwaites	TRATHWAITES(1)	1.0

Table 6.8: FLOWer parameter for transition prediction on CAST10 airfoil using the AHD criterion.

The convergence behaviour of the density residual and the coefficients is shown in figure B.8. A restart with activated transition prediction, performed after 2700 iteration, initially disturbs the converged state of the lift and drag coefficient. This influence calms after 2500 iterations (10 prediction steps). The density residual decreases rapidly, resulting in good convergence of the coefficients. Due to the laminar flow regions, the drag coefficient decreases by 23% while the lift coefficient slightly increases by 9%.

The convergence behaviour of transition positions predicted by the van Driest & Blumer criterion is shown in figure B.9. On the airfoil's upper side, a laminar separation point is detected at the trailing edge, travelling in upstream direction during the first three prediction steps. Transition onset is then detected by the van Driest & Blumer criterion and smoothly converges in upstream direction to a position of 25% chord length. For the lower side, a laminar separation point is detected near the trailing edge at 81% chord length at the first prediction step. During the second prediction step, a more upstream located onset is predicted by the criterion, followed again by a laminar separation point. The onset position detected by the van Driest & Blumer criterion converges in upstream direction after nine steps at 39% chord length.

A comparison between the computed and experimental pressure distribution and onset locations is given in figure B.10. The predicted transition onset on the airfoil's upper side is located downstream of the first pressure minimum, 16% upstream of the experimental location. On the lower side the predicted onset is located slightly ahead of the global pressure minimum, resulting in a 23% upstream difference to the experimental location. For the CAST10 testcase, transition locations detected by the van Driest & Blumer criterion show a robust convergence behaviour and are in fair agreement with the experimental data.

6.2.4 AHD

As fourth case, the AHD criterion was used for the prediction of transition onset. The momentum thickness is approximated according to Thwaites [22], the displacement thickness is used in integral form. The parameters used for the transition prediction process are summarized in table 6.8.

As can be seen in figure B.11, convergence behaviour with activated transition prediction is good after the restart at iteration cycle 2700. The influence of transition prediction

process causes initial perturbations of the coefficients. After 3500 iteration cycles (12 prediction steps), the coefficients converge and residual density decreases progressively. The laminar flow region decreases the drag coefficient by 29%, the lift coefficient increases by 8%.

The history of the predicted transition onsets on upper and lower side is given in figure B.12. On the airfoil's upper side, the second and third predicted onset is found to be a laminar separation point. Transition onset developes smoothly from the trailing edge in upstream direction, converging at 26% chord. On the lower side, transition onset shifts from an initial trailing edge position to a laminar separation point at 56% chord length during the second prediction step. This location is held constant throughout the remaining prediction steps. This behaviour indicates the use of a relaxation mechanism preventing abrupt, large upstream shifts between predition steps (see chapter 5.5). Transition onset detected by the AHD criterion, is located more than 30% chord length upstream of the laminar separation position. To avoid conflicting transition onset points, the relaxation method preserves the laminar separation location as onset point.

A comparison of the predicted and experimentally measured transition onset positions is shown in figure B.13. Transition onset on the airfoil's upper side is predicted by the AHD criterion at the end of the first positive pressure gradient, upstream of the experiment's location by 20% of chord. On the lower side, transition onset is predicted downstream of the pressure minimum, using the laminar separation criterion. The onset is located upstream of the experiment's location by 6% chord length. Transition prediction for the lower side is in good agreement with experiment, while the onset position on the upper side shows fair agreement.

6.2.5 Conclusion

For the CAST10 airfoil testcase, differences between calculated and experimentally measured pressure distribution show on the upper side. The computed pressure distribution shows a more adverse pressure gradient, generally favouring an earlier transition onset. Agreement of the pressure distribution on the lower side is good though. This circumstance has been previously observed in [8] and should be taken into account when comparing the predicted and measured onset locations.

On the airfoil's lower side, onset is best predicted by laminar separation resulting in good agreement to experimental data (6% chord length offset in upstream direction). This is accomplished by using a restrictive underrelaxation factor (see table 6.8).

On the airfoil's upper side, Michel, van Driest & Blumer as well as AHD show a moderate offset to the experimental data (20% chord length in upstream direction). This can be attributed to the previously mentioned difference in calculated and experimental pressure distribution. The predicted onset is physically feasible though in the context of the computed pressure distribution.

The convergence behaviour was stable during the employed prediction strategy.

The minimum pressure criterion proofs as not suited for the CAST10 testcase, since it detects onset too early on the lower side. This is due to a suction peak near the leading edge, resulting from the negative angle of attack. Slight onset oscillations can be observed

on the upper side.

7 Verification test case - ONERA 7A rotor

To test and verify the transition prediction method of chapter 5 for a hovering rotor, the ONERA 7A rotor testcase is used. Since no experimental data with respect to transition onset is available in the literature for the 7A rotor, the test computations are compared to ONERA results [5]. The ONERA results are based on an Euler code coupled to a boundary layer code (WAVES/MI3DI). Inside the MI3DI boundary layer code, the AHD criterion is used for transition prediction due to longitudinal instabilities [3]. The ONERA approach has been succesfully validated for a Dauphin rotor at hover [4].

For the FLOWer computation, an analytically generated six block mesh is used, as shown in figure C.1. Each block consists of a C mesh with 177 points in wall tangential direction, 65 in wall normal direction and, 13 points in spanwise direction. The boundary layer is resolved by approximately 20 grid points. The C meshes are lined up in radial direction of the rotor blade and add to a total of 897.390 grid points. The computational domain houses one rotor blade and covers an azimuthal section of $90°$, modelling the four bladed layout of the 7A rotor. Periodic boundary conditions are defined at the azimuthal block faces. The boundary condition at the root cutout is set to Euler slip wall condition. Far field boundary conditions with characteristic variables are used at the inlet, outlet and outer radial face of the computational domain.

Tip mach number is $M_{tip} = 0.617$ at a Reynolds number of $Re = 1.93 \cdot 10^6$. Geometric angle of attack at 70% rotor radius is $\Theta_c = 11.3°$. The SST-kω turbulence model is used for the computation.

The prodecure for transition prediction is divided into two steps:

1. a fully turbulent computation (full multigrid) over 4500 cycles to converge the thrust and power coefficients;

2. a restart (simple multigrid) with activated transition prediction and laminar initialization over 3750 cycles;

Transition prediction will be performed at intervalls of 250 cycles.

For prediction, the empirical cirteria according to the minimum pressure, Michel, van Driest & Blumer and AHD criterion will be used.

Option	Setting	FLOWer parameter	Value
Stagnation point detection	c_p-max	TRACSTAGMETH	1
Relaxation	none	TRACRELAX	1.0
Prediction frequency	user specified	TRACFREQ	250
Laminar zone thickness	user specified	TRACTHICKN	41

Table 7.1: FLOWer parameter used for transition prediction on ONERA 7A rotor using the minimum pressure criterion.

7.1 Minimum pressure

The first case for transition prediction on the 7A rotor uses the minimum pressure criterion. No boundary layer parameters have to be evaluated. Table 7.1 summarizes the FLOWer transition prediction parameter used for the computation.

The convergence history of the density residual, thrust and power coefficient is shown in figure C.2. After a restart with activated transition prediction from iteration 4.500, an initial deflection of the thrust and power coefficient can be observed, flattening after approximately 1.000 iterations. The coefficients then converge to a constant level. The density residual reduces progressively without oscillations during the complete transition prediction process. After the last prediction step, the power coefficient shows a minor decrease of 2% compared to the fully turbulent value while the thrust coefficient remains practically unchanged.

The initially detected transition onset positions remain very stable throughout the prediction process, as shown in figure C.3 for selected prediction steps. On the upper side, a small laminar band at the blade's tip can be observed to change to a fully turbulent state. The lower side shows no changes between prediction steps.

The constant position of transition onset indicates a stable pressure distribution along the blade's surface during the computation. Pressure distributions at selected airfoil sections are shown in figure C.4. As can be seen from the LTFLAG distribution, the minimum pressure criterion reliably detects the suction peak at the section's upper side and the pressure minimum located near the trailing edge of the lower side as transition onset point.

Globally, transition onset detected by the minimum pressure criterion starts at 10% chord on the rotor's upper side and on 75% on the lower side, as can be seen in C.5.
Taking a closer look at the blades upper side, transition onset follows an almost linear distribution along the leading edge, running from the cutout to approximately 80% rotor radius. For the remaining span onwards to the rotor tip, the laminar running length decreases, which corresponds to the locally increasing Reynolds number. The tip is fully turbulent.

On the blade's lower surface, transition onset follows a line parallel to the trailing edge up to approximately 85% rotor radius. The remaining span to the tip shows a slight increase of laminar running length. The rotor tip shows transitional and turbulent flow areas.

A comparison of the achieved results to an Euler/boundary layer computation (WAVES/MI3DI) for the 7A rotor is given in C.5.

Option	Setting	FLOWer parameter	Value
Stagnation point detection	c_p-max	TRACSTAGMETH	1
Relaxation	none	TRACRELAX	1.0
Prediction frequency	user specified	TRACFREQ	250
Laminar zone thickness	user specified	TRACTHICKN	41
Calculation of δ_2	Thwaites approximation	TRATHWAITES(1)	1.0

Table 7.2: FLOWer parameter used for transition prediction on ONERA 7A rotor using the Michel criterion.

As can be observed, the minimum pressure criterion closely captures the trend of the WAVES/MI3DI computation. For the upper side, the results indicate a slightly more upstream location of transition onset. Decrease of laminar running length with rotor radius is indicated 14% earlier.
On the lower side, transition onset is predicted slightly upstream of the WAVES/MI3DI computation, up to 75% rotor span. For the remaining span, the increase of laminar running length matches well with the WAVES/MI3DI computation.

7.2 Michel criterion

The Michel criterion [18] is used for the second case. The momentum thickness is approximated according to Thwaites [22]. The employed transition prediction parameter are given in table 7.2.

Figure C.6 shows the convergence history for the density residual, thrust and power coefficient. The computation with activated transition prediction starts at iteration cycle 4.500, initially introducing a disturbance to the coefficients. The disturbance flattens after 1.000 iteration cycles. Looking at the power coefficient, a mild oscillation sets in, repeating every 500 iterations. The thrust coefficient shows minimal signs of oscillations. The density residual initially converges progressively after the restart, then changing into small oscillations with peaks every 250 iterations, indicating the execution of prediction steps. The thrust and power coefficients' decrease against the turbulent solution differs by 1%.

The development of laminar and turbulent flow regions between selected prediction steps is shown in figure C.7. The blades upper side, shows a stable, linearily decreasing laminar running length towards the rotor tip. This distribution is superimposed by the build up of two larger laminar areas. The first one developes edgewise along the rotor cutout to 35% rotor radius, the second forms a triangular shape at 75% rotor radius.
The blades lower side is completely covered by a fully laminar flow throughout all prediction steps, with the exception of two turbulent spots near the tip's trailing edge. For the remaining blade, no transition onset is found by the Michel or laminar separation criterion, which sets the transition onset point to the trailing edge position.

Figure C.8 shows the pressure and LTFLAG distribution at selected airfoil sections at the end of the prediction process.
When looking at the blade's upper side, transition onset is detected downstream of the suction peak. The downstream distance is strongly reduced near the blade's tip and shifts

Option	Setting	FLOWer parameter	Value
Stagnation point detection	c_p-max	TRACSTAGMETH	1
Relaxation	none	TRACRELAX	1.0
Prediction frequency	user specified	TRACFREQ	250
Laminar zone thickness	user specified	TRACTHICKN	41
Calculation of δ_2	Thwaites approximation	TRATHWAITES(1)	1.0
Michel, factor	-	TRAMICHEL(1)	1.174
Michel, exponent	-	TRAMICHEL(2)	0.46

Table 7.3: FLOWer parameter used for transition prediction on ONERA 7A rotor using the Michel criterion (version 1952) [19].

towards the pressure minimum. On the rotor blades lower side, no transition onset location can be found, as indicated by the LTFLAG distribution. Thus, the onset point is set to the trailing edge initializing the lower side to fully laminar.

For completeness of the discussion, a comparison between the transition onset positions using the Michel criterion and former results using an Euler/boundary layer code (WAVES/MI3DI) is presented in figure C.9.
Examining the blade's upper side between 35% and 75% rotor radius, the predicted transition onset is located donwstream of the WAVES/MI3DI results, showing a light linear dependency with increasing rotor radius. From the cutout to 35% radius, deviation of the onset distribution is large in downstream direction. The same holds true for the triangular laminar area at 75% rotor radius.
On the blade's lower side, the flow is set to fully laminar. With respect to the WAVES/MI3DI results, the laminar running length is overestimated for the complete rotor span.

7.3 Michel criterion (version 1952)

A computation with the version of the Michel criterion as published 1952 in [19] is done in order to further investigate the transition detection behaviour. The momentum thickness is approximated according to Thwaites [22]. Table 7.3 summarizes the FLOWer transition prediction parameter used for the computation.

Figure C.10 shows the convergence history for the density residual, thrust and power coefficient. The execution of the first transition prediction step at 4.750 iterations introduces a small disturbance to the thrust and power coefficient. The disturbance of the coefficient flattens after 1.500 iterations, this equals six prediction steps. Compared to the fully turbulent value, the power coefficient decreases by 1%, as does the thrust coefficient. The density residual decreases progressively during the computation with activated transition prediction procedure.

The development of laminar and turbulent flow regions between selected prediction steps is shown in figure C.11. The blade's upper surface, shows a stable LTFLAG distribution throughout the prediction steps. The laminar running length decreases linearily towards the rotor tip. Minimal shifts of transition onset can be observed near the blade's tip.

Option	Setting	FLOWer parameter	Value
Stagnation point detection	c_p-max	TRACSTAGMETH	1
Relaxation	moderate	TRACRELAX	1.0
Prediction frequency	user specified	TRACFREQ	250
Laminar zone thickness	user specified	TRACTHICKN	41

Table 7.4: FLOWer parameter used for transition prediction on ONERA 7A rotor using the van Driest & Blumer criterion.

The blades lower side is mainly covered by a fully laminar flow throughout all prediction steps. This is due to the fact that no transition onset is found by the Michel or laminar separation criterion, setting the transition onset to the trailing edge. The only exception present two turbulent areas near the tip's trailing edge.

Figure C.12 shows the pressure and LTFLAG distribution at selected airfoil sections at the end of the prediction process.
Looking at the blade's upper side, transition onset is detected downstream of the suction peak. The distance between the suction peak and transition onset location reduces lineary with increasing rotor radius. Near the blade's tip, transition onset coincides with the pressure minimum.
On the blade's lower side, no transition onset location can be found, as indicated by the LTFLAG distribution. Thus, the onset point is set to the trailing edge, initializing the lower side to fully laminar.

A comparison between the transition onset positions using the Michel criterion and an Euler/boundary layer code (WAVES/MI3DI) is shown in figure C.13.
Examining the blade's upper side, the predicted transition onset is located donwstream of the WAVES/MI3DI results, showing a linear dependency in increasing radial direction, up to 85% rotor radius. From 85% radius outwards, the laminar running length strongly decreases.
On the blade's lower side, the flow is set to fully laminar. With respect to the WAVES/MI3DI results, the laminar running length is overestimated for the complete rotor span.

7.4 van Driest & Blumer criterion

For the third case, the van Driest & Blumer criterion is used as transition onset criterion. The boundary layer thickness is analyzed according to Stock & Haase [21]. The transition prediction parameter used for the computation are shown in table 7.4.

During the prediction process, the thrust and power coefficient converge to their initially fully turbulent state, with only minor disturbances during the first 850 iteration cycles of the prediction process. This can be seen in figure C.14. The overall change of the thrust and power coefficient is below 1%, which is surprisingly small. Convergence behaviour of the density residual however is benign and very stable.

The convergence behaviour of the transition onset distribution over the rotor blade is shown in figure C.15.

For the upper side, the onset distribution is very stable during the prediction process. Very small shifts occur near the rotor tip at 83% rotor radius onwards.
On the lower side, a major movement of transtion onset in upstream direction evolves over the prediction process. During the first step, a smooth distribution of transition onset is predicted, mainly parallel to the trailing edge. This distribution shifts in upstream direction, until the ninth prediction step is reached, at iteration cycle 6.500, and then remains constant. Hereby, a kink in the onset distribution forms at 32% radial span near the cutout and persists during the remaining computation. From 72% rotor radius on, the transition onset distribution developes in an slightly S-shaped curve, decreasing the laminar running length near the rotor tip from almost full laminar to half turbulent.

It can be seen from figure C.16, that the onset positions for the blade's upper side, as represented by the LTFLAG distribution, are located slightly downstream to the position of the suction peaks.
On the lower side, it is worthwile noting, that transition onset is predicted upstream of the minimum pressure location near the trailing edge. The van Driest & Blumer criterion accounts for pressure gradient and free-stream turbulence effects [1]. Since the negative pressure gradient on the pressure side is weaker than on the suction side, the influence of free stream turbulence seems to become dominant and induces a more upstream detection. The pressure distribution remains globally constant throughout the prediction process, as was observed during the calculations with the minimum pressure criterion (see chapter 7.1). This explains the constant onset distribution on the upper side.

A comparison between the calculated onset distribution and former results from an Euler/boundary layer code computation (WAVES/MI3DI) is given in C.17. On the blade's upper side, the matching of the onset distrbution is very good. From 80% rotor radius outwards, the decrease of laminar running length developes more clearly.
On the lower side, the onset distribution predicted by the van Driest & Blumer criterion differs apparently from the WAVES/MI3DI solution. Generally, onset is located approximately 20% more upstream. A kink near the cutout forms, which is not present in the former distribution. While the trend of constant transition onset distribution is fairly captured, the degradation of laminar running length near the rotor tip differs from the WAVES/MI3DI results.

7.5 AHD criterion

As fourth case, transition onset is evaluated using the AHD criterion. The momentum thickness is approximated according to Thwaites [22], the displacement thickness is derived as integral parameter from the flow solution. Table 7.5 summarizes the FLOWer transition prediction parameter used for the computation.

Figure C.18 shows the convergence history for the density residual, thrust and power coefficient. With the activation of transition prediction at iteration cycle 4.500, the coefficients show an initial deviation from the fully turbulent solution. After 1.000 iteration cycles, the coefficents converge again to a constant level. The reduction of thrust and power coefficient are below 1%. Throughout the predicition process, the density residual decreases continually.

Option	Setting	FLOWer parameter	Value
Stagnation point detection	c_p-max	TRACSTAGMETH	1
Relaxation	moderate	TRACRELAX	1.0
Prediction frequency	user specified	TRACFREQ	250
Laminar zone thickness	user specified	TRACTHICKN	41
Calculation of δ_1	integral	-	-
Calculation of δ_2	Thwaites approximation	TRATHWAITES(1)	1.0

Table 7.5: FLOWer parameter used for transition prediction on ONERA 7A rotor using the AHD criterion.

As indicated by the steady characteristic of the density residual during activated transition prediction, the development of transition onset locations shows a globally constant behaviour, as can be seen in figure C.19. The blade's upper side shows a constant LTFLAG distribution with minimal onset shifts at 80% rotor radius and near the tip at 95%.
On the lower side, the LTFLAG distribution remains globally stable. Minor shifts of the transition onset near the trailing edge can be observed along the rotor radius. At the tip, a small band, initially turbulent, developes to a completely laminar flow.

Figure C.20 shows chordwise pressure distributions at selected airfoil sections, representing the flow solution at the last transition prediction step. The extent of laminar flow areas is indicated by the LTFLAG distribution. For the blade's upper side, the onset positions are located slightly downstream of the pressure minimum. With increasing rotor radius, the onset position shifts towards the pressure minimum, reducing the laminar running length. On the lower side, transition onset is predicted at the pressure minimum near the trailing edge. This is the case for all presented rotor sections along the radius.

As can be seen in figure C.21, transition onset for the upper side is globally located at approximately 20% chord, while on the lower side the onset is located at 80% chord. Looking at the upper side, the laminar running length decreases almost lineary from approximately 40% chord at the rotor cutout to a fully turbulent flow at the rotor tip. At 85% radius an intensifying decrease of laminar running length sets in.
On the lower side, transition onset runs parallel to the trailing edge until 84% rotor radius, showing a slight variation of laminar running lengths. For the remaining distance to the rotor tip, the laminar running length increasingly expands in downstream direction. The tip is characterized by turbulent flow.

Figure C.21 compares the FLOWer results obtained for the 7A rotor using the AHD criterion to an Euler/boundary layer computation (WAVES/MI3DI). In summary, the LTFLAG distribution on upper and lower side matches the onset distribution of the WAVES/MI3DI computation very well. This can be expected since the ONERA results have also been obtained with the AHD criterion. For the blade's upper side, the laminar running lengths dependency on radial Reynolds number is slightly more developed. A stronger degradation of the laminar running length near the tip can be observed, possibly to 3D flow effects.

7.6 Conclusion

For the ONERA 7A rotor hover testcase, the AHD criterion shows the best applicability among the investigated criteria. The criterion's predicted transition positions matches very well with positions derived using WAVES/MI3DI [5], which also employs the AHD criterion. The WAVES/MI3DI method serves as reference since it has been succesfully validated against experimental transition data on a Dauphin rotor at hover [4]. The AHD criterion featured reliable transition onset detection on both upper and lower side of the blade. The convergence behaviour of the density residual was stable.

The minimum pressure criterion can be seen as an robust alternative with good prediction accuracy, though neglecting the influence of freestream turbulence.

The Michel criterion does not detect transition onset on the blade's lower side. On the upper side, accordance with the WAVE/MI3DI results can only be obtained using the parameter set of Michel (version 1952) [19].

For the van Driest & Blumer criterion, agreement with the WAVES/MI3DI results is good on the blade's upper side. On the lower side however, onset is predicted ahead of the pressure minimum, indicating a high sensitivity of the criterion to freestream turbulence.

8 Application - INROS rotor (reference design)

The transition prediction method is tested with a recent rotor design, representative for industrial applications. As testcase, the INROS reference rotor under hovering conditions is used.

The grid has been generated by EUROCOPTER Deutschland with respect to the CHIMERA technique (see figure D.2). It consists of one child grid, representing the blade's geometry, and a background grid, covering a section of 72° azimuth to represent the five bladed layout.
The child grid consists of 20 blocks with a total of 1 million grid points. The blade's airfoil sections are modeled with 137 points in wall tangential direction and 33 points in wall normal direction. The boundary layer is resolved with approximately 10 grid points. Figure D.1 shows the surface grid.
The background grid features six blocks with a total of 2.2 million grid points. Periodic boundary conditions are defined at the azimuthal block faces. Far field boundary conditions with characteristic variables are used at the inlet, outlet and outer radial face of the computational domain. The inner radial face is defined as EULER slip wall.
Tip mach number is $M_{tip} = 0.588$ for a Reynolds number of $Re = 4.15 \cdot 10^6$. The Wilcox kω turbulence model with modified parameters is used for the computations.

Two different approaches will be tested for transition prediction:

- Approach 1 - prediction based on a fully turbulent solution;
- Approach 2 - immediate prediction without fully turbulent solution;

In the first case, a fully turbulent calculation is performed to bring the coefficients to convergence and subsequently do a restart with activated transition prediction. This represents the approach as used in chapters 6 and 7.

In the second case, an approach is chosen in order to reduce the computational effort. Transition prediction will be activated immediately from the start of a computation, without performing of a fully turbulent calculation in advance.

For transition prediction the AHD criterion is chosen for all computations, because it shows good agreement to experimental data of the Somers airfoil and a robust onset detection behaviour (see chapter 6). The criterion has been succesfully validated for a Dauphin rotor at hover in combination with WAVES/MI3DI [4]. FLOWer verification computations with the AHD criterion for the ONERA 7A rotor testcase were in very good accordance to ONERA results (see chapter 7.5). The momentum thickness is approximated according to

Option	Setting	FLOWer parameter	Value
Stagnation point detection	c_p-max	TRACSTAGMETH	1
Relaxation	none	TRACRELAX	1.0
Prediction frequency	user specified	TRACFREQ	200
Laminar zone thickness	user specified	TRACTHICKN	15
Calculation of δ_1	integral	-	-
Calculation of δ_2	Thwaites approximation	TRATHWAITES(1)	1.0

Table 8.1: FLOWer parameter for transition prediction on INROS rotor (reference design) using the AHD criterion.

Thwaites [22], the displacement thickness is derived as integral parameter from the flow solution.

Table 8.1 summarizes the FLOWer transition prediction parameter used for all computations of the following chapters.

To test the prediction method over a broader range of pitch angles, a polar for the INROS rotor (reference design) is calculated. The influence of laminar/turbulent transition on performance prediction is clarified by comparison to fully turbulent results.

8.1 Prediction based on fully turbulent solution (AHD)

A fully turbulent computation is run over 20.600 iterations as single grid computation to converge the thrust and power coefficients The restart with activated transition prediction is is run for another 10.000 iteration cycles, with transition prediction steps activated every 200 iterations.

As can be observed from figure D.3, a reduction of the power coefficient by 3% sets in with activated prediction, due to the presence of laminar flow regions on the blade's surface. The lift coefficient experiences no change. Both coefficients remain constant throughout the remaining computation. Looking at the density residual, inital convergence rate is progressive for the first 1.000 iterations (5 prediction steps). Having reached a level of 10^{-3}, oscillations start to show at a frequency of 200 iteration cycles, which equals the prediction frequency.

The development of transition onset along the blade's upper and lower side is shown in figure D.4. For both sides, the distribution of transition onset is globally stable. Minimal changes occur near the root's upper side, where a closure between two laminar areas takes place. On the lower side, the development of a laminar area shows near the blade's tip.

Figure D.5 shows the blade's final transition onset in form of a LTFLAG distribution. Laminar running length is mainly 16% chord on the upper side, slightly decreasing with radial direction, and 84% chord on the lower side, slightly increasing towards the blade's tip. Near the root, transition onset is detected in the form of laminar separation close to the trailing edge. The onset extendes in radial direction up to $r/R = 8\%$ on the upper side and $r/R = 4\%$ on the lower side. For the remaining blade, onset is detected by the AHD

Activation	**Total iterations** [-]	c_T [-]	c_P [-]	FM [-]
Restart from fully turbulent solution	30.000	0.010036	0.000928	0.766
Immediate	14.000	0.010041	0.000930	0.765

Table 8.2: Comparison of thrust and power coefficients for two different activation points of transition prediction - INROS rotor (reference design), AHD criterion.

criterion, indicated by a sudden shift towards the leading edge. For the lower side, the laminar running length increases again in downstream direction after the shift. This is in accordance to the presence of a stabilizing (negative) pressure gradient. On the upper side, onset is generally located slightly downstream of the suction peak. With increasing radial direction, the onset shifts upstream towards the pressure minimum. Figure D.6 shows the pressure and LTFLAG distribution at selected radial sections.

8.2 Immediate prediction (AHD)

A computation with immediate transition prediction is run for 14.000 iterations. As before, prediction is executed every 200 iterations. Lift and thrust coefficient converge to a stable level, as shown in figure D.7.

When comparing the coefficients to the results obtained by starting from a fully turbulent calculation, as shown in table 8.2, they proof to be practical identical. The density residual reduces up to a level of 10^{-3}. Then, oscillations occur at a frequency of 200 iterations, resembling the prediction frequency. The oscillations persist throughout the remaining computations.

Looking at the curves of the thrust and power coefficient in figure D.7, a slight 'bump' can be recognized at iteration cycle 9.000, indicating a possible instationary disturbance during the solution process. Looking at figure D.8, one can recognize a major disturbance in transition onset near the blade's root at the same iteration cycles. This disturbance causes areas of laminar flow to diminish with progressing iteration number up to cycle 8.600. Then, turbulent flow regions develop back to laminar until the final state of the computation is reached. Due to the coincidence of the iteration cycles, the AHD criterion seems to reflect the phenomenon, which shows as 'bump' in the thrust and power coefficient. A possible explanation to this phenomenon is given in [15]. During hover computations using the CHIMERA technique, the influence of the blade's root vortex manifestes in a vortex 'fountain', rising in axial direction at the center of rotation. This fountain disturbs the downwash of the rotor flow field near the hub and hence decreases the thrust coefficient. This influence vanishes after approximately 5.000 iterations, resulting in an increased and stabilized thrust coefficient.

The transition onset distribution for the blade's upper and lower side after the final prediction step is shown in figure D.9. The related chordwise pressure and LTFLAG distribution is presented in figure D.10. These results are in accordance to the results obtained with a restart from a fully turbulent solution, as previously described in chapter 8.1. A difference in transition onset near the root can be explained because of the instationary disturbance

mentioned before. The disturbance proofs not to be relevant with respect to performance prediction when comparing the power and thrust coefficients of table 8.2.

8.3 Comparison between transitional (AHD) and turbulent results

The investigation of the previous chapter has shown, that performing a calculation with immediate transition predication yields identical results compared to prediction based on a restart from a fully turbulent calculation. Consequently, immediate prediction is used for the INROS rotor case to calculate the thrust and power coefficients for blade pitch angles in the range of $[-6°, -4°, -2°, 0°, 2°, 4°,$ and $5°]$. Table 8.1 shows the FLOWer transition parameters used for the calculations.

The convergence history for the density residuals as well as thrust coefficients is presented in figure D.11. For the positive pitch angles, 14.000 iteration cycles are necessary to converge the thrust coefficient on the finest grid level. The density residual decreases progressively until a level of 10^{-3}, then changing to a moderate oscillatory behaviour - similar to the charactistic described in chapter 8.2. For pitch angles of $4°$ and $5°$, minor oscillations can be observed for the thrust coefficients.
The negative pitch angles show a more progressive decrease of the density residual until a level of about 10^{-5} is reached. Then, small periodic osciallations start to show throughout the remaining computation. The convergence of the thrust coefficients is not affected and reaches a stable level.

In the following, characteristics for thrust, thrust to power and rotor efficiency are deduced from the computations and compared to fully turbulent results.

8.3.1 Thrust polar

The generated rotor thrust as a function of pitch angle is shown in figure D.12. A comparison to a fully turbulent solution is given, too. As can be seen, the presence of laminar flow areas has practically no influence on the thrust coefficient within the investigated range of pitch angles. Results of the thrust coefficient with and without transition are identical.
A linear behaviour of thrust with pitch can be observed in the range of $-6°$ to $2°$. For pitch angles of $4°$ and $5°$ the slope starts to flatten, possibly indicating the presence of separated flow at the blade due to the increased disc loading.

8.3.2 Thrust to power characteristic

The thrust / power characteristic of the INROS rotor is given in figure D.13. Compared to a fully turbulent solution, the curve representing transition prediction is slight shifted towards lower power coefficients. The power reduction is feasible considering the reduced skin friction coefficient within the present laminar flow areas. The reduction accounts for 6% and decreases with increasing power coefficient. The last two points to the right in

figure D.13, representing pitch angles of $4°$ and $5°$, almost coincide with the fully turbulent solution.

8.3.3 Rotor efficiency

Figure D.14 presents the efficiency for the INROS rotor (reference design) resulting from the calculation with activated transition prediction. A fully turbulent solution is included to clarify the impact of laminar flow regions on rotor performance prediction.
The curve representing the AHD criterion generally shows a similiar characterictic over pitch angles as the fully turbulent curve, but it is shifted towards higher rotor efficiency. This is reasonable recalling the improved thrust / power characteristic of figure D.13. For the far left points, representing pitch angles of $-6°$ and $-4°$, an efficiency increase of about 7% can be observed. The efficiency gain reduces with increasing pitch angle, until almost coinciding with the fully turbulent solution for the far right points, representing pitch angles of $4°$ and $5°$.
While the fully turbulent solution shows a strict linear efficiency decrease at high thrust coefficients, a slight kink can be observed for the curve, representing transition prediction. An explanation may be given by figure D.15, showing the distribution of laminar/turbulent flow regions of the blade for different pitch angles. For angles of $4°$ and $5°$, a sudden decrease of laminar running length at approximately $r/R = 0.9$ sets in, possibly causing the kink.

9 Conclusions

The work presented in this report covered the implementation, verification and validation of a method for transition prediction using empirical criteria in combination with the block structured flow solver FLOWer. Empirical criteria according to minimum pressure, laminar separation, Michel, van Driest & Blumer and Arnal, Habiballah & Delcourt (AHD) were used. The investigations focused on applications with respect to airfoils and rotary wings under stationary flow conditions.

Validation results have been shown for two testcases: the Somers airfoil at low mach number and the CAST10 airfoil at transsonic conditions.

The AHD criterion shows the best applicability among the investigated criteria for the Somers testcase, featuring good agreement to the experimental data (upstream by 4% chord), a robust onset detection, even at high angles of attack, and stable convergence behaviour. The minimum pressure criterion predicts transition onset with fair accuracy, at an average of 15% chord upstream to the experimental locations. Convergence behaviour was robust and the detection of the pressure minimum reliable. The Michel criterion predicts transition onset with very good accuracy (upstream by 3% chord). At angles of attack greater than $8°$, laminar separation points had to be favoured to avoid oscillations in the convergence behaviour. The criterion according to van Driest & Blumer yields good accuracy (upstream by 8% chord), with a robust behaviour over a wide range of angles of attack. The convergence behaviour was stable.
The empirical criteria's location of transition onset have not been found to be significantly influenced by turbulence models, including the Baldwin-Lomax, Spalart-Allmaras, Wilcox k-ω and SST k-ω models. The choice of turbulence models mainly affects the convergence behaviour at angles of attack higher than $\alpha = 12°$. Below $\alpha = 12°$, convergence is stable for all investigated turbulence models. For the AHD criterion, the Baldwin-Lomax and Wilcox k-ω models proof to give stable onset detection over the range of $\alpha = [-4°; 14°]$.

For the CAST10 airfoil testcase, differences between the calculated and experimentally measured pressure distribution show on the upper side, as previously observed in [8]. The computed pressure distribution shows a more adverse pressure gradient, generally favouring an earlier transition onset. Agreement of the pressure distribution on the lower side is good though. This circumstance has to be taken into account when comparing the predicted and measured onset locations.
On the airfoil's lower side, onset is best predicted by laminar separation, with good agreement to the experimental data (6% chord length offset in upstream direction). This is accomplished by using a restrictive underrelaxation behaviour. On the airfoil's upper side, Michel, van Driest & Blumer as well as AHD show a moderate offset to the experimental data (20% chord length in upstream direction). This upstream shift can be attributed to

the previoulsly mentioned difference in calculated and experimental pressure distribution. The computed onset is physically feasible though in the context of the computed pressure distribution. The minimum pressure criterion was not suited to predict transition onset for the CAST10 airfoil's lower side due to early activation by a small suction peak forming close to the leading edge.

To test and verify the FLOWer transition prediction method for a hovering rotor, the ONERA 7A rotor testcase is used. The FLOWer computations are compared to ONERA results [5], since no experimental data with respect to transition onset is available in the literature. The ONERA results are based on a coupling of an Euler and boundary layer code (WAVES/MI3DI), which has been succesfully validated for a Dauphin rotor at hover [4].
For the FLOWer computations of the ONERA 7A testcase, the AHD criterion shows the best applicability. The criterion's predicted transition positions matches very well with the ONERA results. The transition onset detection on both upper and lower side of the blade is reliable. The convergence behaviour of the density residual was stable.
The minimum pressure criterion proofs as a robust and simple alternative for transition prediction. The reliable detection of the minimum pressure location gives comparable onset locations to the ONERA results. The convergence behaviour is stable. The minimum pressure criterion does not account for possible effects of freestream turbulence though.
The Michel criterion does not detect transition onset on the blade's lower side, which results in a completely laminar flow. For the upper side, comparable onset locations to the ONERA results can only be achieved with a parameter set of the Michel criterion, as published 1952. The van Driest & Blumer criterion's results for the upper side match well compared to the ONERA results. Transition detection on the blade's lower side shows an upstream travelling characteristc. Thus, onset was located at a more upstream position, indicating a high sensitivity of the criterion to free-stream turbulence.

Finally, the transition prediciton method was applied to a recent rotor blade design in hover, representing an industrial application. Using the AHD criterion, the impact of transition on rotor performance prediction is clarified by comparison to fully turbulent calculations. An increase in figure of merit of up to 7% can be observed at low pitch angles. The power coefficient decreases by 6% due to the presence of laminar flow regions. The thrust coefficient remains unchanged. The positive effect of transition on figure of merit and power coefficient weakens to nearly fully turbulent values with increasing pitch angle. The AHD criterion captures the instationary flow behaviour near the blade's root.

10 Outlook

Based on the experiences gained during the verification and validation of the transition prediction method, the following topics have been identified as possible future developments:

- improved robustness of the boundary layer edge detection, especially in transitional and turbulent flow regions;
- compressibility correction for approximated boundary layer quantities;
- influence of integral evaluation of the boundary layer quantities on prediction accuracy;
- extension and application of the prediction method to instationary problems like oscillating airfoils and rotors in forward flight;
- application of sophisticated transition prediction methods in combination with linear stability codes;
- generation of experimental data for rotors at hover and forward flight conditions.

A brief comment to each of the above points is given.

Currently the boundary layer edge is detected according to a method by Stock & Haase [21]. This method proofed as reliable in the areas of laminar flow, which is necessary to correctly determine the boundary layer parameters for the empirical transition criteria. In transitional and turbulent flow regions, however, the method tended to detect the boundary layer edges too close to the no-slip walls (see chapter 5.3). This phenomenon occurs especially at high angles of attack. Alternative methods for boundary layer edge detection could be tried to improve detection robustness.

During the validation of the transsonic CAST10 testcase (see chapter 6.2), the transition onset locations detected by the Michel and AHD criterion showed fair agreement with experimental data. A compressibility correction for the approximated momentum and displacement thickness could provide a mean to improve the prediction quality of the (incompressible) empirical criteria at transsonic conditions.

As an alternative to compressibility corrections, the boundary layer parameters can be directly integrated from the flow solution in their compressible form to determine the momentum and displacement thickness. This approach requires meshes with sufficient resolution of the boundary layer thickness (70 points and more). The influence on the

prediction accuracy as well as grid dependency would be of interest during this investigation.

To enable transition prediction for a broader operational envelope of rotary wings, the prediction algorithm would have to be adapted and tested for instationary problems, like an oscillating airfoil and a rotor in forward flight. Due to the broad range of flow conditions encountered at even moderate advance ratios, the validity of incompressible empirical criteria would have to be questioned for such applications. A possible approach could be the coupling of the flow solver FLOWer to a linear stability code in combination with a more sophisticated transition prediction method, as for example the e^N method.

Regardless from the points above, it is essential to improve the knowledge of transition behaviour on rotary wings by experimental data, in both hovering and forward flight conditions, since reference in the literature is sparse. The experimental data should be understood as an vital element of gaining further confidence in the numerical results of transition prediction methods and will serve as a decisive guideline during the development and adaption of enhanced methods to rotary wing applications.

Acknowledgements

The author would like to thank Andreas Krumbein (DLR) for helpfull discussions and provision of the Somers and CAST10 airfoil test cases, Frederic LeChuiton (ECD) for the introduction to the transition prediction implementation of the FLOWer code, Manfred Imiela (DLR) for provision of the ONERA 7A rotor grid and Andree Altmikus (ECD) for provision of the INROS rotor grid. Further thanks go to Jochen Raddatz (DLR) and Normann Krimmelbein (DLR) for very helpfull discussions.

Bibliography

[1] ARNAL, D.: *Description and prediction of transition in two-dimensional, incompressible flow*. AGARD Report No 709, Toulouse Cedex, 1984

[2] ARNAL, D.: *Three-dimensional boundary layers: laminar-turbulent transition*. AGARD Report No 741, Toulouse Cedex, 1987

[3] BEAUMIER, P., HOUDEVILLE R.: *3D laminar-turbulent boundary layer calculations on helicopter rotors in forward flight: application to drag prediction*. 21st European Rotorcraft Forum, Saint-Petersburg, August 30th - September 1st, 1995

[4] BEAUMIER, P., CASTELLIN, C., ARNAUD, G.: *Performance prediction and flowfield analysis of rotors in hover, using a coupled Euler/boundary layer method*. 24th European Rotorcraft Forum, Marseilles, France, 1998

[5] BEAUMIER, P., CHELLI E., PAHLKE, K.: *Navier-Stokes prediction of helicopter rotor performance in hover including aero-elastic effects*. 56th Annual Forum, American Helicopter Society, Virginia Beach, United States, 2000

[6] CLIQUET, J., HOUDEVILLE, R., ARNAL, D.: *Application of laminar-turbulent transition criteria in Navier-Stokes computations*. 45th AIAA Aerospace Sciences Meeting and Exhibit, Reno, Nevada, United States, 2007

[7] FLOWER: *Manual for FLOWer transition features*. Institut für Aerodynamik und Strömungstechnik, Deutsches Zentrum für Luft- und Raumfahrt, 2009

[8] GARTEUR AD(AG35): *Application of Transition Criteria in Navier Stokes Computations*. Group For Aeronautical Research And Technology In Europe, GARTEUR/TP-137, 2003

[9] HILL, J.L, SHAW, S.T., QIN, N.: *Engineering prediction of laminar/turbulent transition for isolated helicopter rotors in hover*. RAeS Aerospace Aerodynamics Resource Conference, London, 2004

[10] KROLL, N., ROSSOW, C. C., SCHWAMBORN, D., BECKER, K., HELLER, G.: *MEGAFLOW - a numerical flow simulation tool for transport aircraft design*. 23rd International congress of the aeronautical sciences, Toronto, 2002

[11] KROLL, N., FASSBENDER, J.K. (EDS.): *MEGAFLOW - Numerical Flow Simulation for Aircraft Design*. Notes on Numerical Fluid Mechanics and Multidisciplinary Design, Volume 89, Springer, 2005

[12] KROLL, N., BECKER, K., RIEGER, H., THIELE, F.: *Ongoing activities in flow simulation and shape optimization within the german MEGADESIGN project*. 25th International congress of the aeronautical sciences, Hamburg, 2006

[13] KRUMBEIN, A.: *Automatic transition prediction and application to 3D wing configurations*. Journal of Aircraft, Volume 3, 2007

[14] LEISHMAN, J.G.: *Principles of Helicopter Aerodynamics*. Cambridge University Press, 2nd edition, New York, 2006

[15] MACK, A.: *Nutzung der Chimera-Technik für wirbelbehaftete Strömungen*. Diplomarbeit am Institut für Entwurfsaerodynamik, DLR, Braunschweig, 1999

[16] MATSUDA, N.: *Anwendung und Validierung empirischer Umschlagskriterien in FLOWer*. Diplomarbeit am Institut für Aerodynamik und Gasdynamik, Universität Stuttgart, 2009

[17] MCCROSKEY, W. J.: *Measurements of boundary layer transition, separation and streamline direction on rotating blades*. NASA Technical Note, NASA TN D-6321, Washington, 1971

[18] MICHEL, R.: *Etude de la transition sur les profils d'aile; Etablissement d'un critere de determination du point de transition et calcul da la trainee de profil incompressible*. Technical Report, ONERA, Report1/1578A, 1951

[19] MICHEL, R.: *Determination du point de transition et calcul de la trainee des profiles d'ailes en incompressible*. ONERA, 1952

[20] SOMERS, D.A.: *Design and experimental results for a natural laminar flow airfoil for general aviation applications*. NASA Technical Paper 1861, Scientific and technical information branch, 1981

[21] STOCK, H.W., HAASE, W.: *Feasibility-Study of e^N Transition Prediction in Navier-Stokes Methods for Airfoils*. AIAA, Vol. 37, No. 10, p.1187-1196, 1999

[22] THWAITES, B.: *Approximate calculation of the laminar boundary layer*. Aeron. Quarterly, Vol.1, 1949

[23] VAN DRIEST, E.R., BLUMER, C.B.: *Boundary Layer Transition: Freestream Turbulence and Pressure Gradient Effects*. AIAA-J, Vol. 1 / No. 6, 1963

[24] WALZ, A.: *Strömungs- und Temperaturgrenzschichten*. Bestell-Nr. 4241, Verlag G. Braun, Karlsruhe, 1966

A Figures - Somers testcase

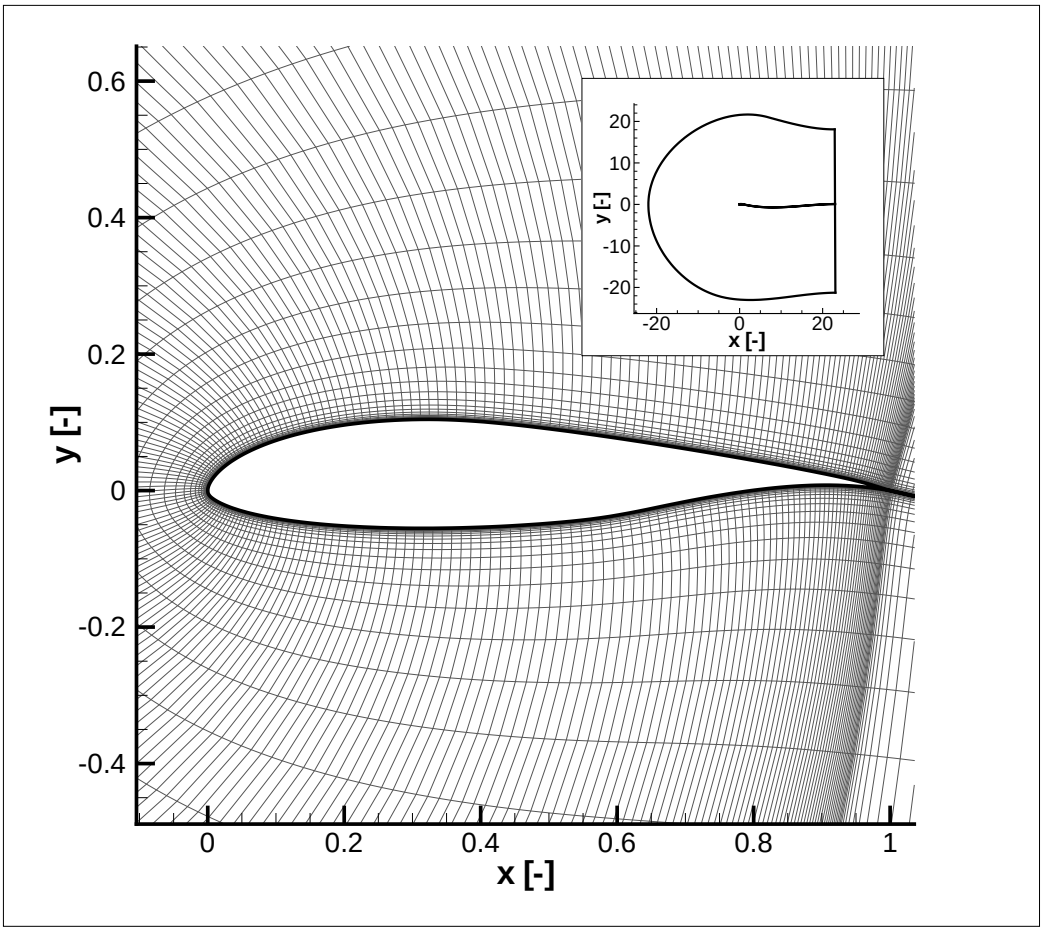

Figure A.1: Somers airfoil - computational grid.

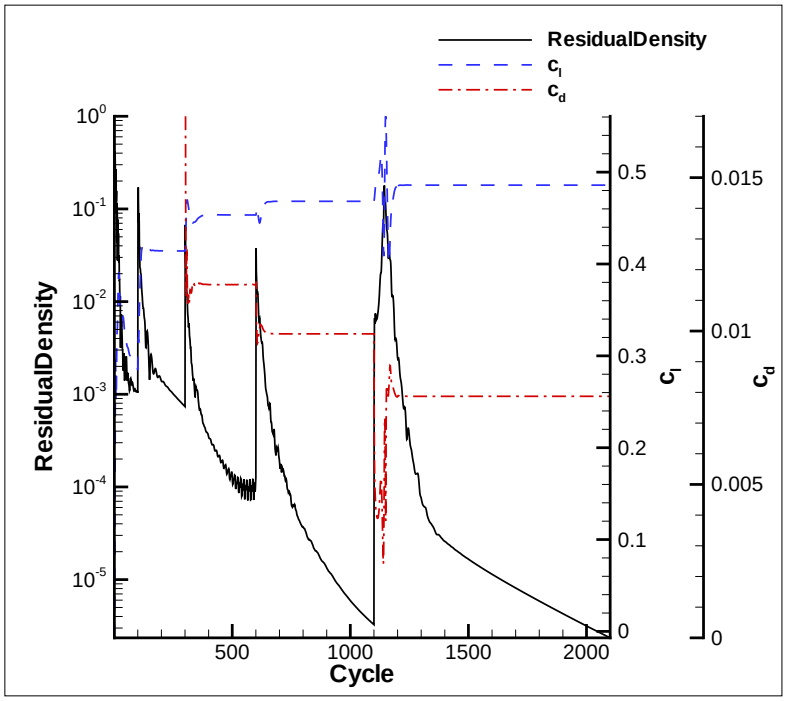

Figure A.2: Somers airfoil - convergence history for the density residual, lift and drag coefficient using the minimum pressure criterion for $\alpha = 0$.

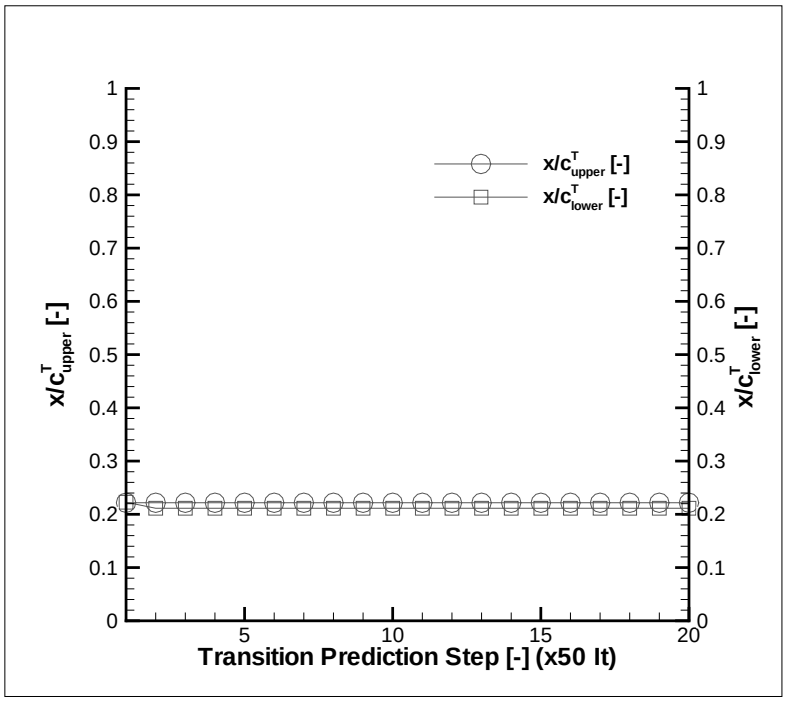

Figure A.3: Somers airfoil - convergence of the predicted transition locations using the minimum pressure criterion for $\alpha = 0$.

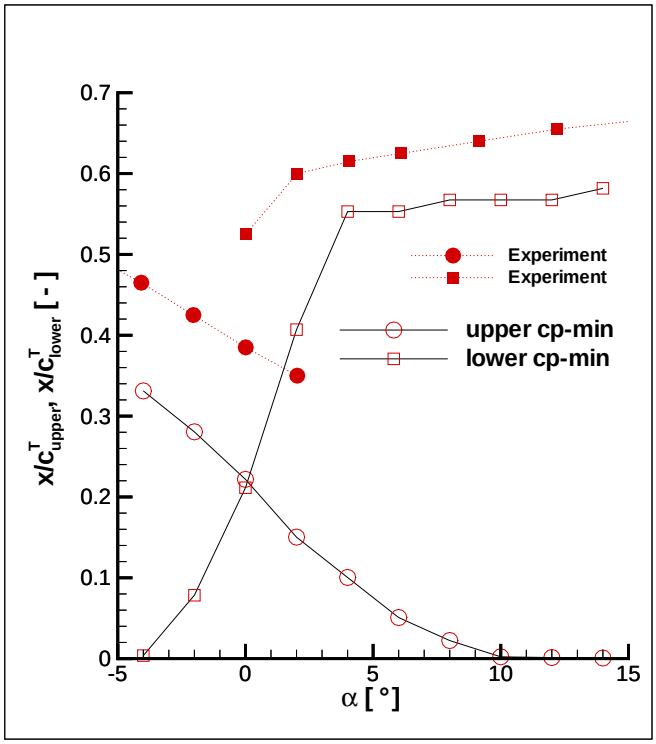

Figure A.4: Somers airfoil - experimental and computed transition locations using the c_p-min criterion.

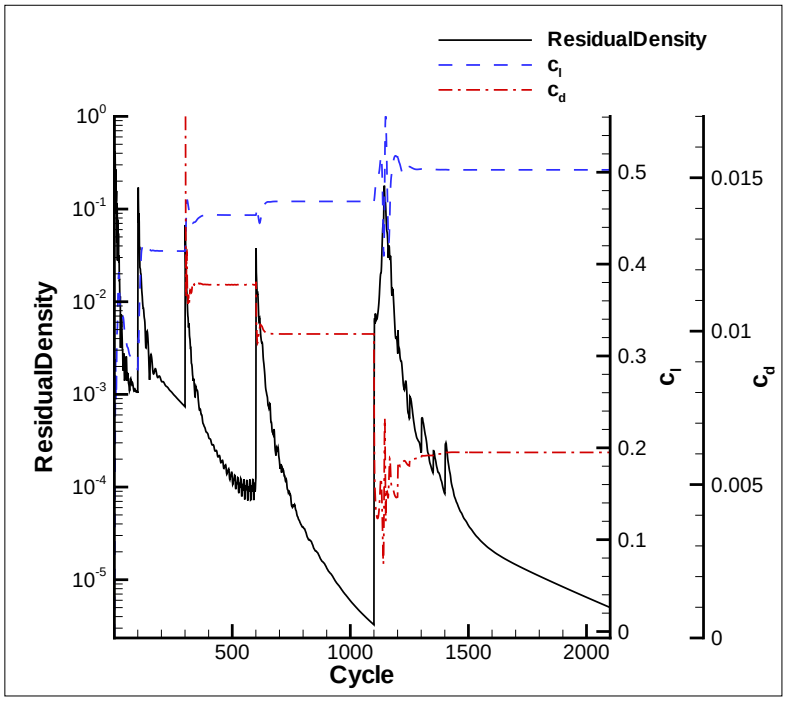

Figure A.5: Somers airfoil - convergence history for the density residual, lift and drag coefficient using the Michel criterion for $\alpha = 0$.

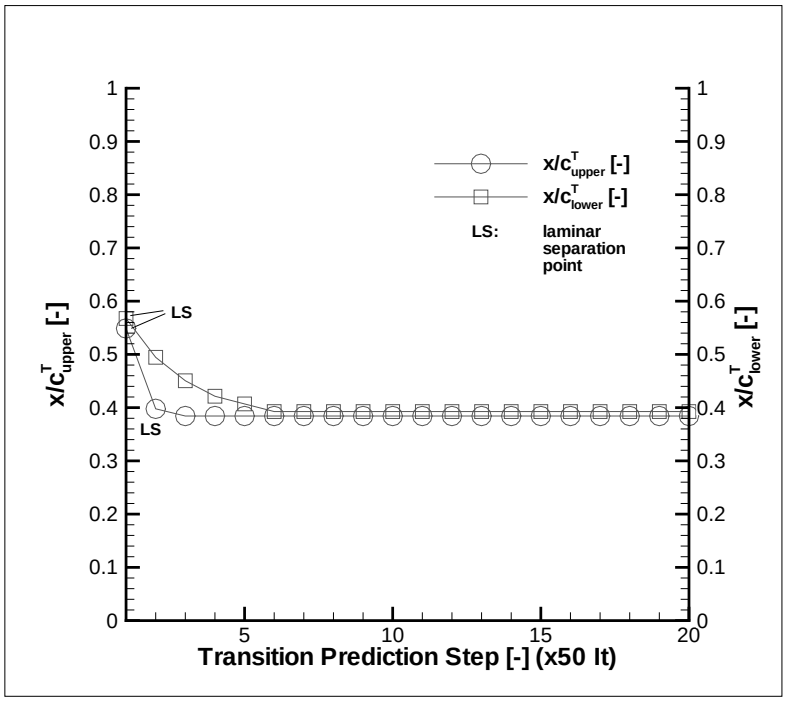

Figure A.6: Somers airfoil - convergence of the predicted transition locations using the Michel criterion for $\alpha = 0$.

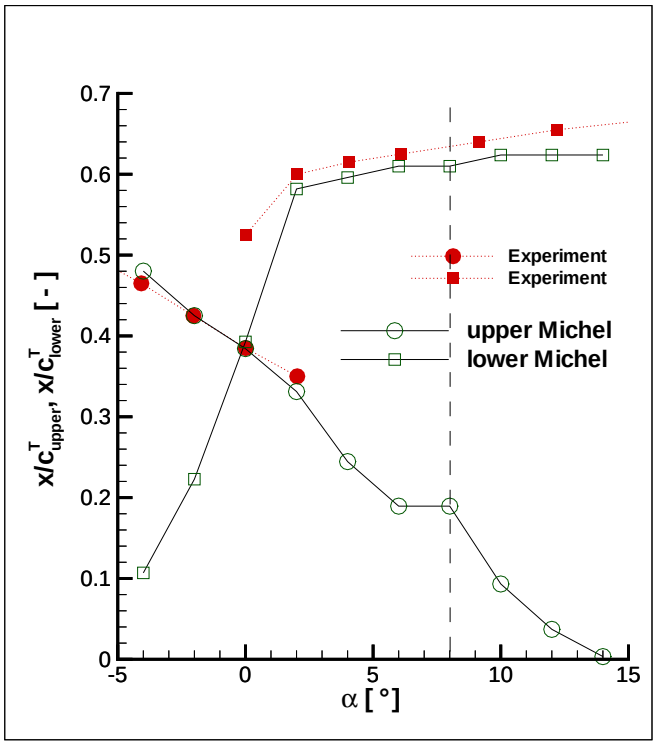

Figure A.7: Somers airfoil - experimental and computed transition locations using the Michel criterion; from $\alpha = 8°$ on, transition onset is detected by laminar separation.

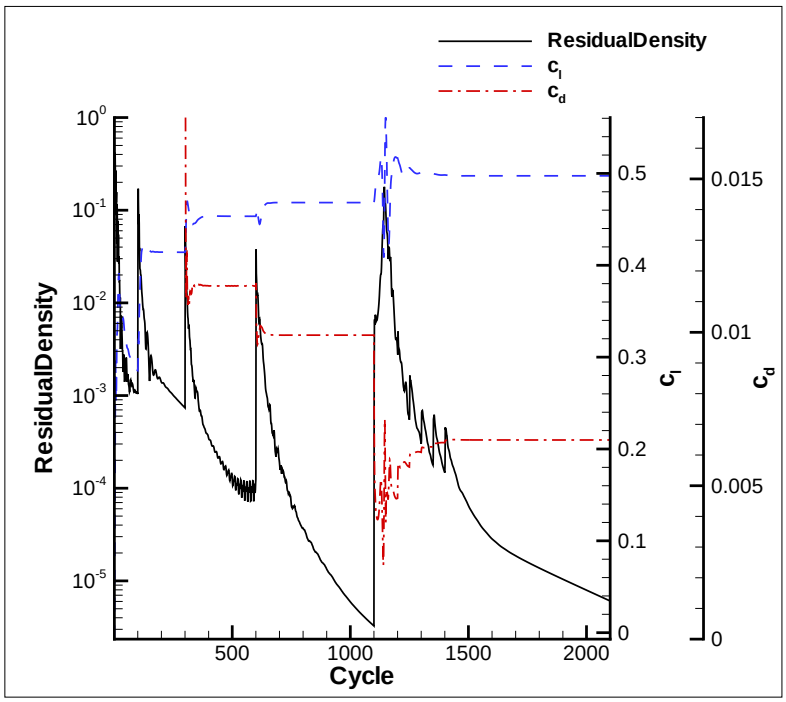

Figure A.8: Somers airfoil - convergence history for the density residual, lift and drag coefficient using the van Driest & Blumer criterion for $\alpha = 0$.

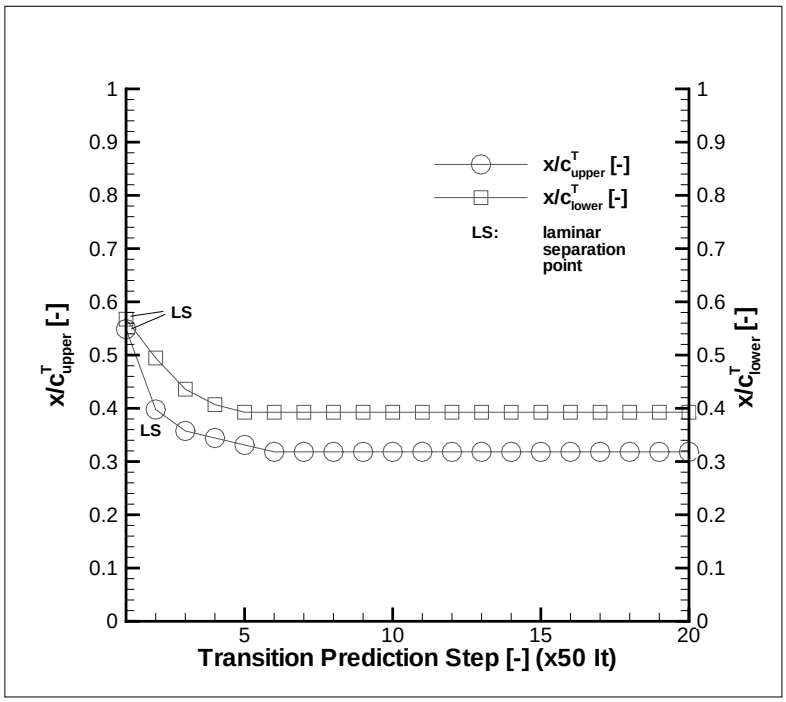

Figure A.9: Somers airfoil - convergence of the predicted transition locations using the van Driest & Blumer criterion for $\alpha = 0$.

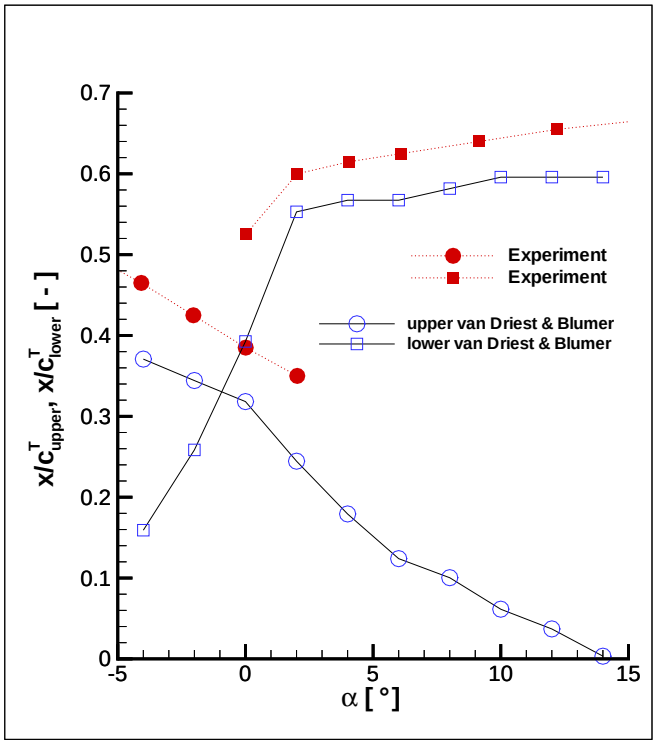

Figure A.10: Somers airfoil - experimental and computed transition locations using the van Driest & Blumer criterion.

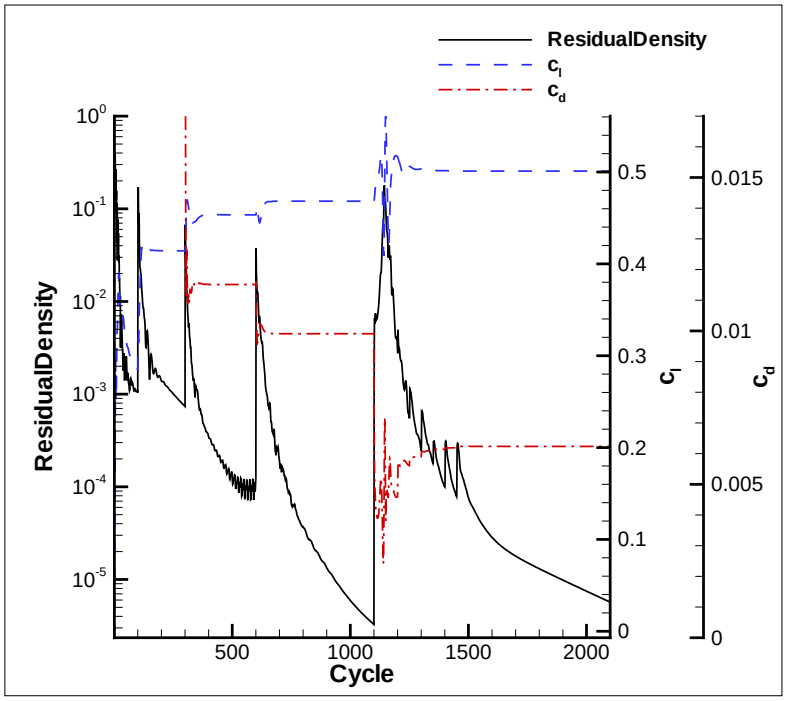

Figure A.11: Somers airfoil - convergence history for the density residual, lift and drag coefficient using the AHD criterion for $\alpha = 0$.

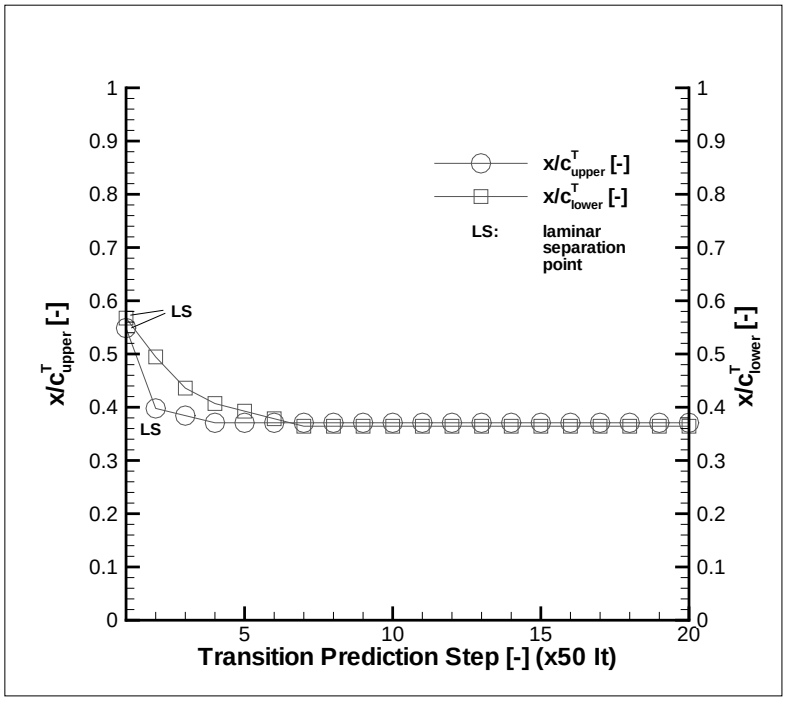

Figure A.12: Somers airfoil - convergence of the predicted transition locations using the AHD criterion for $\alpha = 0$.

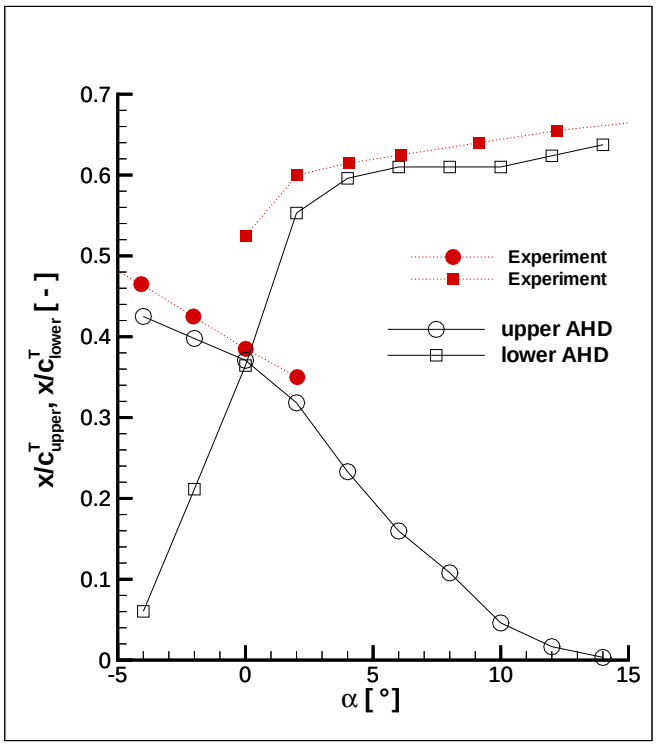

Figure A.13: Somers airfoil - experimental and computed transition locations using the AHD criterion.

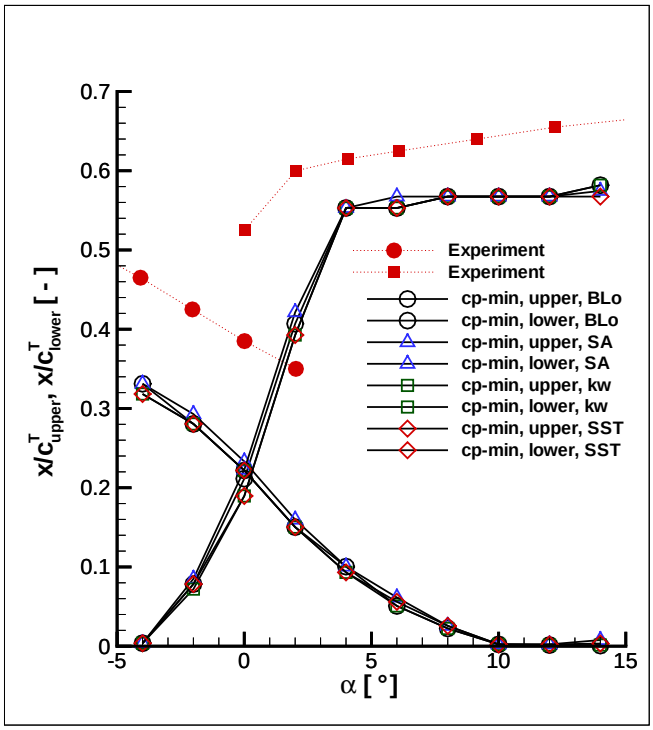

Figure A.14: Somers airfoil - experimental and computed transition locations using the minimum pressure criterion in combination with the Baldwin-Lomax, Spalart-Allmaras, Wilcox k-ω and SST k-ω turbulence models.

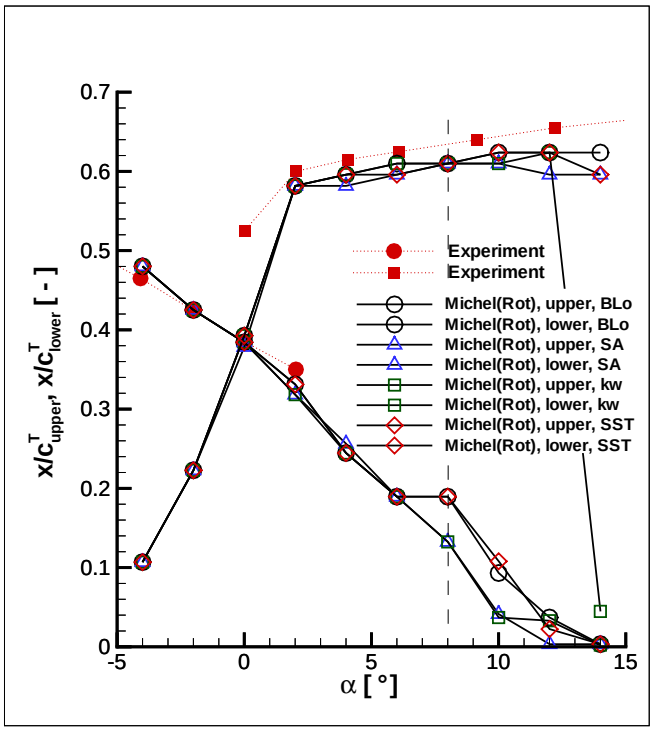

Figure A.15: Somers airfoil - experimental and computed transition locations using the Michel criterion in combination with the Baldwin-Lomax, Spalart-Allmaras, Wilcox k-ω and SST k-ω turbulence models.

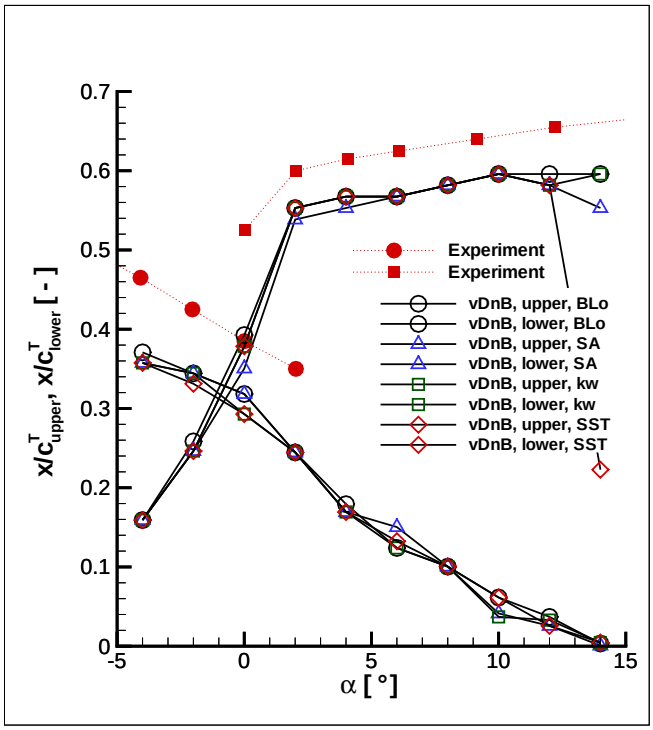

Figure A.16: Somers airfoil - experimental and computed transition locations using the van Driest & Blumer criterion in combination with the Baldwin-Lomax, Spalart-Allmaras, Wilcox k-ω and SST k-ω turbulence models.

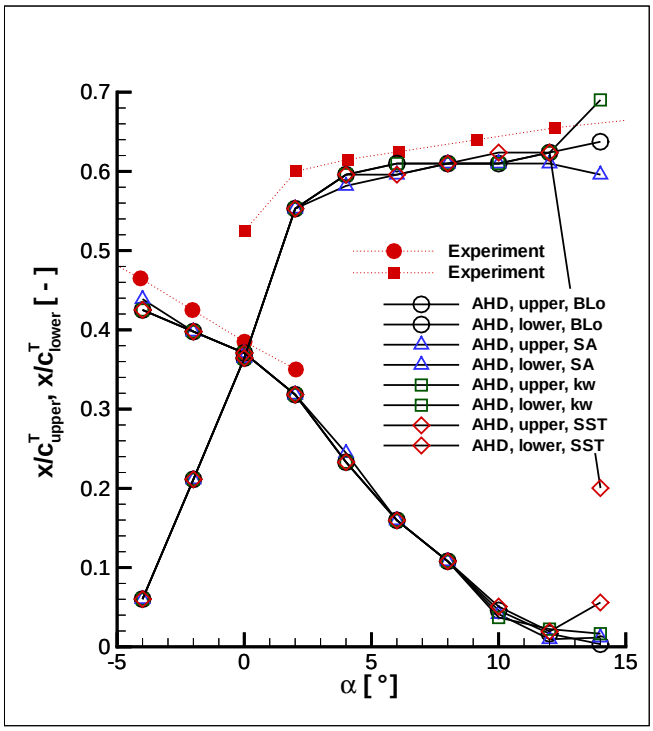

Figure A.17: Somers airfoil - experimental and computed transition locations using the AHD criterion in combination with the Baldwin-Lomax, Spalart-Allmaras, Wilcox k-ω and SST k-ω turbulence models.

B Figures - CAST10 testcase

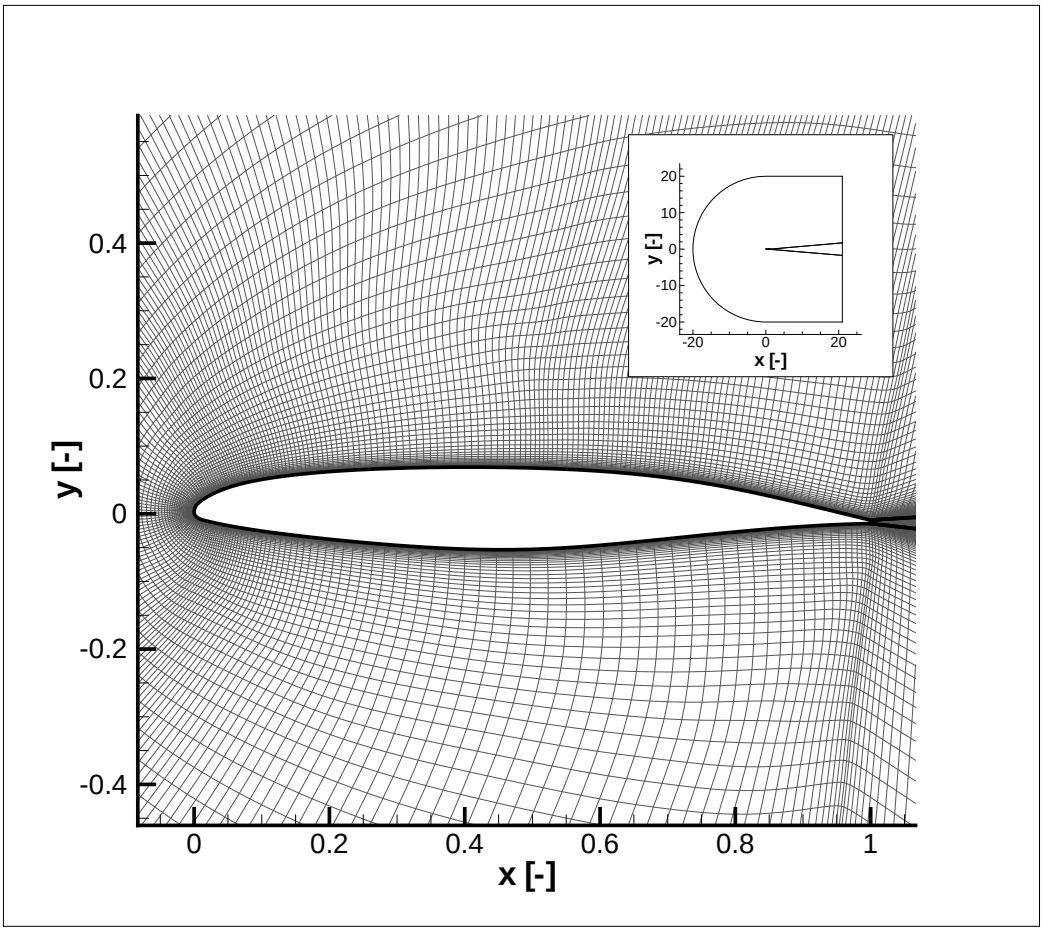

Figure B.1: CAST10 airfoil - computational grid.

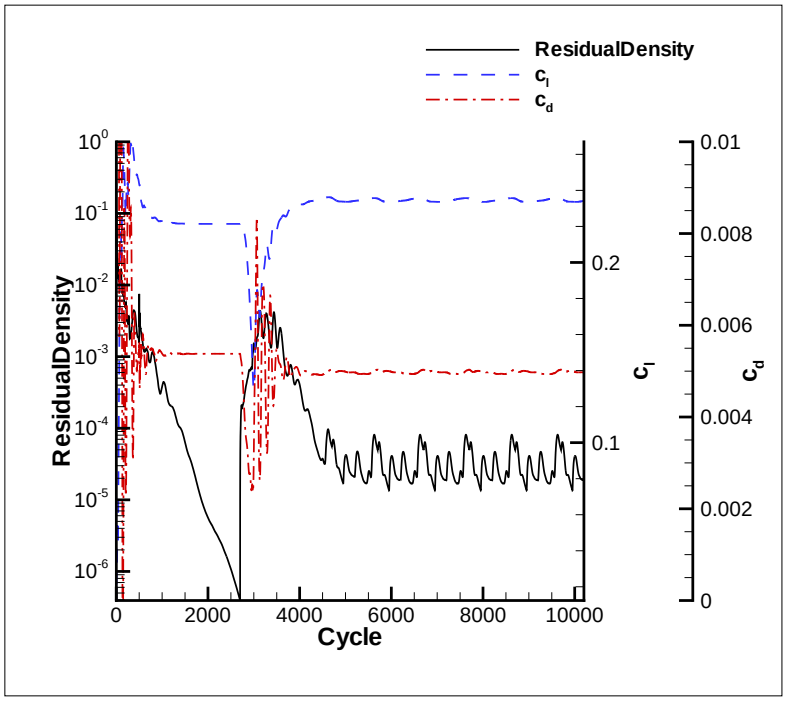

Figure B.2: CAST10 airfoil - convergence history for the density residual, lift and drag coefficient using the minimum pressure criterion for $\alpha = -0.25°$.

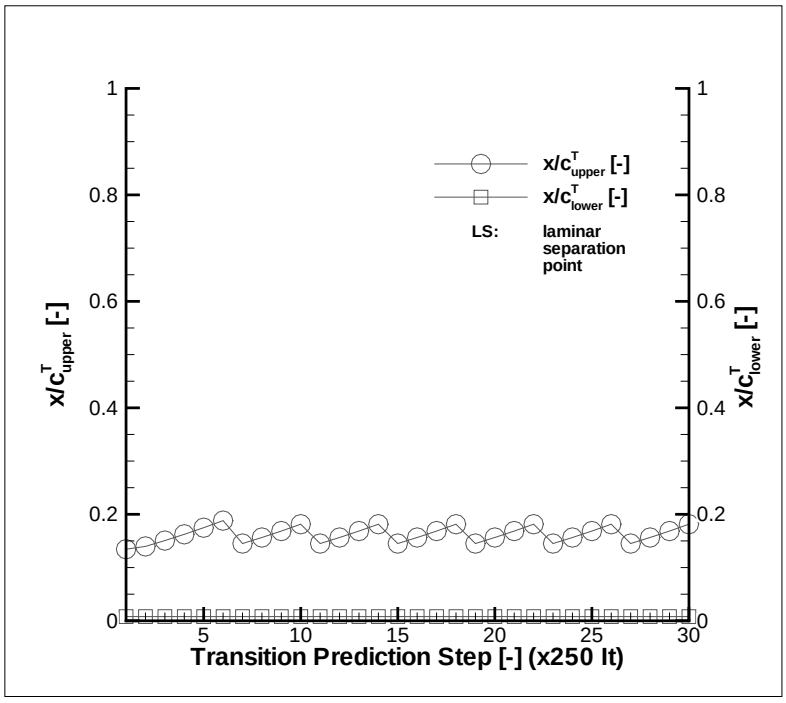

Figure B.3: CAST10 airfoil - convergence of the predicted transition locations using the minimum pressure criterion for $\alpha = -0.25°$.

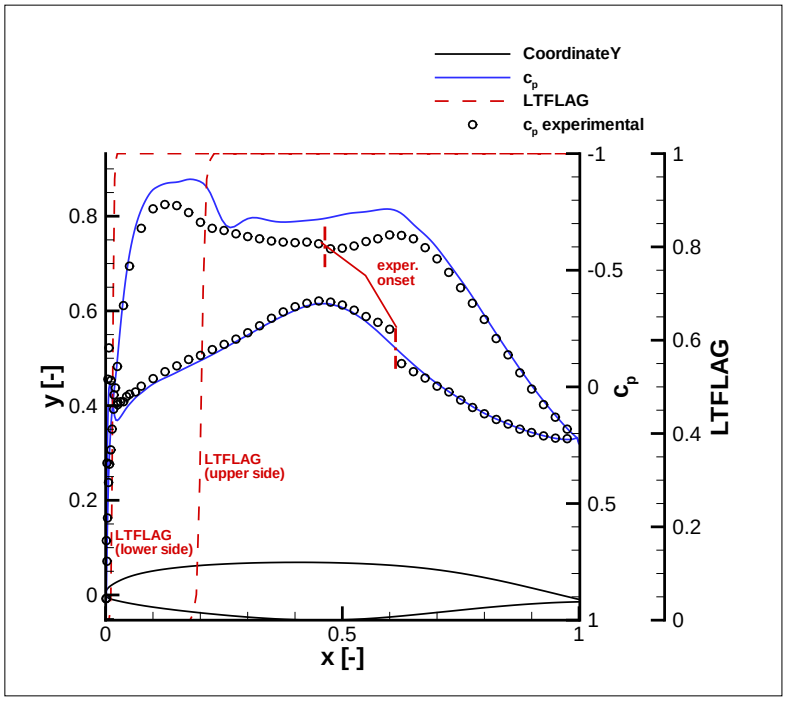

Figure B.4: CAST10 airfoil - pressure distribution and chordwise LTFLAG status with comparison to experimental data (minimum pressure criterion).

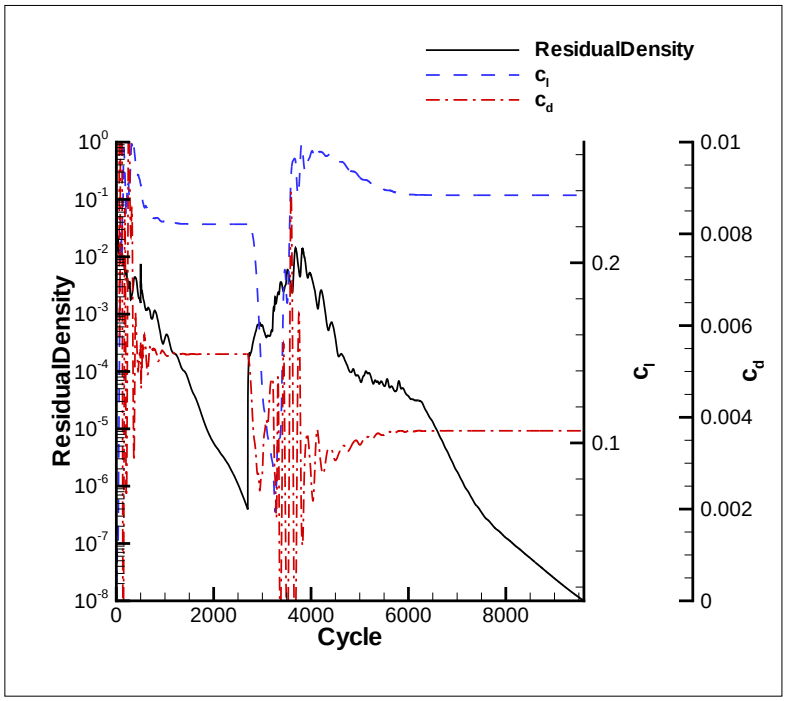

Figure B.5: CAST10 airfoil - convergence history for the density residual, lift and drag coefficient using the Michel criterion for $\alpha = -0.25°$.

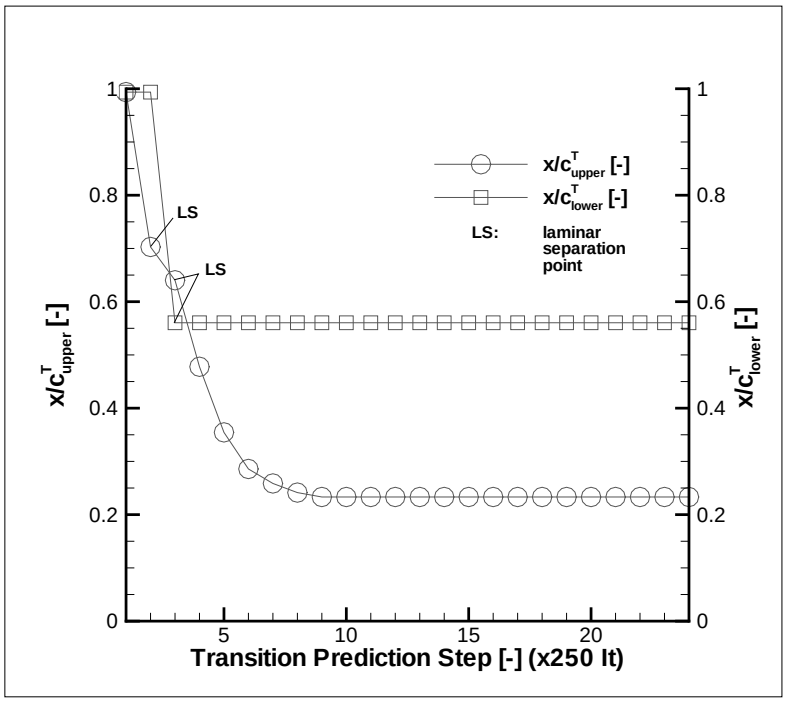

Figure B.6: CAST10 airfoil - convergence of the predicted transition locations using the Michel criterion for $\alpha = -0.25°$.

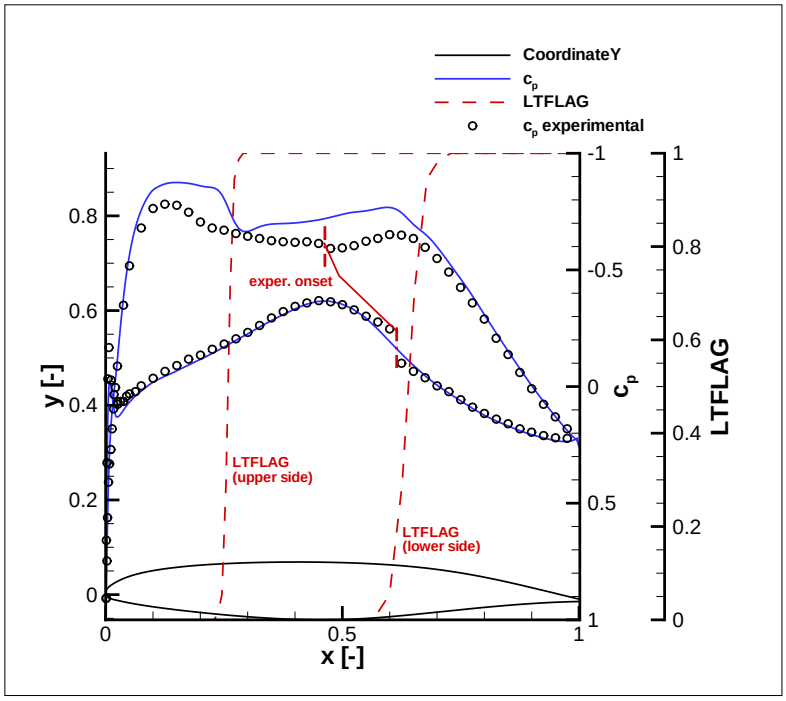

Figure B.7: CAST10 airfoil - pressure distribution and chordwise LTFLAG status with comparison to experimental data (Michel criterion).

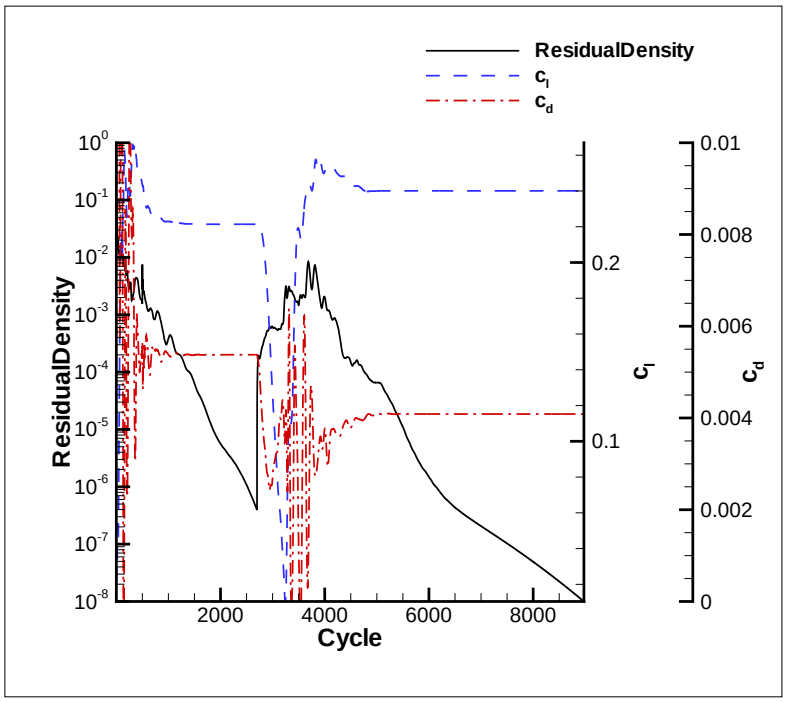

Figure B.8: CAST10 airfoil - convergence history for the density residual, lift and drag coefficient using the van Driest & Blumer criterion for $\alpha = -0.25°$.

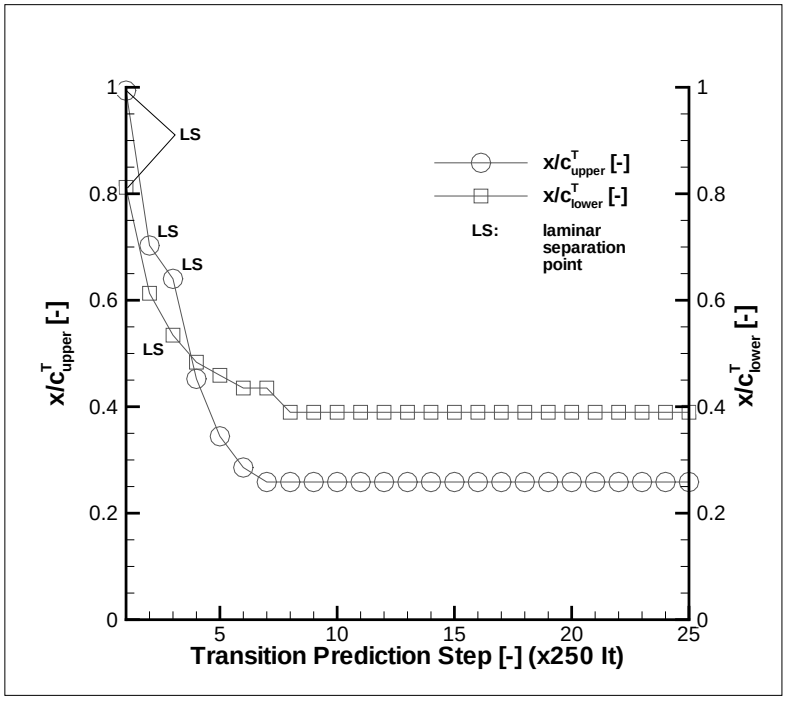

Figure B.9: CAST10 airfoil - convergence of the predicted transition locations using the van Driest & Blumer criterion for $\alpha = -0.25°$.

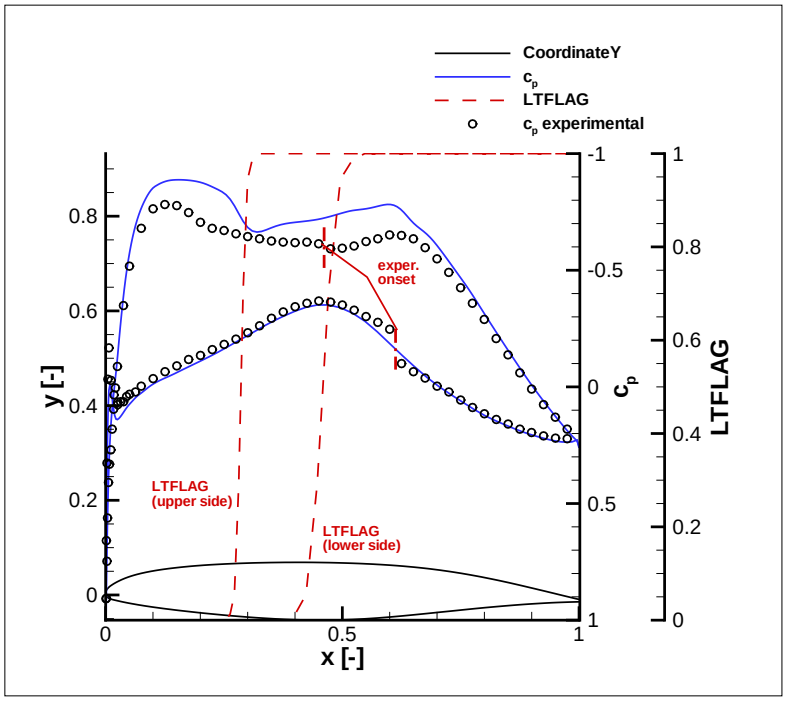

Figure B.10: CAST10 airfoil - pressure distribution and chordwise LTFLAG status with comparison to experimental data (van Driest & Blumer criterion).

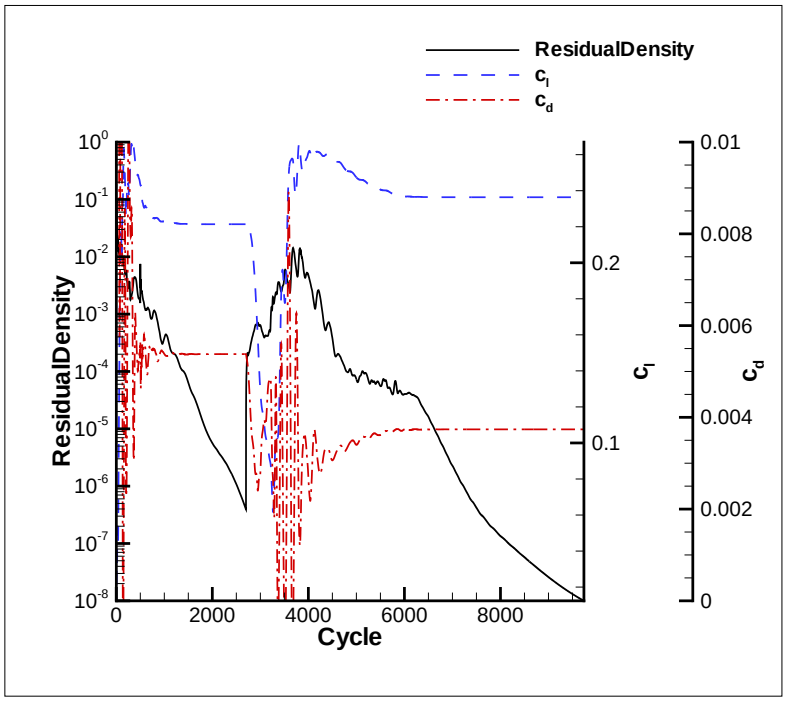

Figure B.11: CAST10 airfoil - convergence history for the density residual, lift and drag coefficient using the AHD criterion for $\alpha = -0.25°$.

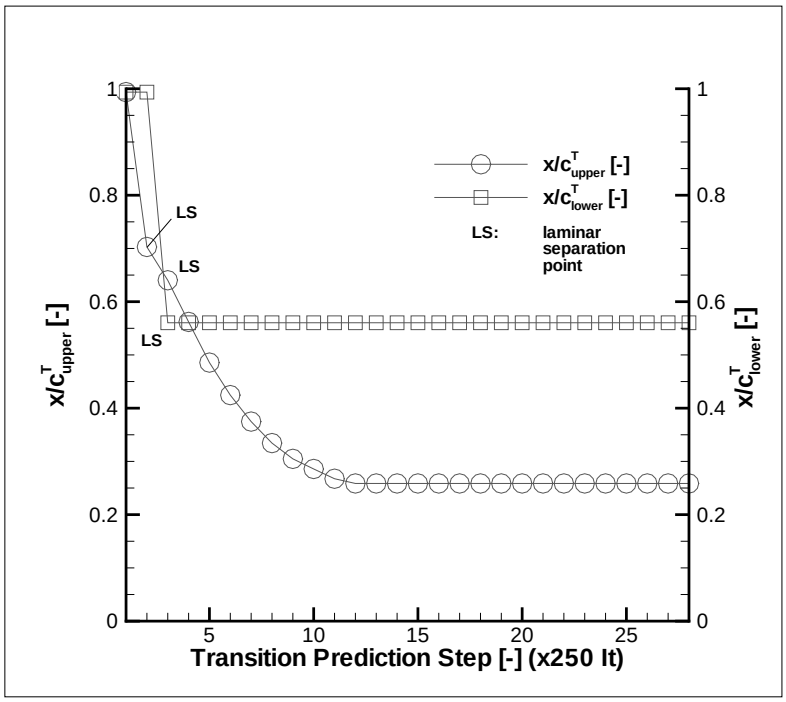

Figure B.12: CAST10 airfoil - convergence of the predicted transition locations using the AHD criterion for $\alpha = -0.25°$.

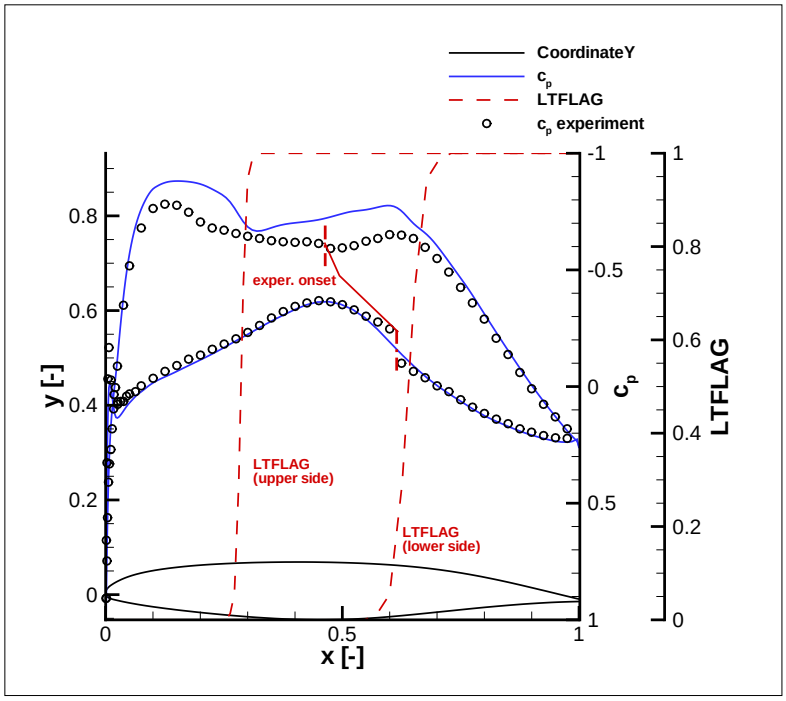

Figure B.13: CAST10 airfoil - pressure distribution and chordwise LTFLAG status with comparison to experimental data (AHD criterion).

C Figures - ONERA 7A rotor testcase

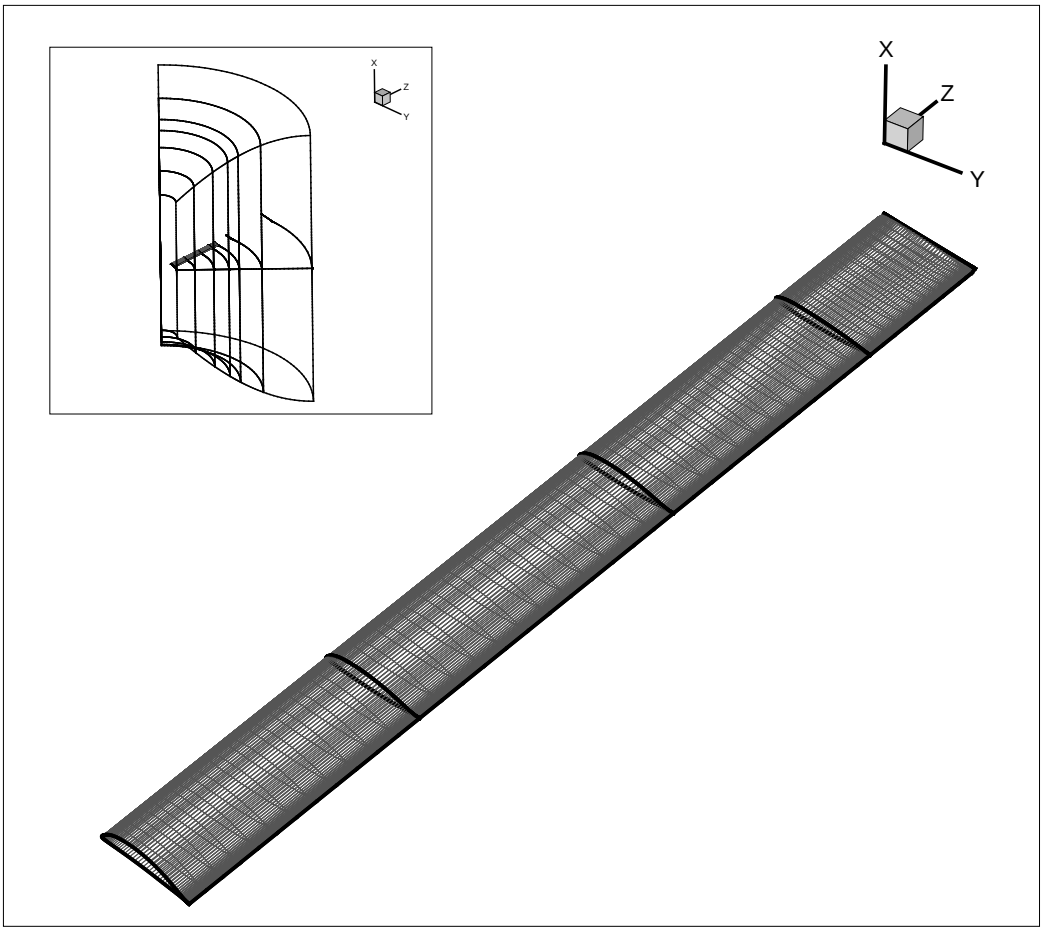

Figure C.1: ONERA 7A rotor - computational grid.

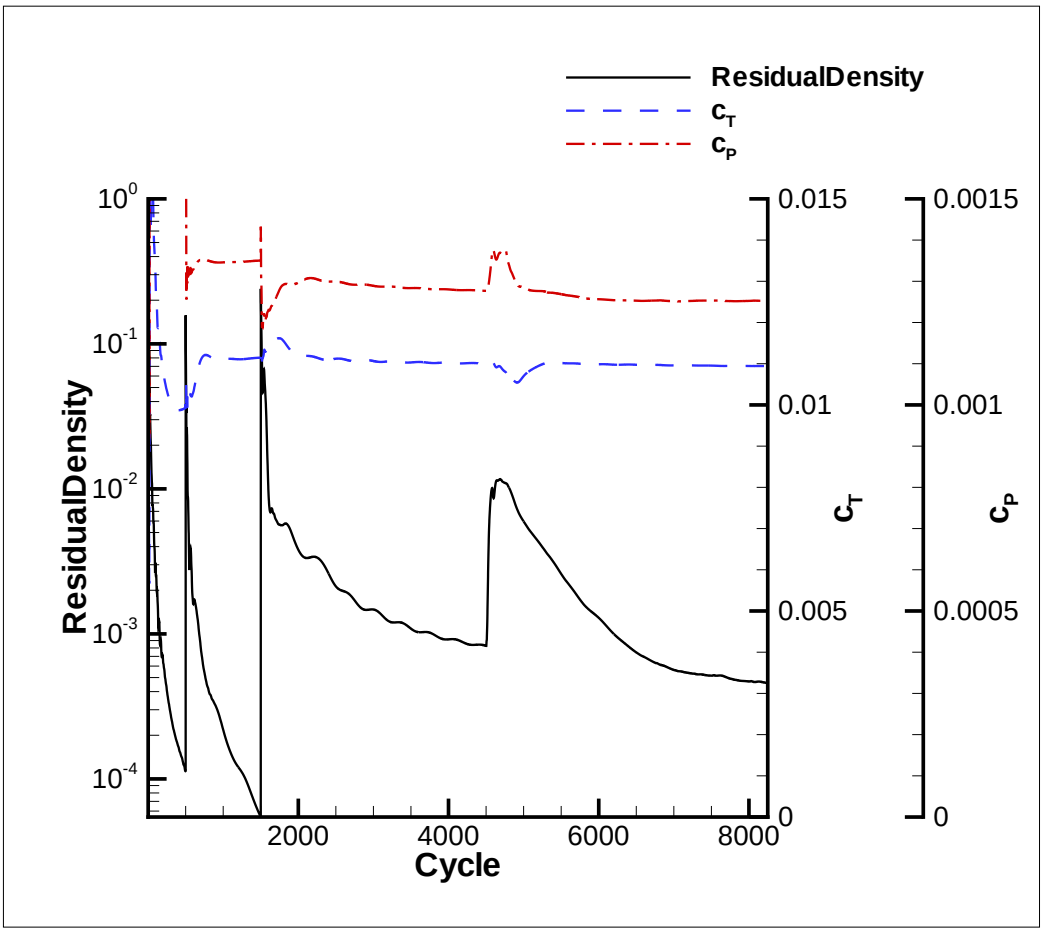

Figure C.2: ONERA 7A rotor - convergence history for the density residual, thrust and power coefficient using the minimum pressure criterion.

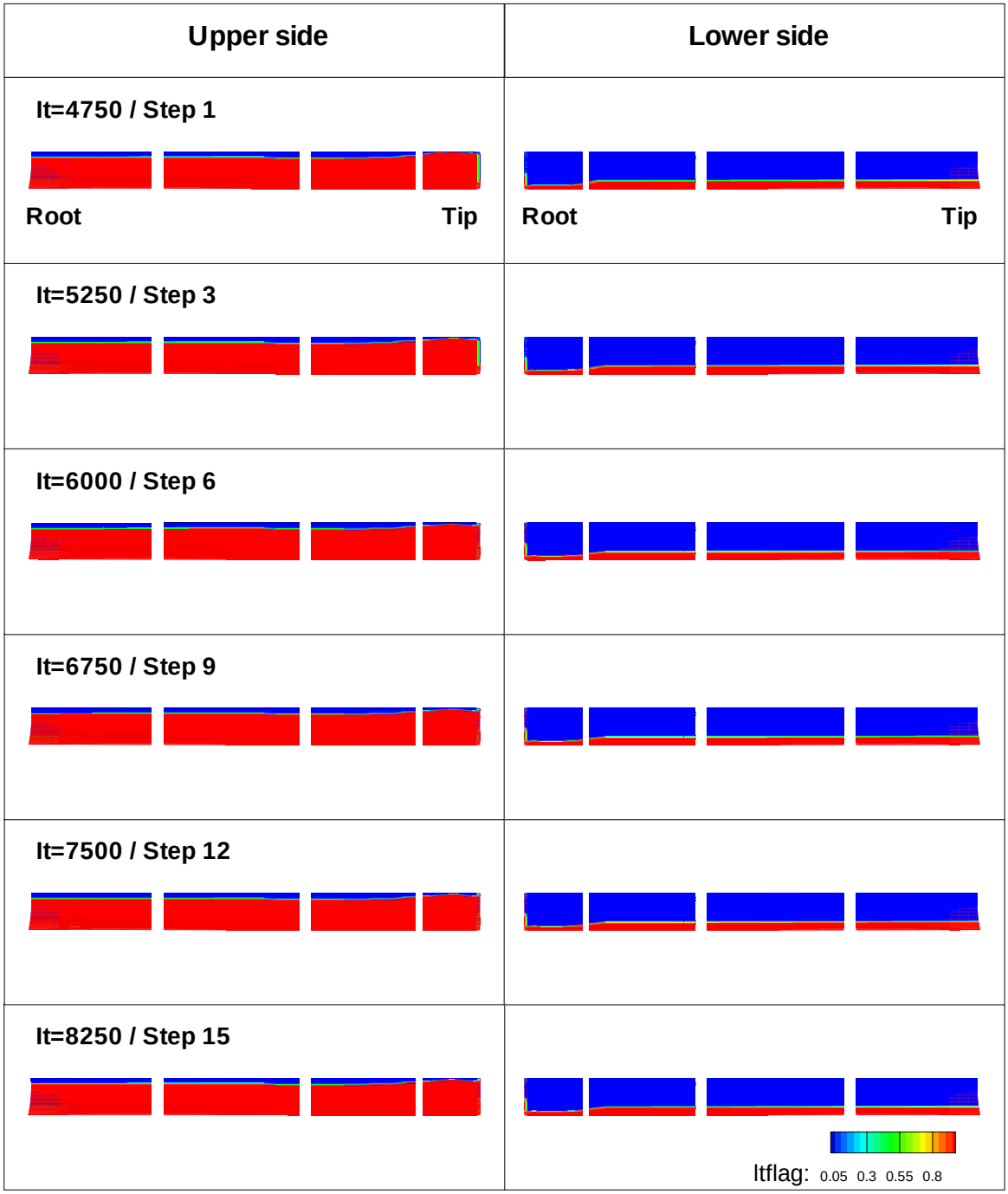

Figure C.3: ONERA 7A rotor - development of laminar and turbulent flow regions between selected transition prediction steps using the minimum pressure criterion.

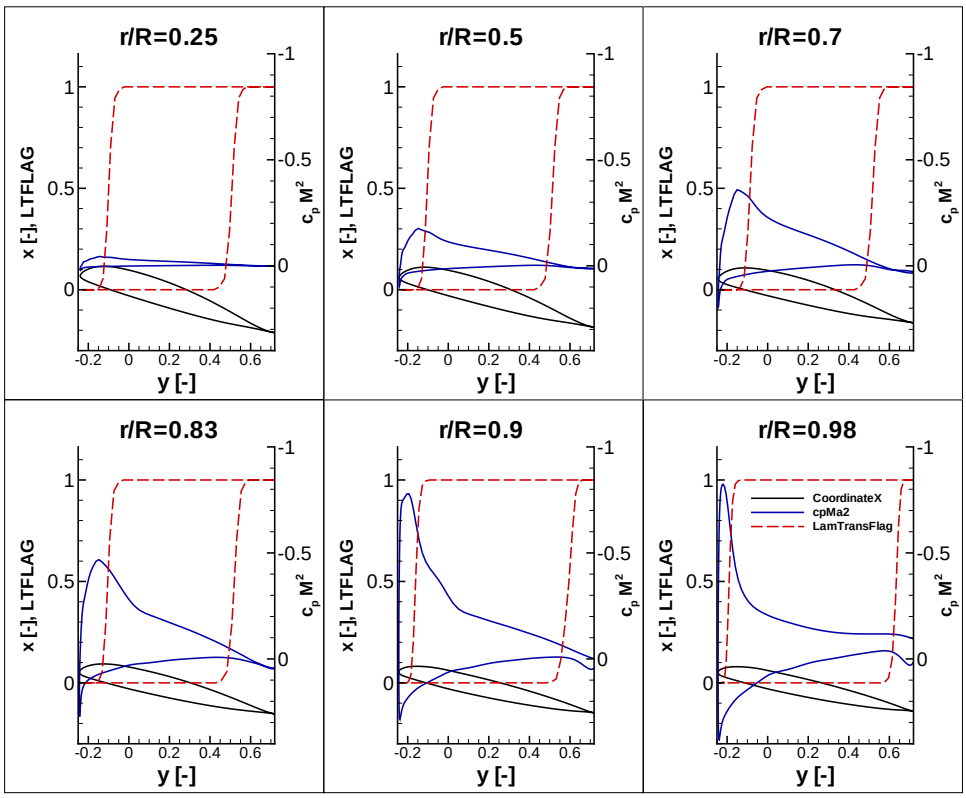

Figure C.4: ONERA 7A rotor - pressure and LTFLAG distribution at selected airfoil sections for prediction step 15 using the minimum pressure criterion.

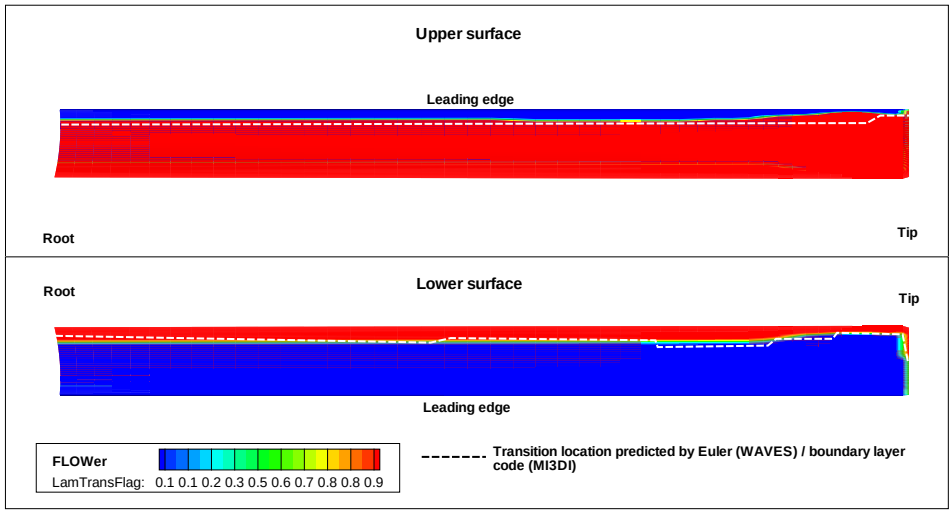

Figure C.5: ONERA 7A rotor - predicted transition onset using the FLOWer minimum pressure criterion in comparison to an Euler/boundary layer code (WAVES/MI3DI) [4].

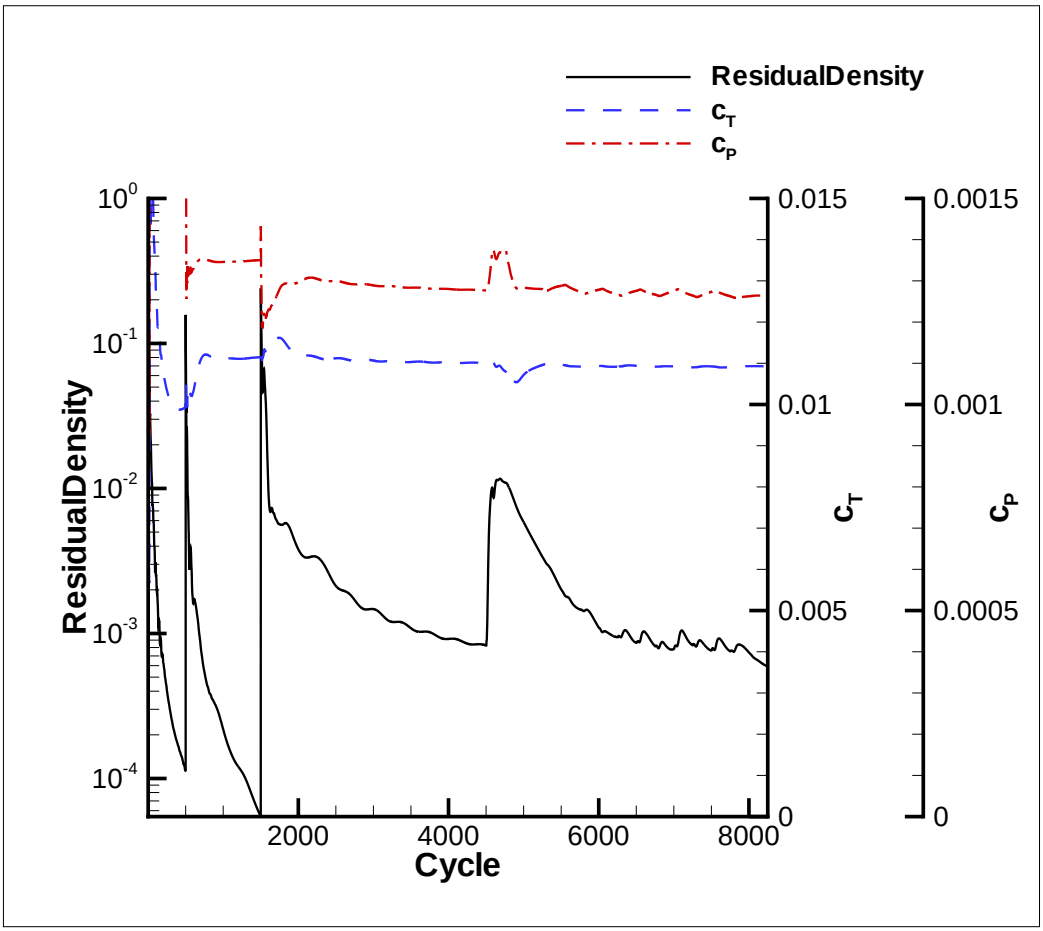

Figure C.6: ONERA 7A rotor - convergence history for the density residual, thrust and power coefficient using the Michel criterion.

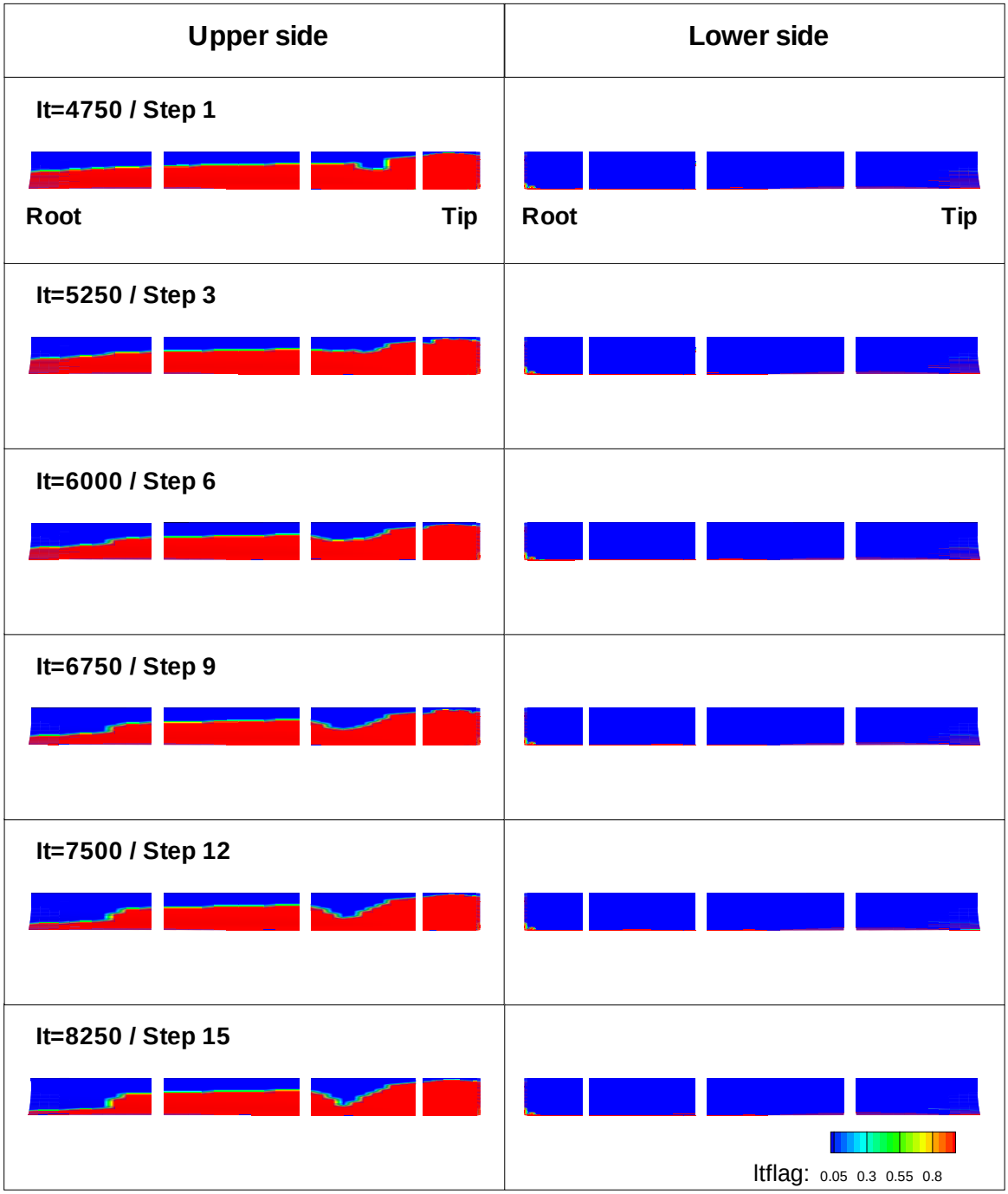

Figure C.7: ONERA 7A rotor - development of laminar and turbulent flow regions between selected transition prediction steps using the Michel criterion.

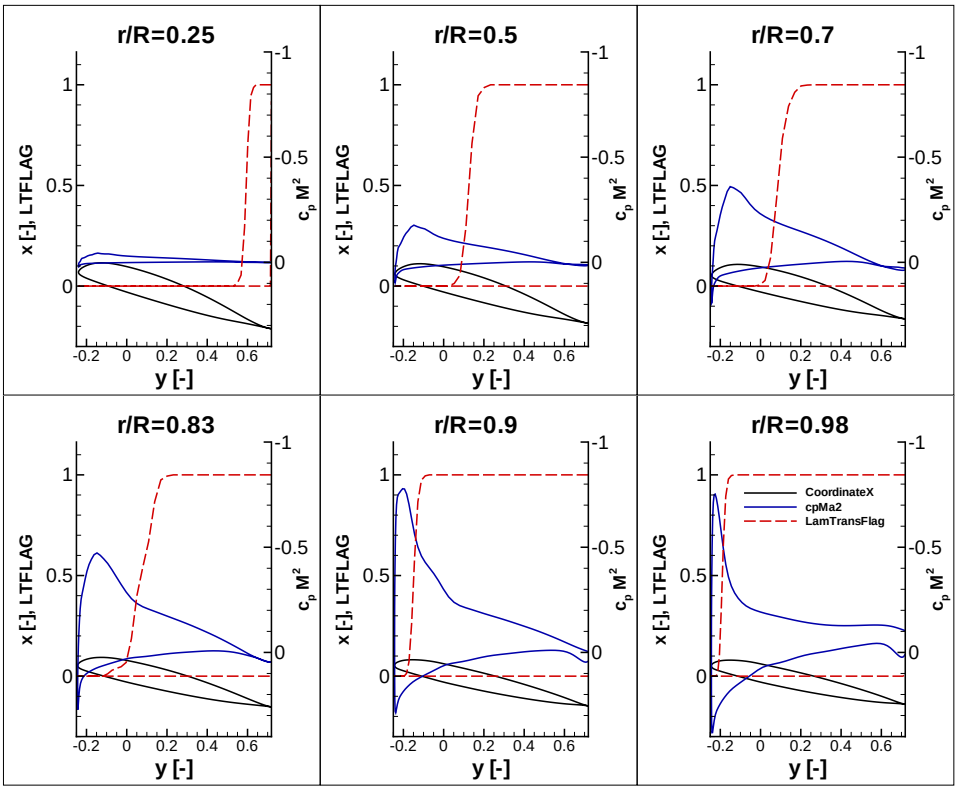

Figure C.8: ONERA 7A Rotor - pressure and LTFLAG distribution at selected airfoil sections for prediction step 15 using the Michel criterion.

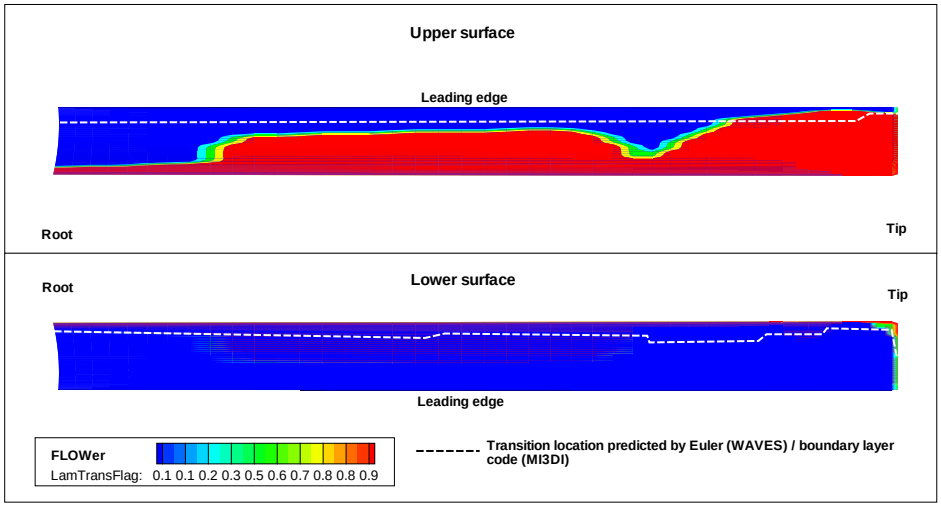

Figure C.9: ONERA 7A rotor - predicted transition onset using the FLOWer Michel criterion in comparison to an Euler/boundary layer code (WAVES/MI3DI) [4].

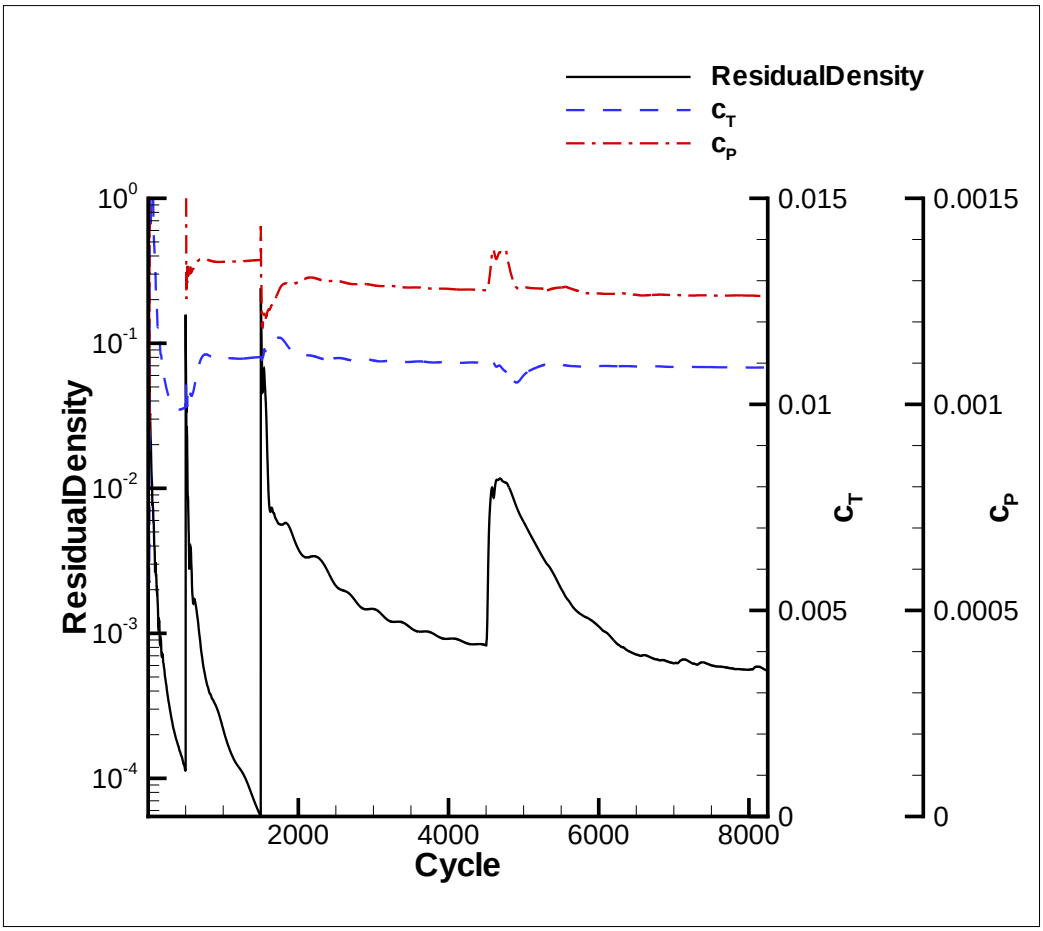

Figure C.10: ONERA 7A rotor - convergence history for the density residual, thrust and power coefficient using the Michel criterion (version 1952 [19]).

Figure C.11: ONERA 7A rotor - development of laminar and turbulent flow regions between selected transition prediction steps using the Michel criterion (version 1952 [19]).

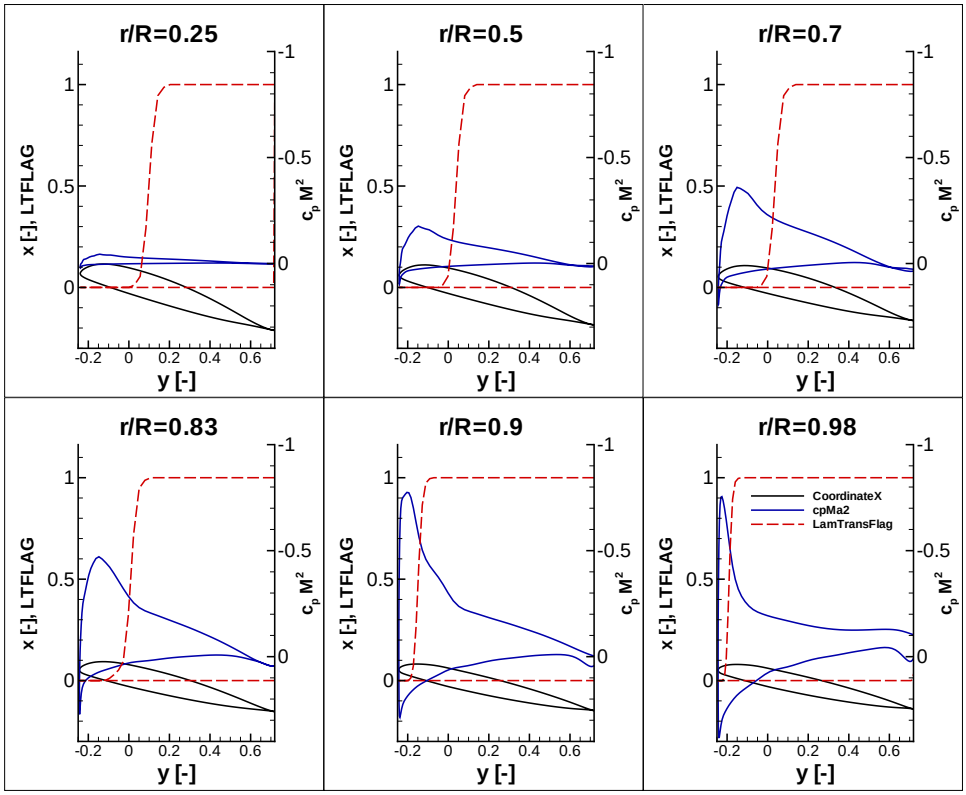

Figure C.12: ONERA 7A Rotor - pressure and LTFLAG distribution at selected airfoil sections for prediction step 15 using the Michel criterion (version 1952 [19]).

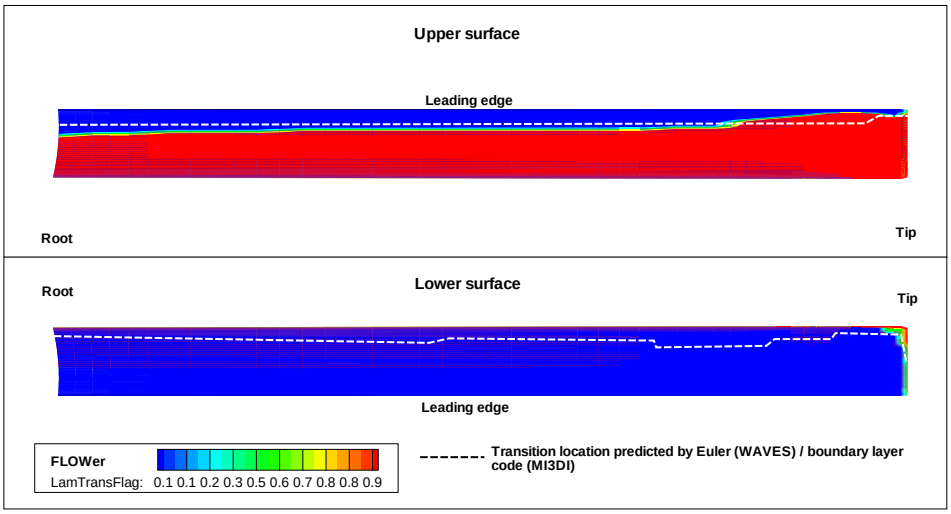

Figure C.13: ONERA 7A rotor - predicted transition onset using the FLOWer Michel criterion (version 1952 [19]) in comparison to an Euler/boundary layer code (WAVES/MI3DI) [4].

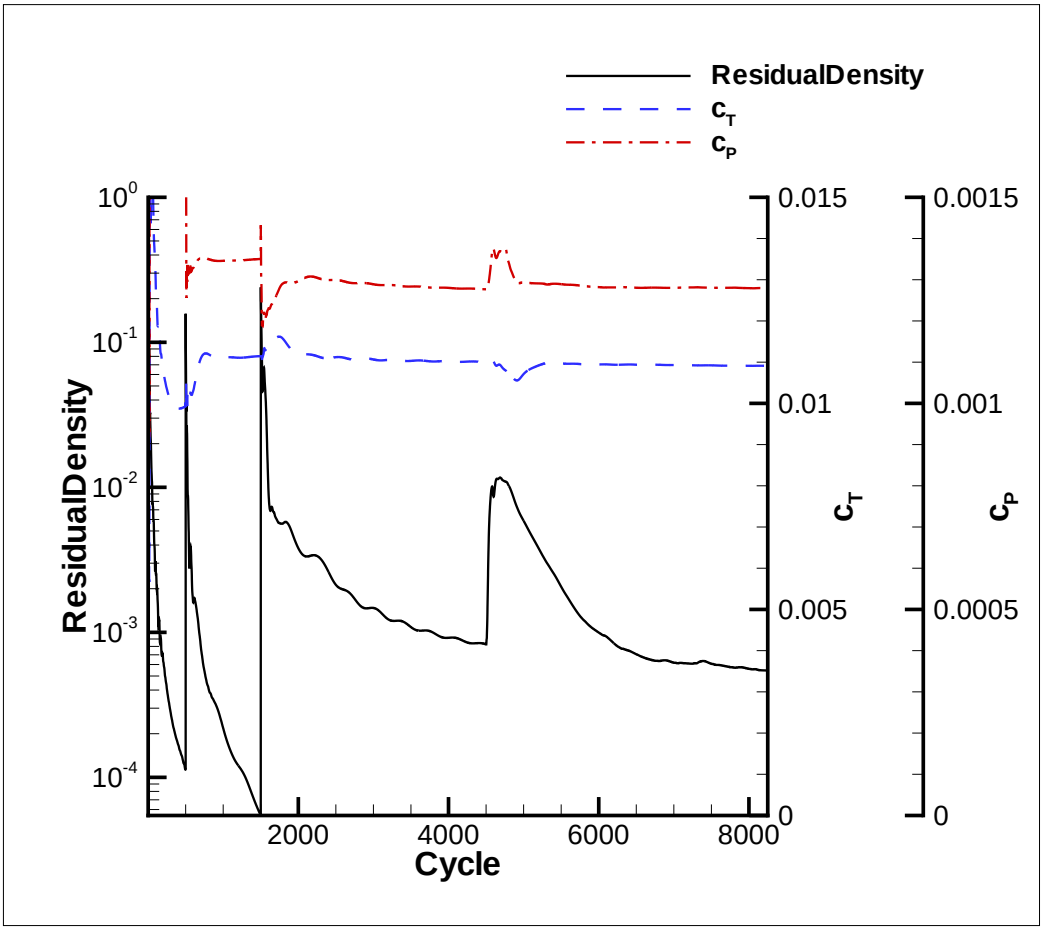

Figure C.14: ONERA 7A rotor - convergence history for the density residual, thrust and power coefficient using the van Driest & Blumer criterion.

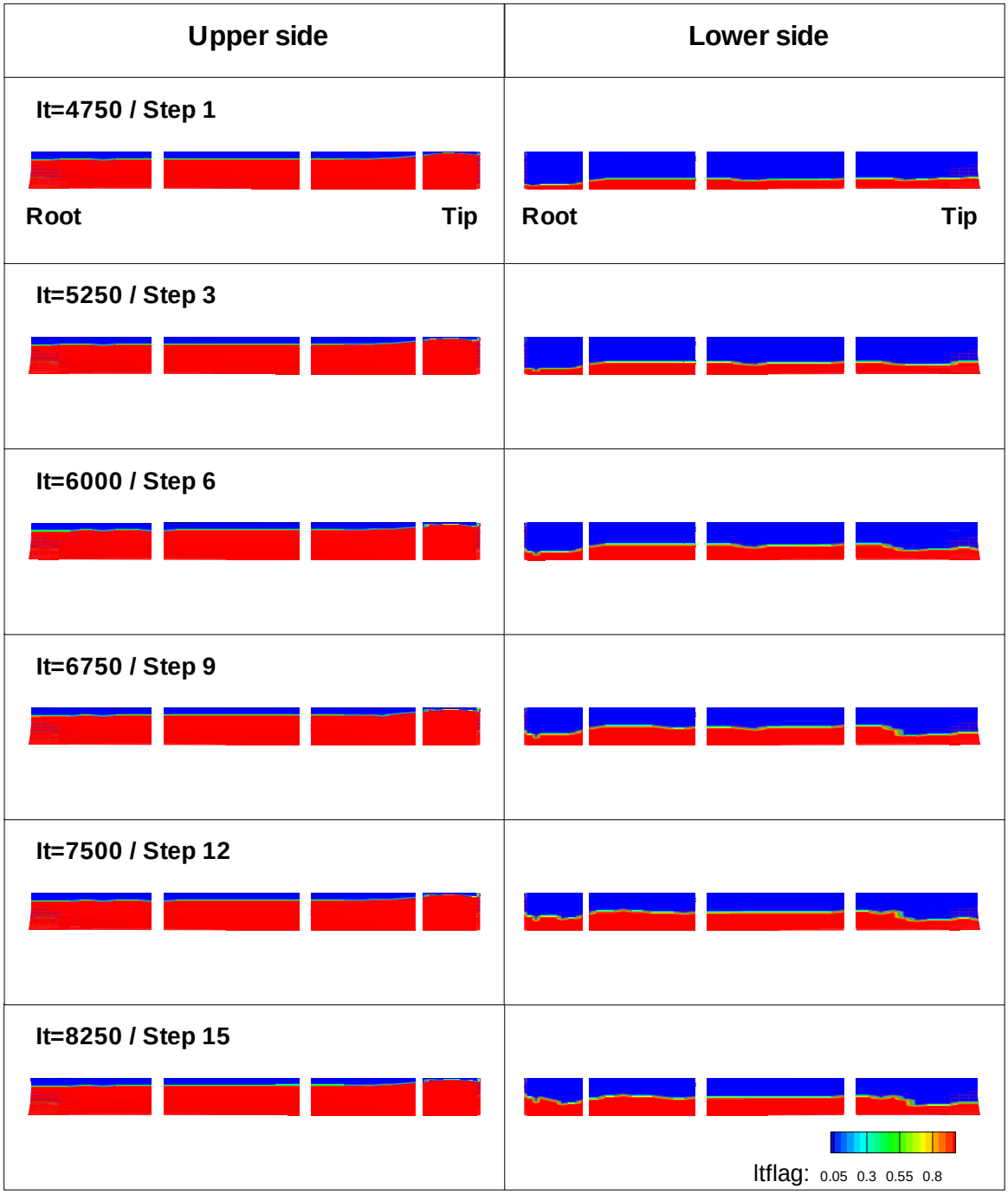

Figure C.15: ONERA 7A rotor - development of laminar and turbulent flow regions between selected transition prediction steps using the van Driest & Blumer criterion.

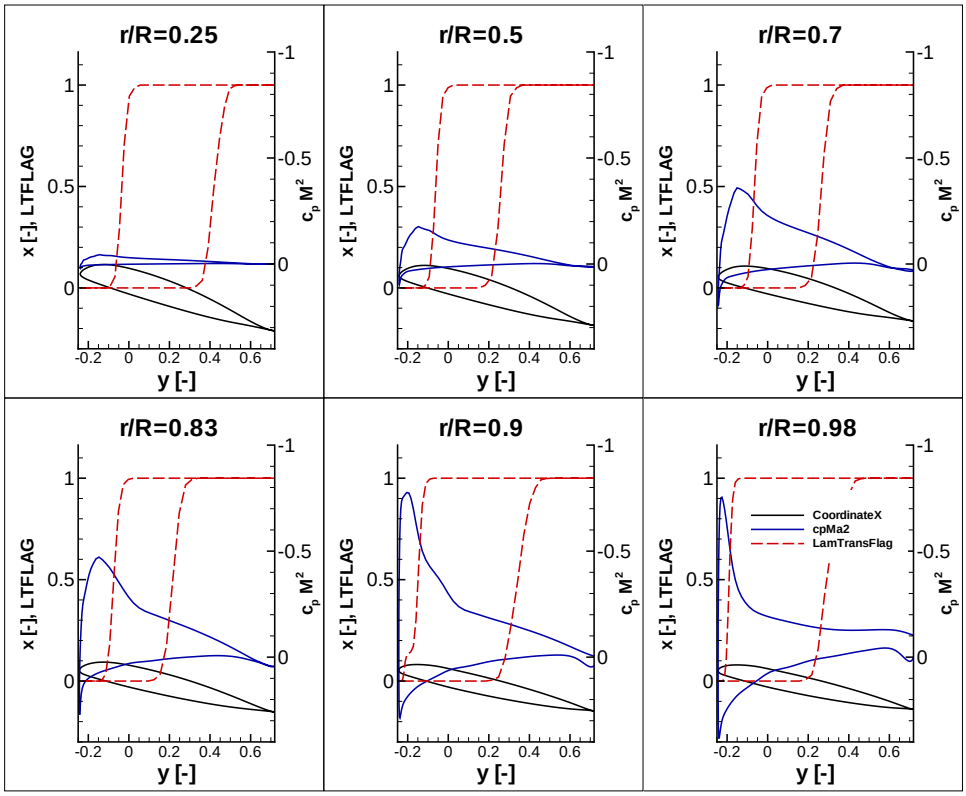

Figure C.16: ONERA 7A rotor - pressure and LTFLAG distribution at selected airfoil sections for prediction step 15 using the van Driest & Blumer criterion.

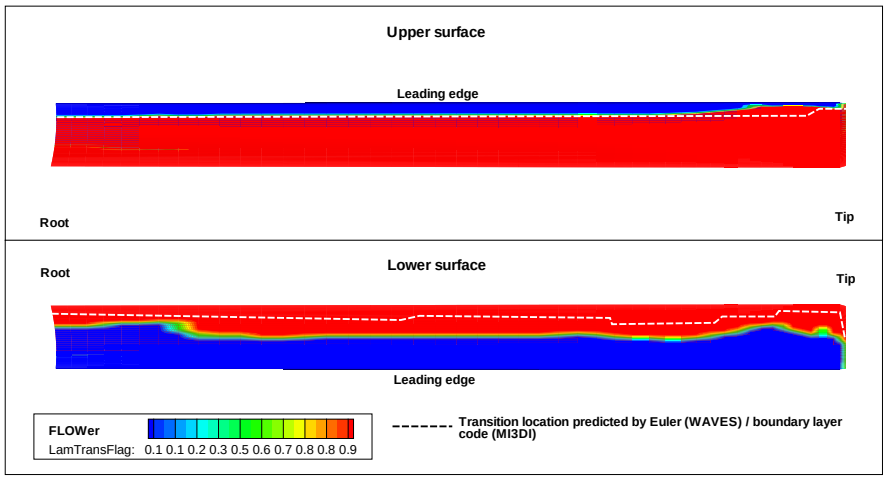

Figure C.17: ONERA 7A rotor - predicted transition onset using the FLOWer van Driest & Blumer criterion in comparison to an Euler / boundary layer code (WAVES/MI3DI) [4].

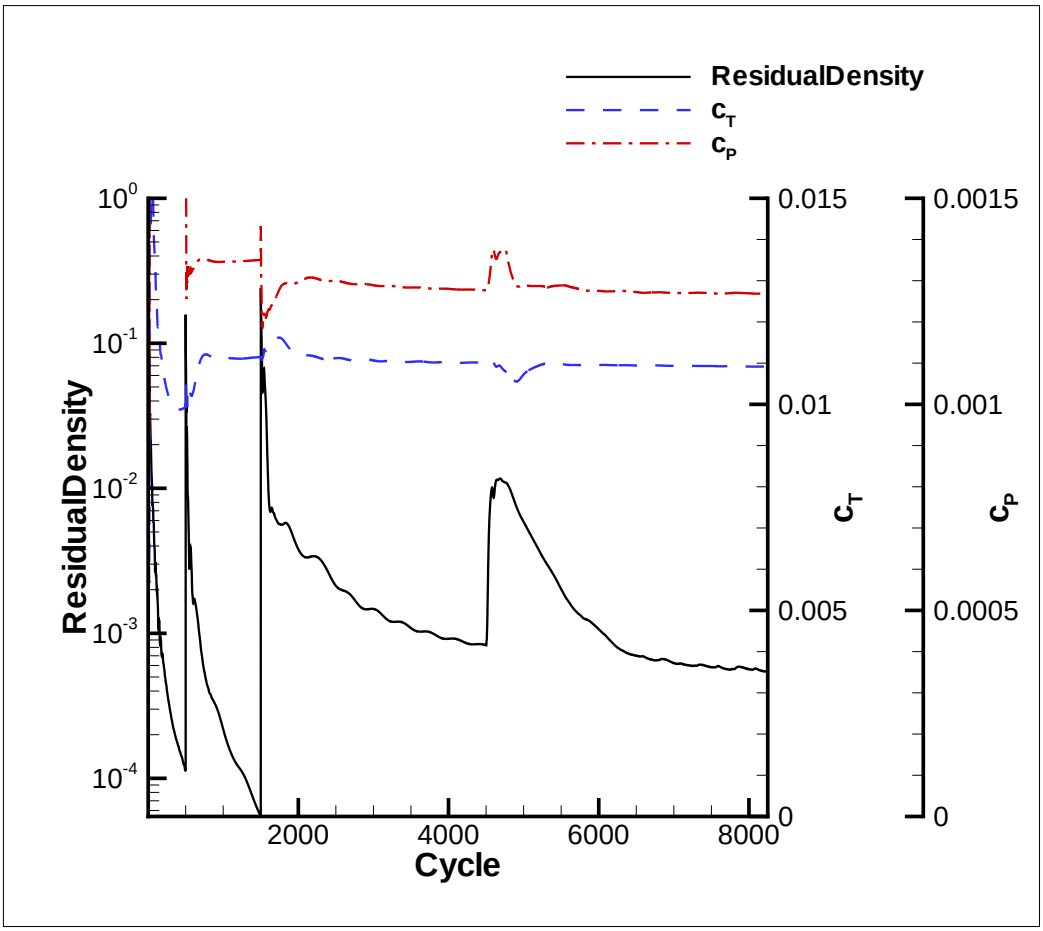

Figure C.18: ONERA 7A rotor - convergence history for the density residual, thrust and power coefficient using the AHD criterion.

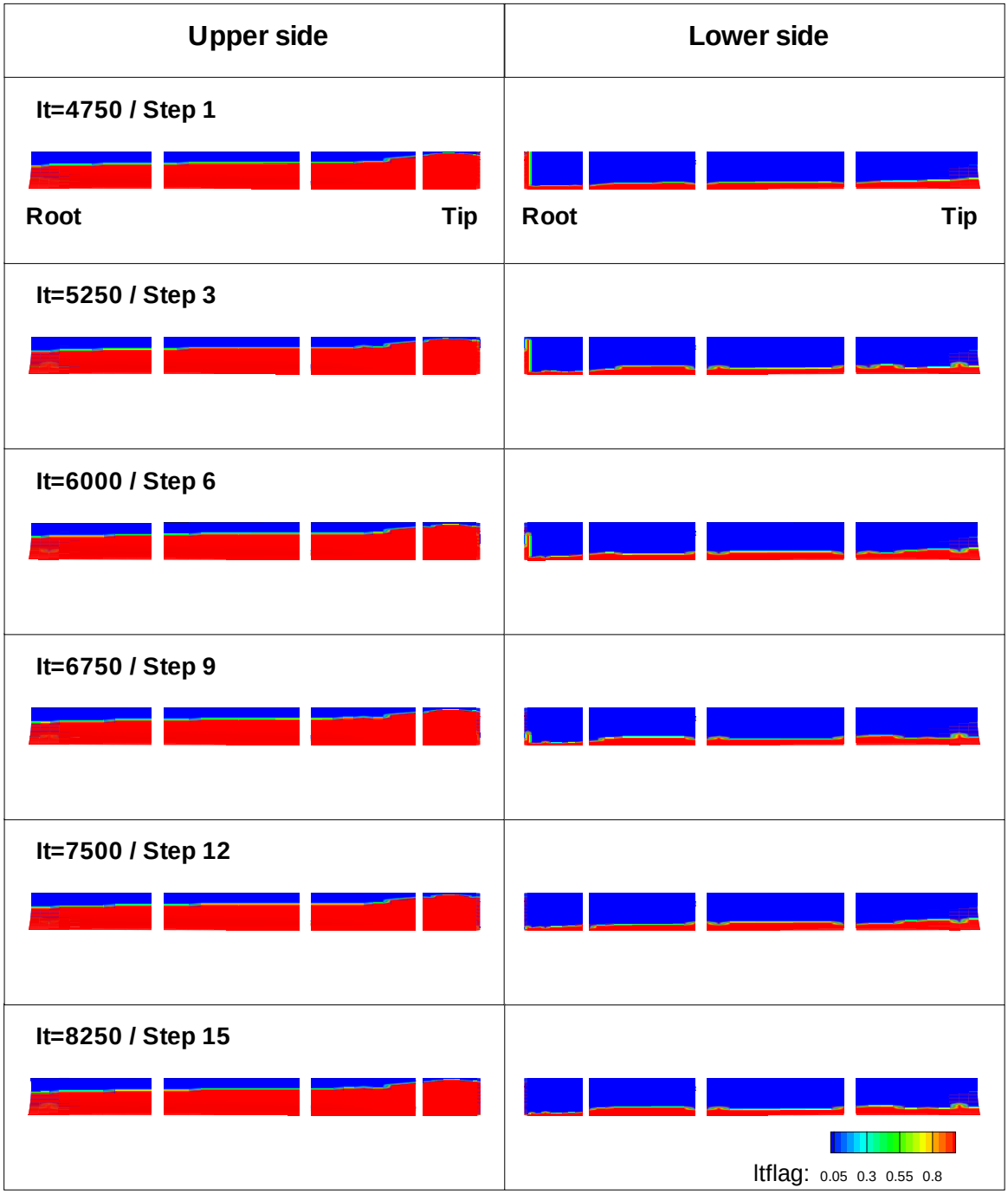

Figure C.19: ONERA 7A rotor - development of laminar and turbulent flow regions between selected transition prediction steps using the AHD criterion.

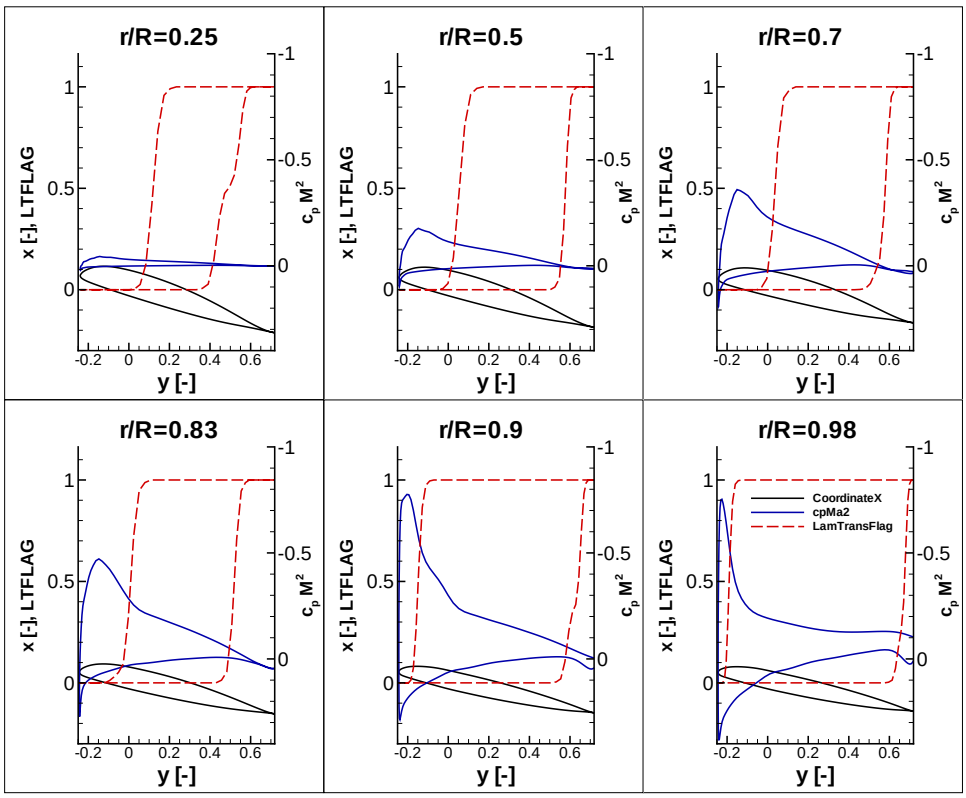

Figure C.20: ONERA 7A rotor - pressure and LTFLAG distribution at selected airfoil sections for prediction step 15 using the AHD criterion.

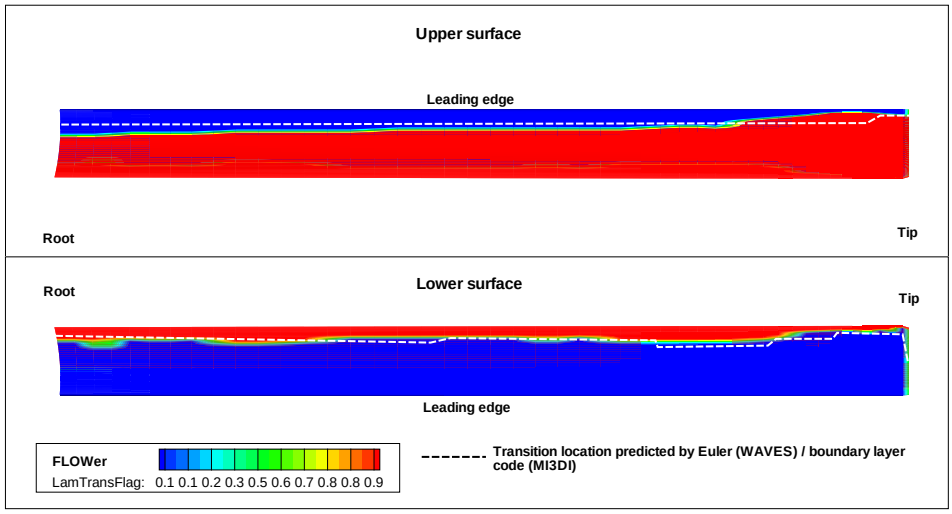

Figure C.21: ONERA 7A rotor - predicted transition onset using the FLOWer AHD criterion in comparison to an Euler / boundary layer code (WAVES/MI3DI) [4].

D Figures - INROS rotor (reference design) testcase

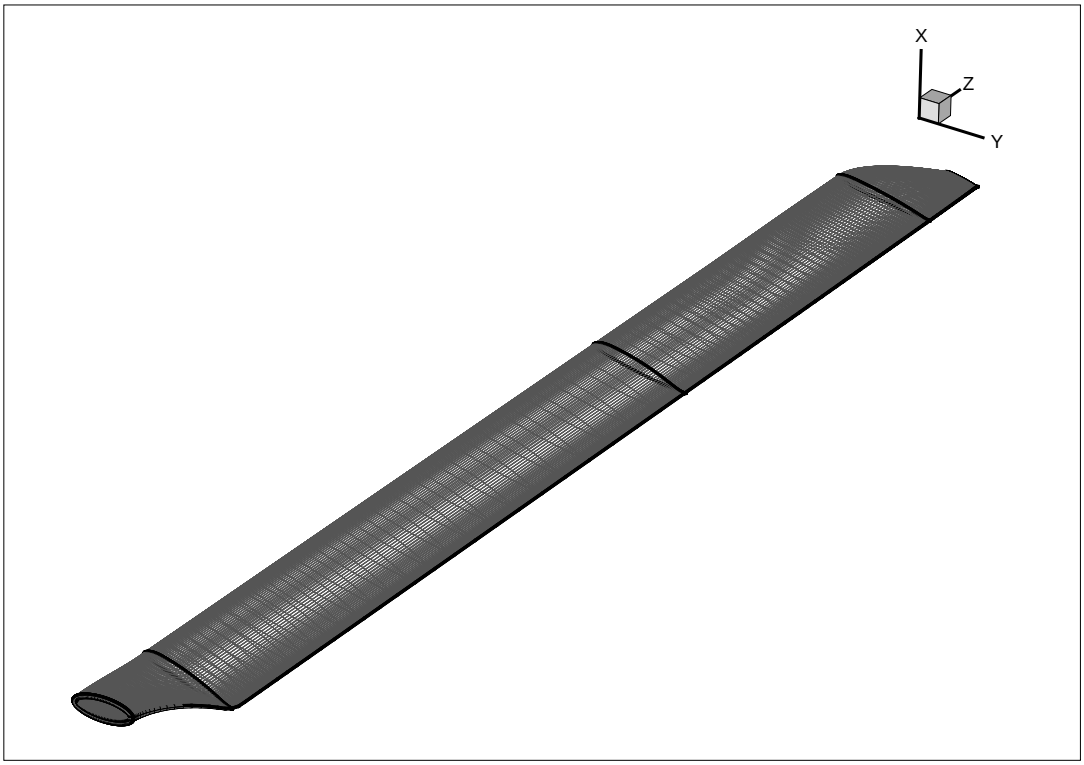

Figure D.1: INROS rotor (reference design) - surface grid.

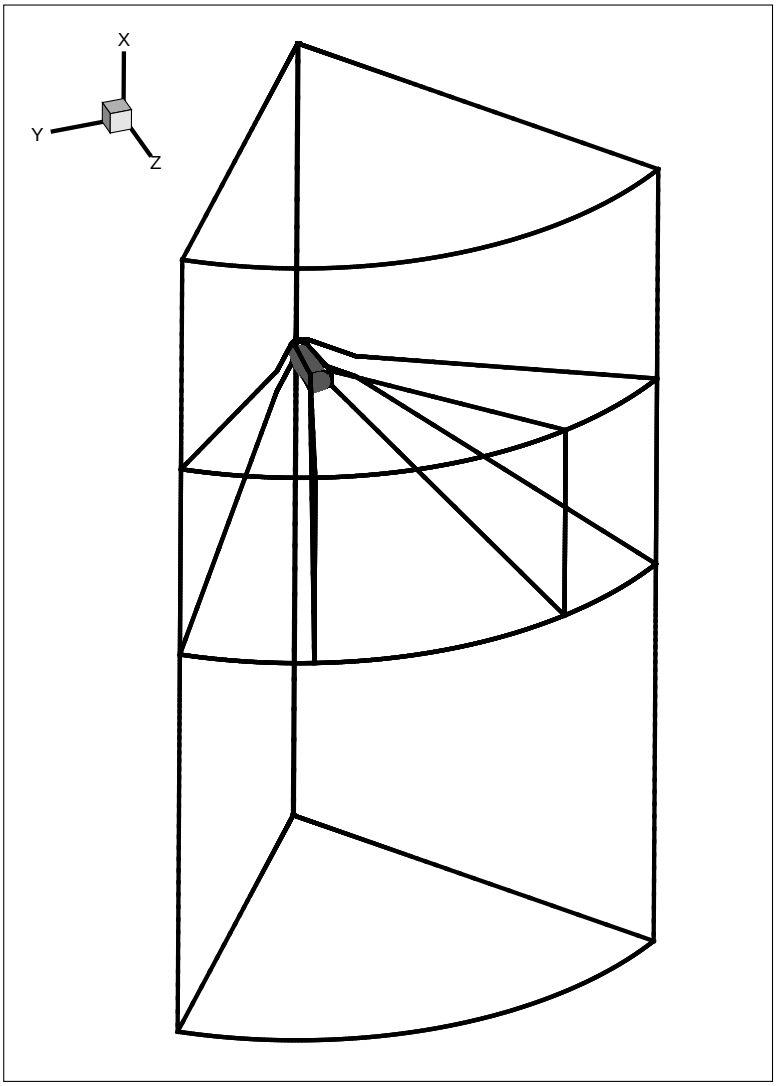

Figure D.2: INROS rotor (reference design) - grid topology.

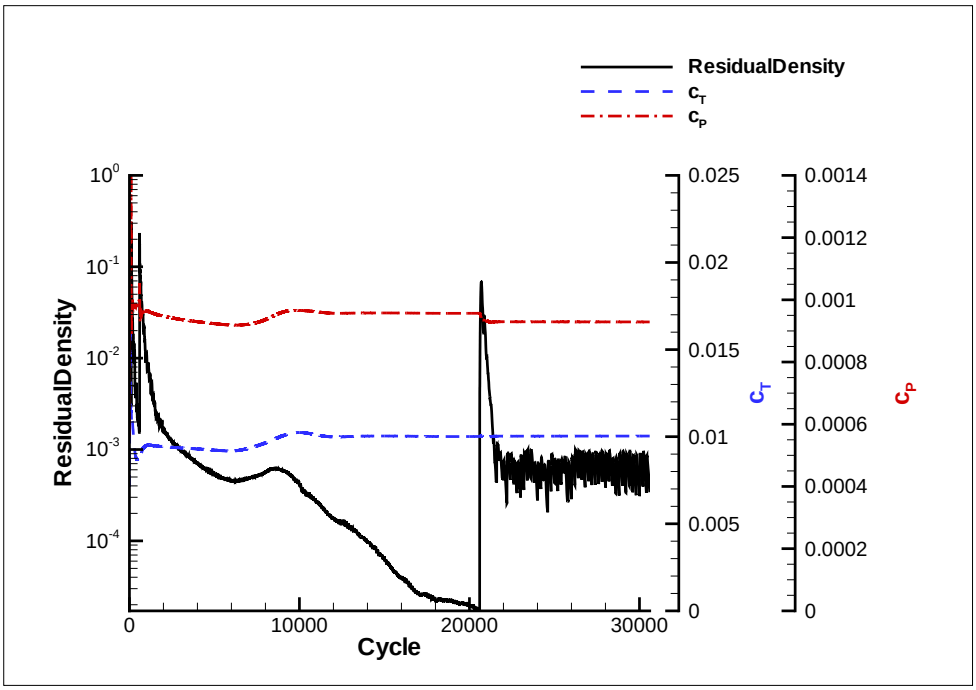

Figure D.3: INROS rotor (reference design) - convergence history for the density residual, thrust and power coefficient with restart from fully turbulent calculation using the AHD criterion.

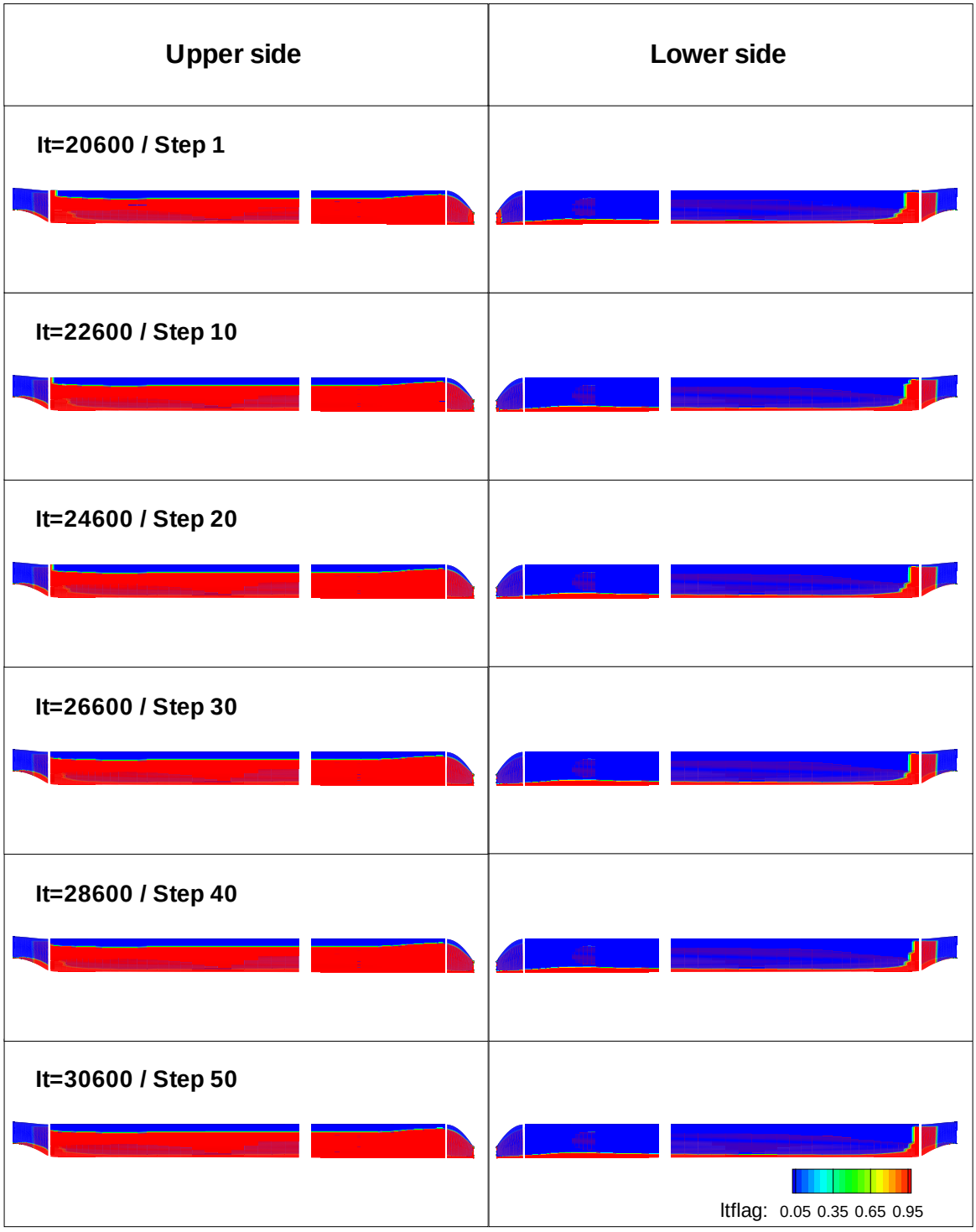

Figure D.4: INROS rotor (reference design) - development of laminar and turbulent flow regions between selected transition prediction steps using the AHD criterion.

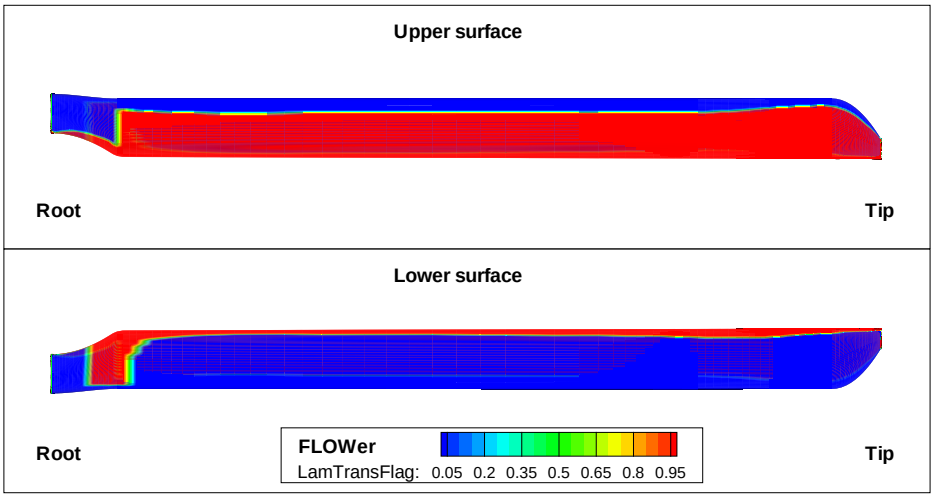

Figure D.5: INROS rotor (reference design) - predicted transition onset using the FLOWer AHD criterion with restart from fully turbulent calculation.

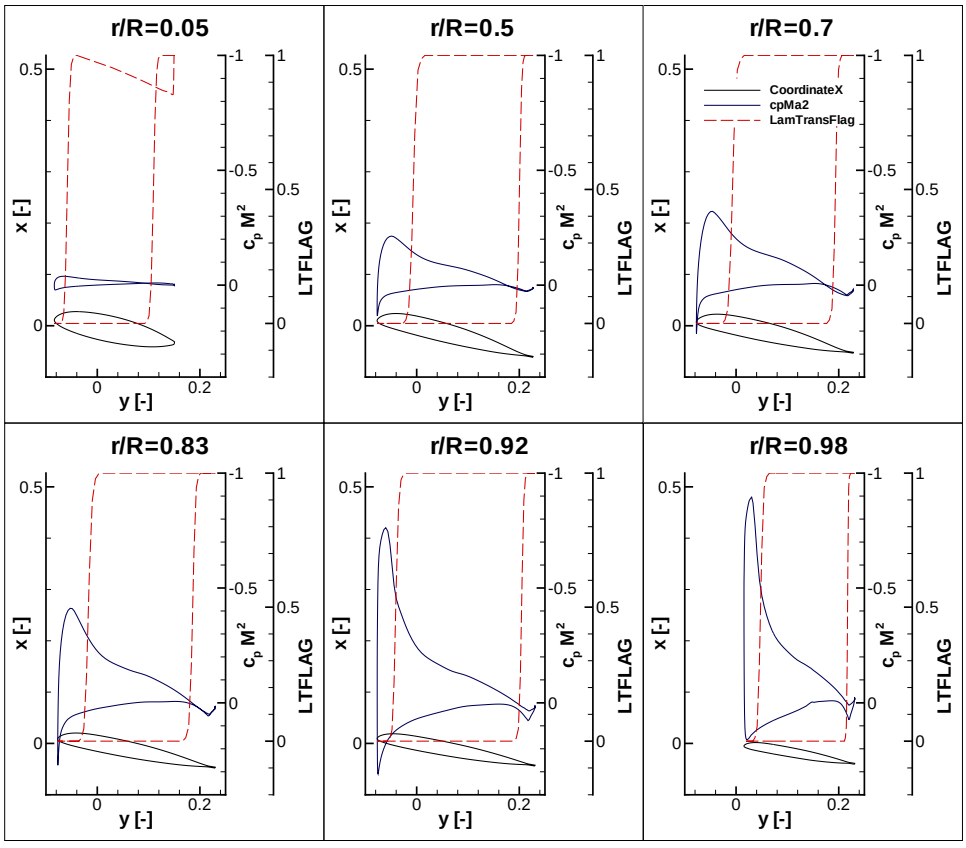

Figure D.6: INROS rotor (reference design) - pressure and LTFLAG distribution at selected airfoil sections using the AHD criterion.

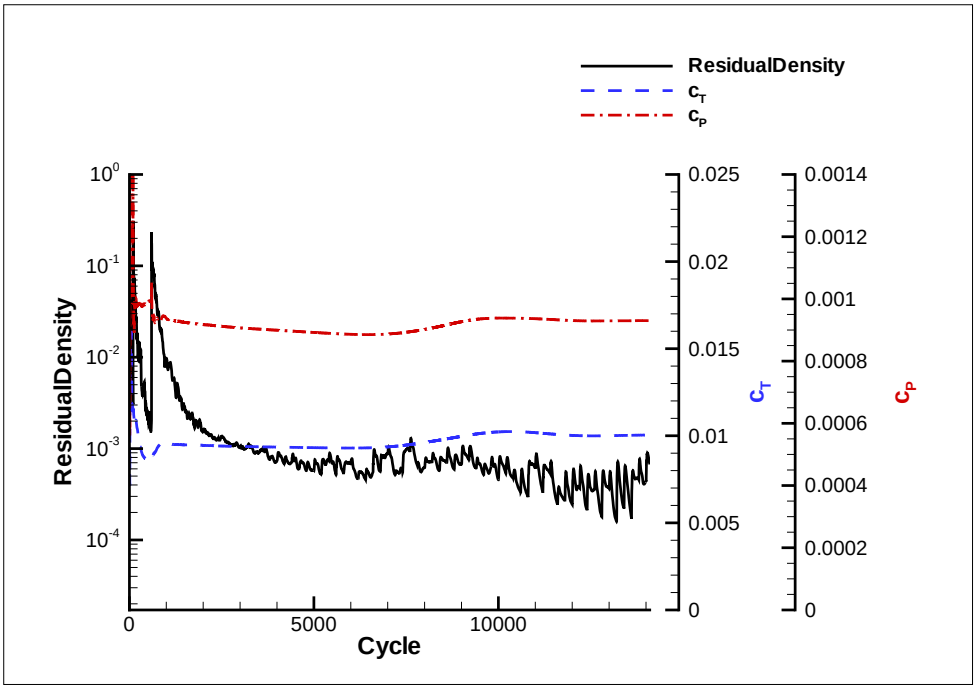

Figure D.7: INROS rotor (reference design) - convergence history for the density residual, thrust and power coefficient using the AHD criterion.

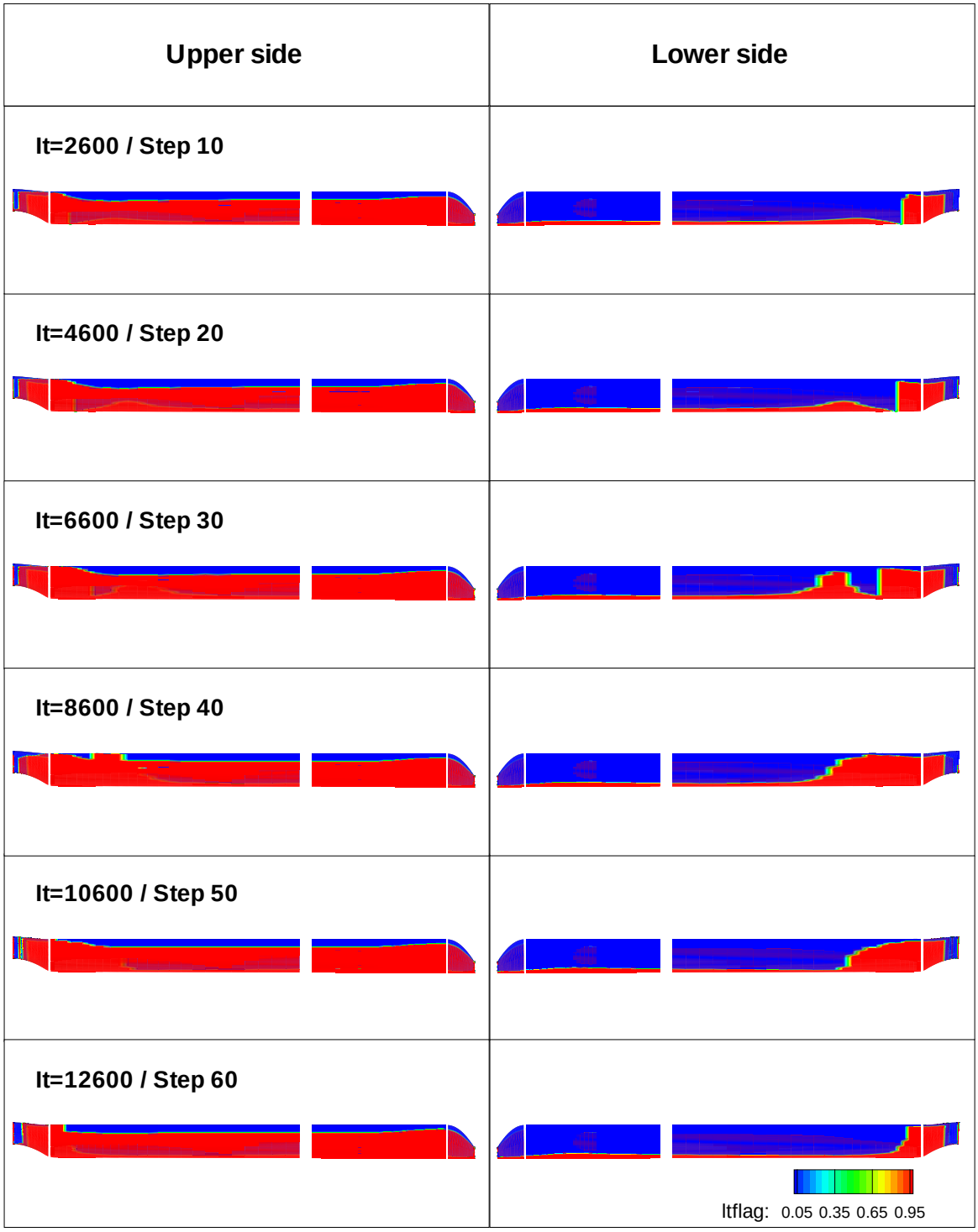

Figure D.8: INROS rotor (reference design) - development of laminar and turbulent flow regions between selected transition prediction steps using the AHD criterion.

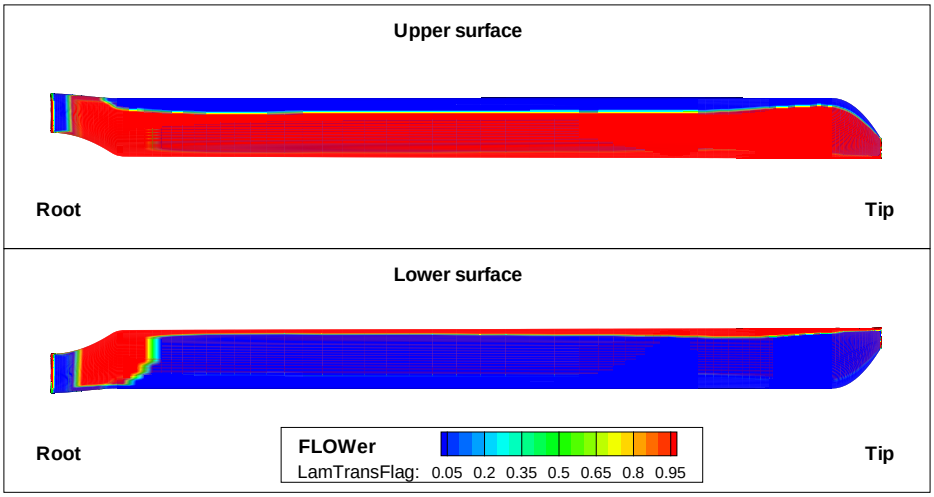

Figure D.9: INROS rotor (reference design) - predicted transition onset using the AHD criterion.

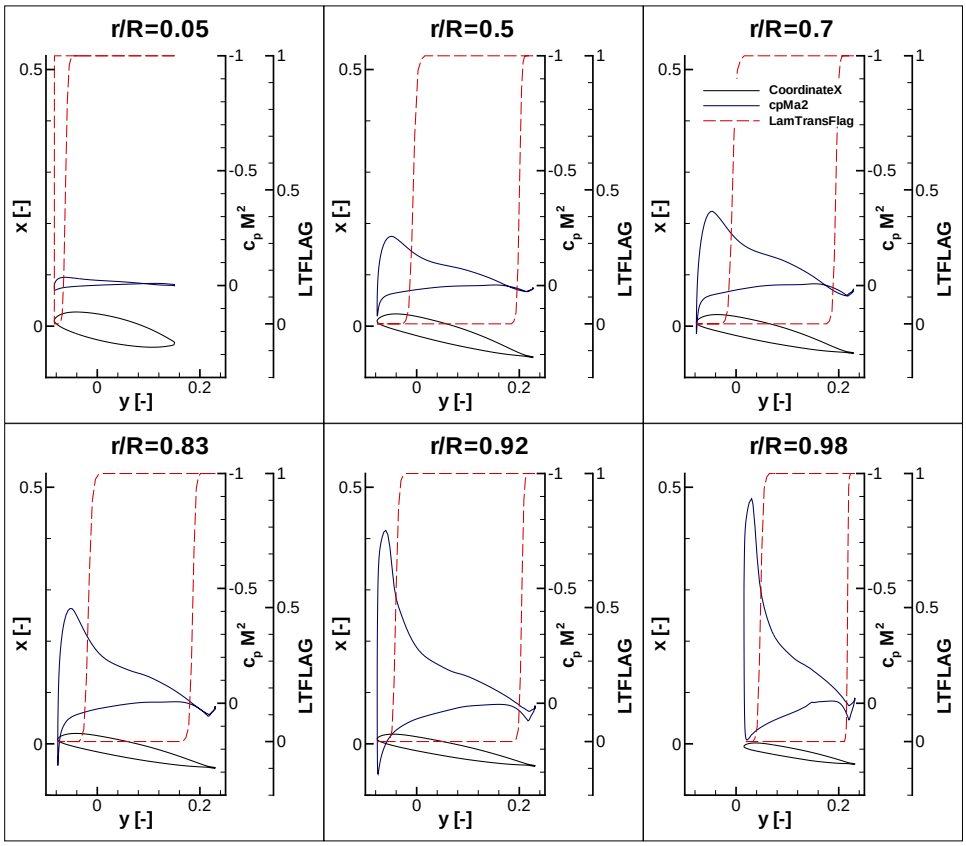

Figure D.10: INROS rotor (reference design) - pressure and LTFLAG distribution at selected airfoil sections using the AHD criterion.

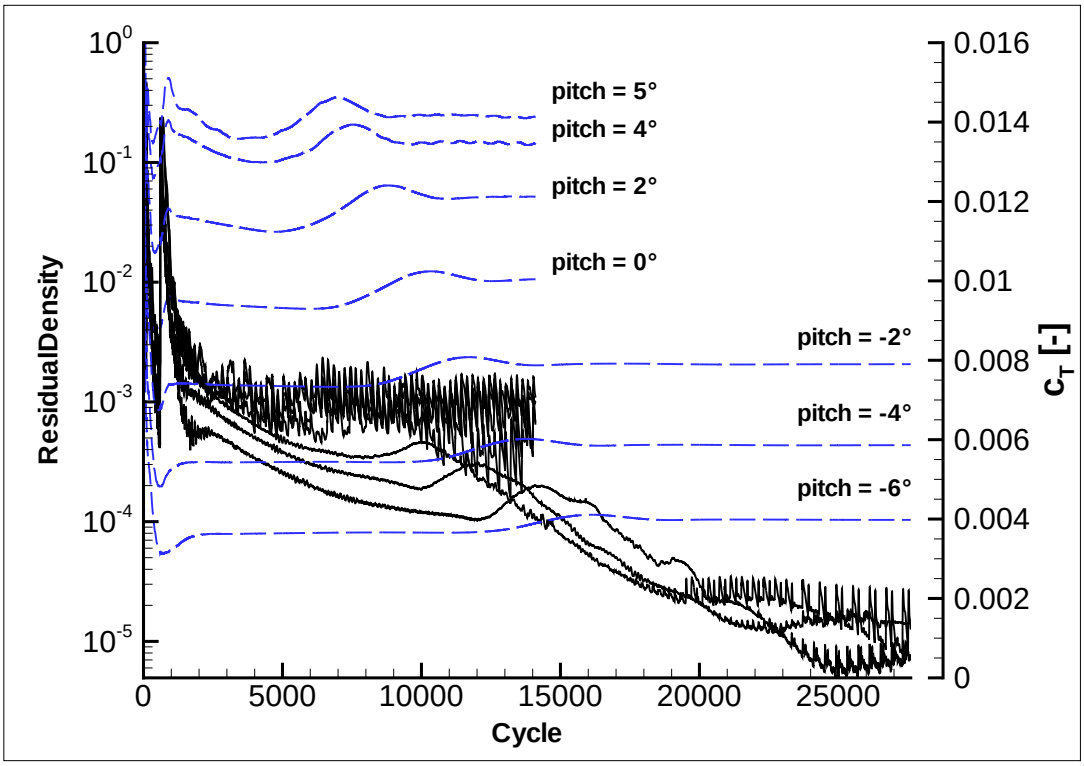

Figure D.11: INROS rotor (reference design, AHD criterion) - convergence history for density residual and thrust coefficient for different pitch angles.

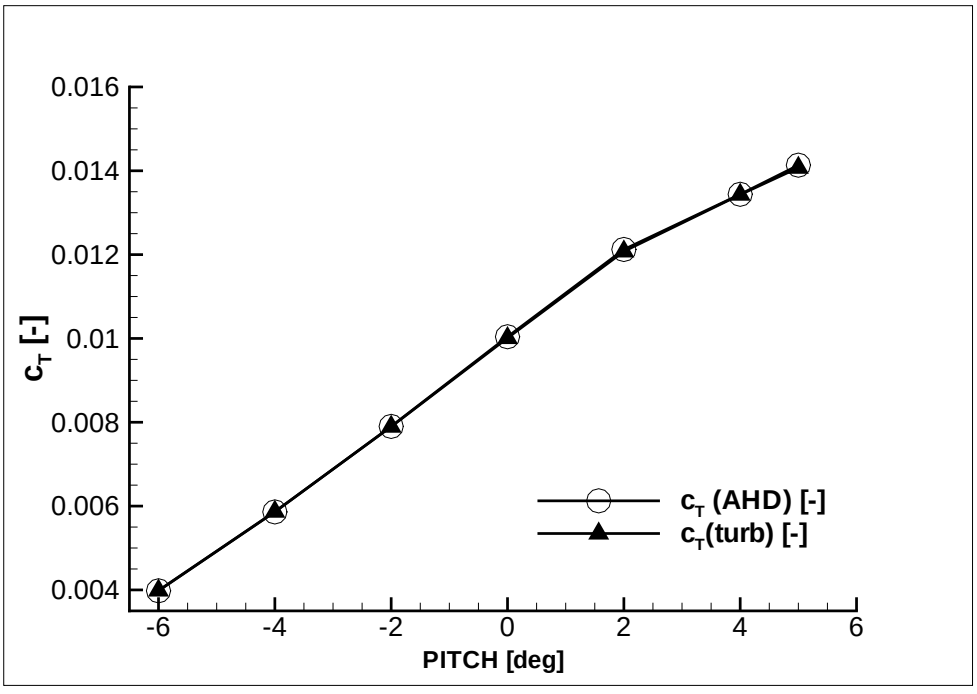

Figure D.12: INROS rotor (reference design, AHD criterion) - comparison of thrust polar for fully turbulent and transitional calculation.

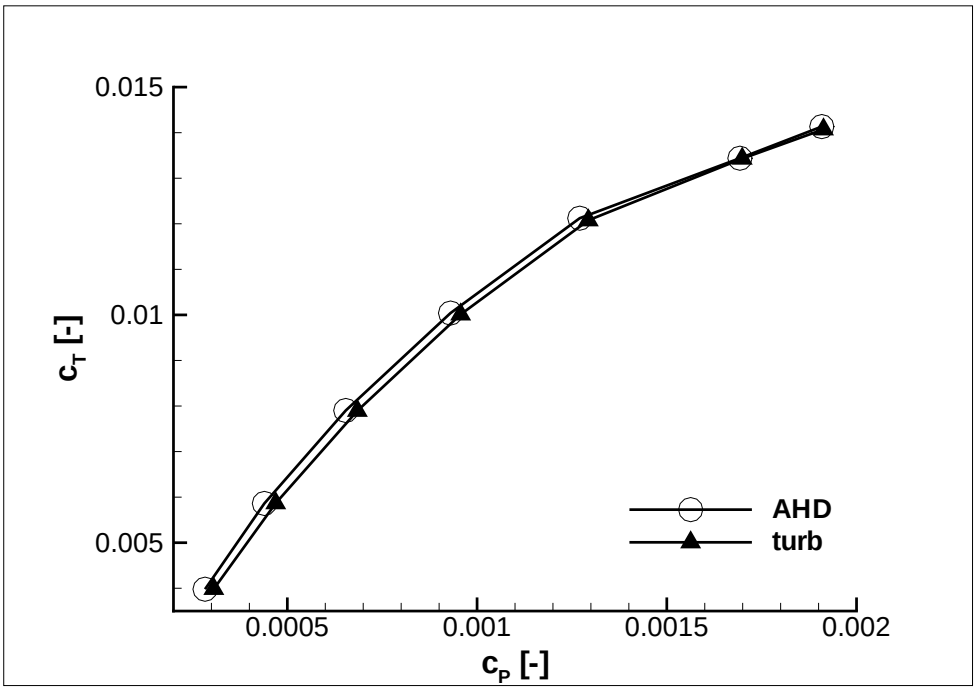

Figure D.13: INROS rotor (reference design, AHD criterion) - comparison of thrust/power characteristic for fully turbulent and transitional calculation.

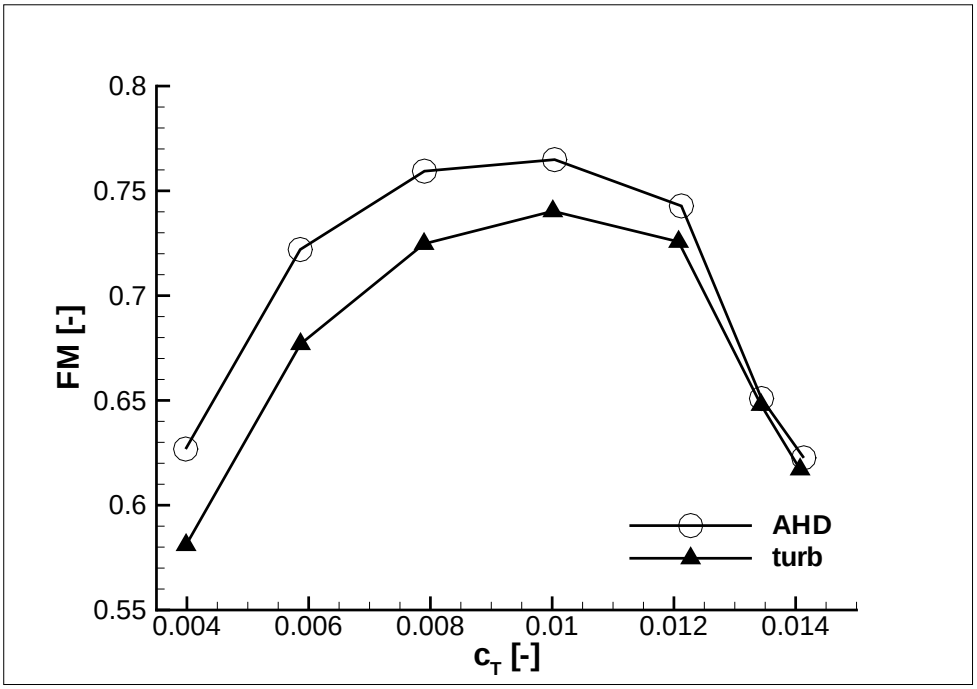

Figure D.14: INROS rotor (reference design, AHD criterion) - comparison of rotor efficiency for fully turbulent and transitional calculation.

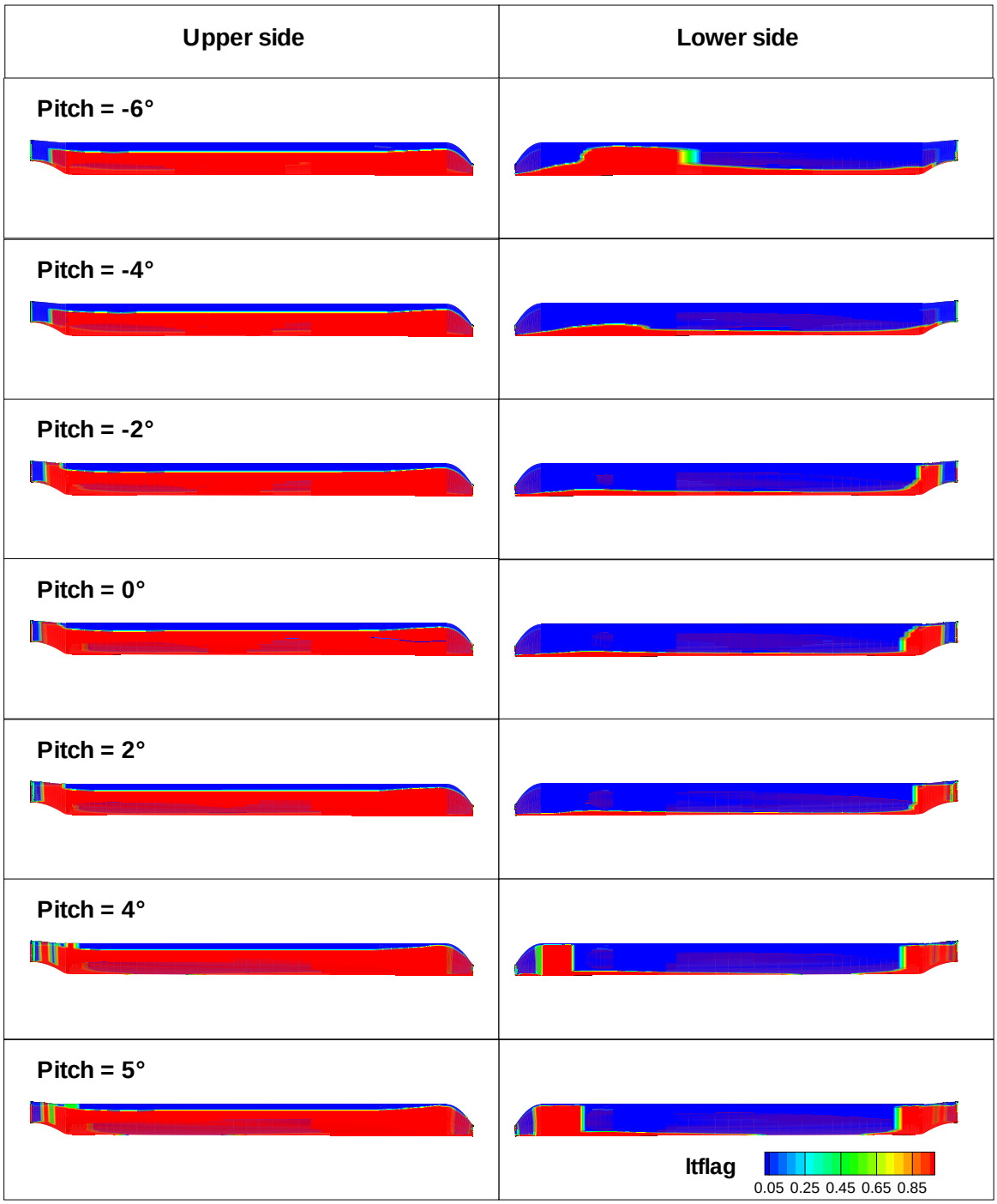

Figure D.15: INROS rotor (reference design, AHD criterion) - distribution of laminar / turbulent flow regions for different pitch angles.

E FLOWer input parameters (selection)

A summary of the FLOWer parameters mentioned in this report is summarized in table E.1. For a complete listing of all available parameters for transition prediction please refer to [7].

FLOWer parameter	Description
TRATHWAITES	Transition switch and coefficient of Thwaites formula [22] for the momentum loss thickness. trathwaites(1) = 0. - integral calculation trathwaites(1) = 1. - Thwaites' approximation (default) trathwaites(2) = 0.450 (default)
TRACSTAGMETH	Transition component stagnation method. Detection method for stagnation points. 1 - maximum pressure 2 - tangential velocity reversal and maximum pressure
TRACRITERION	Identifier of criterion for transition prediction. 1 - cp-min 2 - Michel*) [19] 3 - van Driest & Blumer*) [23] 4 - AHD*) [2] *) will be overruled by laminar separation
TRACRELAX	Transition component prediction relaxation. Relaxation coefficient on the location of transition onset. Will not affect locations predicted by laminar separation!
TRACFREQ	Transition prediction frequency per component. Frequency of calls of transition prediction.
TRACTHICKN	Transition component thickness number of cells. This is the thickness of the laminar zone of a given component in terms of laminar cells above the surface.

Table E.1: FLOWer input parameters for transition prediction (selection)

F Grid requirements

The implemented method is intended for rotary wing applications, assuming a geometrical representation of the surface grid resembling

- airfoils,
- wing geometries or
- rotor blades.

The grid should satisfy the following requirements in order to work properly with the implemented algorithms for empirical transition criteria:

- a continuous, this means not subdivided, wall segment around the body's upper and lower surface (mandatory);
- C or O block grid topology for airfoils (2D) or wings/rotor blades (3D);
- grid lines alligned parallel to the general flow direction;
- grid lines alligned normal to the wall surface;
- optional sharp or blunt trailing edge;
- one or more grid blocks in spanwise direction (3D);

Figure F.1 schematically summarizes the above mentioned grid requirements.

If integral, laminar boundary layer profiles are to be computed directly from the RANS grid, the following additional requirements should be satisfied:

- sufficient resolution of boundary layer thickness (best practice: approximately 70 equidistant points to resolve direction normal to wall);
- sufficient mesh point density along profile chord direction (best practice: approximately 250 points to resolve upper or lower side);
- sufficient mesh point density at leading edge for accurate stagnation point detection;

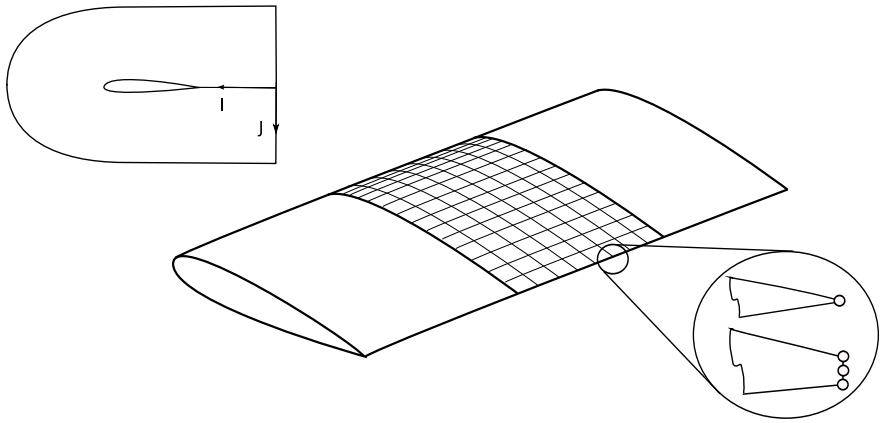

Figure F.1: Schematic of grid requirements for transition prediction

G Best practice guidelines

Based on the experiences gained during the computations done for this report, some recommendations for required FLOWer settings are given in the following:

- **Choice of transition prediction frequency**
  The convergence of the transition onset location showed to be sensitive to the chosen prediction intervall, defined by 'TRACFREQ'. For the low Mach number Somers airfoil, a trend of decreasing 'TRACFREQ' with increasing angle of attack could be observed to obtain stable results. A value of 'TRACFREQ=50' proved as good value to avoid oscillations for all employed criteria. For the transsonic flow of the CAST10 airfoil, 'TRACFREQ=250' showed the best convergence behaviour to avoid oscillations. Based on the experience from the CAST10 testcase, the value of 'TRACFREQ=250' was adapted for the 7A and INROS rotor at hover.

- **Amount of transition prediction steps**
  For stationary 2D problems, convergence of the transition onset location could be achieved after 8 (Somers testcase), repectively 15 prediction steps (CAST10 testcase). For the quasi stationary 3D problem of the 7A rotor at hover, transition onset converged after 15 steps.

- **Choice of relaxation setting**
  To avoid oscillating behaviour of transition onset, a value of 'TRACRELAX=[0.3, 0.5]' showed good results for the Somers testcase. For high angles of attack, a low relaxation factor (< 0.5) is recommended. For the Michel criterion [9], 'TRACRELAX=0' had to be used to keep the laminar separation location as transition onset point at high angles of attack.
  To avoid suppression of instationary flow phenomena in the transition onset behaviour, 'TRACRELAX=1.0' (no relaxation) was employed for the ONERA 7A and INROS rotor at hover.

- **Choice of stagnation point detection**
  For the Somers and CAST10 computations, the method of flow reversal and c_p-max ('TRACSTAGMETH=2') reliably detected the stagnation point.
  For the 7A rotor case, this method detected stagnation points on the blades upper side, indicating a none feasible negative angle of attack. Using the simple c_p-max detection ('TRACSTAGMETH=1') resolved this problem. This method also worked well for the Somers, CAST10 and INROS rotor testcase.

- **Choice of laminar zone thickness**
  The thickness of a laminar envelope is defined by 'TRACTHICKN'. A save value for

the thickness can approximated by the Prandtl relation for a turbulent flat plate boundary layer thicknes: $\delta = \frac{0.37}{Re_{tip}^{\frac{1}{5}}} \cdot c$.

- **Definition of transition components**
  Grid blocks with an extension of just one grid point in spanwise direction should not be declared as transition components in the grid logic file. Otherwise this will lead to an error caused by the leading edge detection algorithm.

IB 124-2010/2

Implementation, verification and validation of empirical transition criteria for airfoil and rotary wing applications using the DLR FLOWer code

Christoph Heister

Verteiler:

Institut für Aerodynamik und Strömungstechnik, BS	1	Exemplar
Institut für Aerodynamik und Strömungstechnik, GÖ	1	Exemplar
Verfasser ..... je	1	Exemplar
Prof. Dr.-Ing. habil. C. Rossow	1	Exemplar
Prof. Dr.-Ing. N. Kroll	1	Exemplar
Dr.-Ing. D. Schwamborn	1	Exemplar
Dr.-Ing. H. Freiherr Geyr von Schweppenburg	1	Exemplar
Dipl.-Ing. J. Raddatz	1	Exemplar
EUROCOPTER Deutschland GmbH	2	Exemplare
Technische Informationsbibliothek Hannover	1	Exemplar
Niedersächsische Landesbibliothek Hannover	1	Exemplar
Deutsche Bibliothek Frankfurt am Main	2	Exemplare
Niedersächsische Landesbibliothek Hannover	1	Exemplar
Technische Informationsbibliothek Hannover	1	Exemplar
Zentralbibliothek	2	Exemplare
Reserve	5	Exemplare
	23	Exemplare